

THE STRUCTURAL DYNAMICS OF HUMAN LIPOXYGENASES  
ENZYMATIC AND REGULATORY MECHANISMS

By

Kristin Diane Droege

Dissertation

Submitted to the Faculty of the  
Graduate School of Vanderbilt University in  
partial fulfillment of the requirements for the  
degree of

DOCTOR OF PHILOSOPHY

in

Chemistry

August 11, 2017

Nashville, Tennessee

Approved:

John A. McLean, Ph.D.

Charles R. Sanders, Ph.D.

Camelo J. Rizzo, Ph.D.

Brian O. Bachmann, Ph.D.

Alan R. Brash, Ph.D.

*To my Mom and Dad, for the support and love along  
the way.*

*To my sister, Stacie, for always inspiring me.*

*To Nathan, for helping me believe I can accomplish  
anything.*

*In memory of Dr. Richard Neil Armstrong for  
dedicating his life in the pursuit of knowledge and  
teaching others.*

## ACKNOWLEDGEMENTS

I would like to express my gratitude to the following people:

My research advisor, Dr. Richard Armstrong, for providing support, encouragement, and scientific advice during my first years of graduate research. I thank him for the opportunity to learn from his extensive scientific experience, and the opportunity to be part of his research group. I also thank Dr. Chuck Sanders, for becoming my research advisor after Dr. Armstrong's passing. Dr. Sanders stepped in and created a smooth transition through a difficult time period. He has provided essential academic support. This work would not have been completed without his help and guidance over the last two years.

I thank the outstanding members of my thesis committee, Dr. Alan Brash, Dr. Camelo Rizzo, Dr. Brian Bachmann, and Dr. John McLean. I am grateful for the guidance throughout the years. I especially want to thank Dr. John McLean for becoming the head of my committee and for the kindness and academic support he has given.

I need to thank Dr. Wade Calcutt and Julie Coleman of the mass spectrometry research center for the hours of troubleshooting and assistance. I also want to acknowledge the late Dr. Laura Busenlehner for the time she took to train us during the initial troubleshooting and planning of hydrogen deuterium exchange. I also appreciate the academic support and materials provided by Dr. Marcia Newcomer from University of Louisiana. I also want to thank members of the Biochemistry Department staff for the assistance in organizing meetings, and ordering supplies for the lab.

I thank Bill Miller for all of the writing assistance. I appreciate the help and friendship provided by former members of the Armstrong lab including Mary Keithly, Matthew Thompson,

Mike Goodman, Merced Malabanan, and Kevin Jagessar. I have enjoyed all of the research discussions, lunch outings, movie nights, and encouragement over the years. I will always love my lab family. Much the work presented herein could not have been accomplished without the assistance from Mary Keithly, who spent hours troubleshooting with me. I also need to specially thank Matt Thompson for the emotional and academic support in the last two years.

I thank my family and friends, for the love, patience, and support. This journey was overwhelming at times and I would not have made it without them. Specifically, I want to thank Mom and Dad for all of the pep talks. They pushed me to challenge myself and it took me places I never expected. I also thank Stacie for being the best sister and role model imaginable. I am very grateful for Nathan Hoover for providing day to day support and love over the past several years. In addition, for the hours of discussions centered on my research and academic career.

These studies were funded by the National Institute of Health (RO1 GM030910) and the Department of Chemistry at Vanderbilt University.

## TABLE OF CONTENTS

	Page
DEDICATION.....	iii
ACKNOWLEDGEMENTS.....	iv
LIST OF TABLES.....	viii
LIST OF FIGURES.....	ix
LIST OF ABBREVIATIONS.....	xii
Chapter	
I. INTRODUCTION.....	1
Inflammation.....	1
Eicosanoids.....	3
Leukotrienes.....	6
Lipoxins.....	10
Resolvins.....	12
The Lipoxygenase Superfamily.....	13
5-Lipoxygenase.....	20
15-Lipoxygenase.....	26
5-Lipoxygenase Activating Protein.....	32
Hydrogen Deuterium Exchange-Mass Spectrometry.....	36
Purpose of These Studies.....	40
II. MATERIAL AND METHODS.....	44
Materials.....	44
Methods.....	44
III. EXAMINATION OF 15-LOX-2 STRUCTURAL DYNAMICS IN SOLUBLE AND MEMBRANE ASSOCIATED STATES.....	60
Results.....	60
Discussion.....	70

IV.	ANALYSIS OF 15-LIPOXYGENASE-2 CONFORMATIONAL CHANGES UPON LIGAND BINDING.....	78
	Results.....	78
	Discussion.....	85
V.	EFFORTS TOWARDS DETERMINING 5-LIPOXYGENASE AND 5-LIPOXYGENASE ACTIVATING PROTEIN COMPLEX INTERACTIONS.....	93
	Results.....	93
	Discussion.....	102
VI.	CONCLUSIONS.....	107
	Discussion.....	107
	Future Directions.....	111
Appendix		
	A. Amplitudes and rate constants for amide H/D exchange profiles.....	114
	B. Additional H/D exchange profiles for 15-LOX-2.....	118
	C. Supplemental information for Chapter III.....	122
	D. Supplemental information for Chapter IV.....	123
	E. Curriculum vitae.....	124
	REFERENCES .....	130

## LIST OF TABLES

Table	Page
1. Phospholipids that promote LOX membrane association.....	75
2. Amplitudes and rate constants for amide H/D exchange profiles in Figure 17.....	114
3. Amplitudes and rate constants for amide H/D exchange profiles in Figure 22.....	115
4. Amplitudes and rate constants for amide H/D exchange profiles in Figure 23.....	116
5. Amplitudes and rate constants for amide H/D exchange profiles in Figure 25.....	117

## LIST OF FIGURES

Figure	Page
1. PUFA chemical structures.....	4
2. LT biosynthesis.....	8
3. LX biosynthesis.....	11
4. LOXs oxygenation sites on AA.....	15
5. The catalytic cycle of LOXs.....	16
6. Crystal structure of Stable 5-LOX.....	21
7. Similarities of LOXs crystal structures.....	23
8. Crystal structure of 15-LOX-2.....	27
9. 15-LOX-2 active site.....	38
10. Alignments of LOX PLAT domains.....	31
11. The 4.0 resolution crystal structure of FLAP.....	33
12. The Linderstrøm-Lang model of H/D exchange.....	37
13. H/D exchange MS experimental method.....	38
14. Scheme of 15-LOX-2 <i>in vivo</i> activity.....	42
15. Peptide map of 15-LOX-2.....	61
16. Structural dynamics of ligand- and substrate-free 15-LOX-2.....	64
17. Impact of Ca <sup>2+</sup> binding and membrane association of H/D exchange for the PLAT domain of 15-LOX-2.....	65
18. 15-LOX-2 binding to lipids on “strips” to screen for the lipid binding preference of this enzyme.....	67
19. Association of 15-LOX-2 with nanodiscs.....	68



20. Effect of DDM micelles effect on deuterium incorporation.....	70
21. Comparison of membrane association domains in 15-LOX-2 and PKC $\alpha$ .....	74
22. Deuterium exchange in the catalytic domain in 15-LOX-2 upon lipid binding.....	79
23. Deuterium exchange in the PLAT domain in 15-LOX-2 upon lipid binding.....	81
24. AA dose dependence of deuterium incorporation.....	82
25. Effects of ligand binding to 15-LOX-2.....	84
26. Sequence alignments of LOXs to demonstrate conserved $\pi$ -cation interaction.....	87
27. The conserved $\pi$ -cation bridge that binds the PLAT and catalytic domain.....	88
28. Comparison of H/D exchange upon 15-HpETE and 13-HODE binding to 15-LOX-2.....	90
29. SDS-page gel of purified FLAP.....	94
30. SEC profile of FLAP.....	95
31. UV-Vis spectrum of 5-LOX enzymatic activity.....	96
32. 5-LOX loss of enzymatic activity.....	97
33. Preliminary peptide map of 5-LOX.....	98
34. Peptide map of FLAP.....	99
35. Structural dynamics of apo-FLAP.....	101
36. H/D exchange profiles for FLAP peptides.....	102
37. AA binding induces changes in H/D exchange kinetics in FLAP.....	105
38. H/D exchange kinetic profiles for 15-LOX-2 as a function of Ca $^{2+}$ binding and nanodisc-association, Resides 1-364.....	118
39. H/D exchange kinetic profiles for 15-LOX-2 as a function of Ca $^{2+}$ binding and nanodisc-association, Resides 366-676.....	119
40. H/D exchange kinetic profiles for 15-LOX-2 as a function of AA and 15-HpETE binding, Resides 1-354.....	120

41. H/D exchange kinetic profiles for 15-LOX-2 as a function of AA and 15-HpETE binding, Residues 345-676.....	121
42. SDS-page gel of 15-LOX-2 associated with nanodiscs.....	122
43. H/D exchange for 15-LOX-2 associated with nanodiscs containing AA.....	122
44. HPLC chromatogram of LOX products.....	123

## LIST OF ABBREVIATIONS

AA	Arachidonic acid
ATP	Adenosine triphosphate
BLT1	Leukotriene B receptor-1
BLT2	Leukotriene B receptor-2
BSA	Bovine Serum Albumin
Ca <sup>2+</sup>	Calcium ions
C8E4	Tetraethylene glycol monoethyl ether
CHAPS	(3-((3-cholamidopropyl) dimethylammonio)-1-propanesulfonate
CL1	Cytosolic loop 1
CL2	Cytosolic loop 2
CMC	Critical micelle concentration
COX	Cyclooxygenase
cPLA <sub>2</sub>	Cytosolic phospholipase A <sub>2</sub>
CYP	Cytochrome P450
Cys-LT	Cysteinyl leukotrienes
DAG	Diacylglycerol
DC	Dendritic cells
DDM	n-Dodecyl-β-maltoside detergent
DHA	Docosahexaenoic acid
EPA	Eicosapentaenoic acids
ESI	Electrospray ionization

FDR	False discovery rate
FLAP	5-lipoxygenase activating protein
FLIM	Fluorescence life-time imaging microscopy
FPR2/ALX	Formyl-peptide receptor-2/ Lipoxin receptor
FRET	Fluorescence resonance energy transfer
GGT	$\gamma$ -Glutamyl transpeptidase
GLA	$\gamma$ -Linolenic acid
GPCR	G protein-coupled receptor
H/D	Hydrogen/ deuterium
HETE	Hydroxyeicosatetraenoic acid
HODE	Hydroxyoctadecadienoic acid
HpETE	Hydroperoxyeicosatetraenoic acid
HPLC	High-performance liquid chromatography
Ig	Immunoglobulin
IL	Interleukin
IP <sub>3</sub>	D-myo-inositol-1,4,5-triphosphate
IPTG	Isopropyl $\beta$ -D-1-thiogalactopyranoside
LA	Linoleic acid
LB	Luria-bertani
LC	Liquid chromatography
LOOH	Lipid hydroperoxides
LOX	Lipoxygenase
LPS	Lipopolysaccharide

LT	Leukotriene
LTA <sub>4</sub> H	Leukotriene A <sub>4</sub> hydrolase
LTC <sub>4</sub> S	Leukotriene C <sub>4</sub> synthase
LX	Lipoxin
MALDI	Matrix-assisted laser desorption/ ionization
MAPEG	Membrane-associated proteins in eicosanoid and glutathione metabolism
MAPKAP	Mitogen-activated protein kinase-activated protein kinase
MC	Mast cell
MPGES	Microsomal prostaglandin E synthase
MS	Mass spectrometry
MS/MS	Tandem mass spectrometry
MSP	Membrane scaffolding protein
MWCO	Molecular weight cut off
NMR	Nuclear magnetic resonance
NSAIDS	Nonsteroidal anti-inflammatory drug
PC	Phosphatidylcholine
PI-4,5-BP	Phosphatidylinositol 4,5-bisphosphate
PIP <sub>2</sub>	Phosphatidylinositol 4,5-bisphosphate
PKC	Protein kinase C
PLAT	Polycystin-1, lipoxygenase, $\alpha$ -toxin and triacylglycerol
PMN	Polymorphonuclear
PS	Phosphatidylserine
PUFA	Polyunsaturated fatty acid

RA	Rheumatoid arthritis
RBL	Rat basophilic leukemia
Rv	Resolvin
SEC	Size exclusive chromatography
SUV	Small unilamellar vesicles
TB	Terrific broth
TM	Transmembrane
TNF- $\alpha$	Tumor necrosis factor- $\alpha$
WT	Wild-type
UPLC	Ultra performance liquid chromatography

# CHAPTER I

## INTRODUCTION

### Inflammation

An integral aspect of the innate immune response of cells is the initiation of inflammation. Inflammation is a process characterized by rapid accumulation of immune cells within designated areas with the goals of isolating sites of injury, protecting the organism from potentially harmful threats, and triggering the healing process.<sup>1</sup> Inflammation is initiated and resolved by a series of complex, microscopic events such as changes in regulation of lipid mediators, vascular permeability, and cell recruitment and migration.<sup>2</sup>

Inflammation can be divided into two distinct types based on the length of time during which it is activated within cells. Acute inflammation, the body's immediate response to injury, is an essential step in the healing process and a protective response to threats or injury. It is characterized by pain, redness, swelling, and heat in the afflicted area. However, this response can be transposed to the second type of inflammatory immune response, chronic inflammation. Chronic inflammation, the body's long-term healing byproduct, is traditionally associated with a variety of diseases such as cardiovascular disease, asthma, and rheumatoid arthritis (RA).<sup>3</sup> Recently, researchers have demonstrated connections between chronic inflammation and a number of diseases such as Alzheimer's, certain types of cancer, and diabetes. The chronic inflammatory mechanisms identified in these disorders are fibrosis, metaplasia, and tumor formations.<sup>4</sup>

### *Initiation of Inflammation*

Inflammation is viewed as a complex pathophysiological process that involves hundreds of mediators and differing cell types and tissues. It is initiated by any stimulus that cells identify as a threat. This complexity of mechanism and daunting variety of triggering events makes elucidation of specific processes difficult. For example, inflammation can be initiated by the recognition of foreign material by Immunoglobulin (Ig) E antibodies, a relatively common phenomenon. Activated IgE then binds with high affinity to receptor  $FC\epsilon RI$  in mast cells (MC) and basophils, which initiates a series of pathways that include post-translational modifications of signaling proteins responsible for releasing calcium ions ( $Ca^{2+}$ ) from intracellular storage.<sup>5</sup>  $FC\epsilon RI$  activation also results in the degranulation of cytoplasmic granules containing the pro-inflammatory mediators, an increase in production of eicosanoids, and secretion of cytokines and chemokines. These signaling molecules start cascading events that result in altered blood flow, increased vascular permeability, and constriction of bronchiole muscles.<sup>6</sup> The excess of the inflammatory mediators shifts the physiological manifestations into the symptoms of airborne allergies and asthma.

Inflammation can also be initiated by the classic complement pathway. Antibody IgG and IgM bind directly to antigens, which leads to antibody aggregation. Antibody aggregation begins the formation of the complement complex.<sup>7</sup> This complex is cleaved into individual proteins or peptides that are deposited in the injured tissues. The cleavage products activate the release of pro-inflammatory cytokines from phagocytes. In RA, B-cells and other inflammatory cells that have been activated by the complement pathway infiltrate the synovial membrane and release tumor necrosis factor alpha (TNF- $\alpha$ ), interleukin-1 (IL), and IL-6. These pro-inflammatory mediators increase cell recruitment to the site of inflammation, causing the potential for harm to the tissue to



increase significantly. Without resolution, phagocytosis, or apoptosis, such tissues will experience serious damage.<sup>8</sup> In RA, cell accumulation leads to the synovial lining becoming hyperplastic and expanding, which causes bone and cartilage degradation.<sup>9</sup> Pattern recognition receptors can also activate the complement cascade by recognizing specific antigen-antibody complexes, facilitating the process of initiating inflammation.<sup>10</sup>

## Eicosanoids

Eicosanoids are a group of lipid mediators of inflammation that have been extensively studied over the last 50 years. They act locally as signaling molecules at nanomolar concentrations on their target cells. Granulocytes, macrophages, neutrophils, platelets, MCs, and endothelial cells are involved with eicosanoid production during inflammation.<sup>3</sup> In addition to being heavily involved in initiating inflammation, eicosanoids are integral to the process of resolving inflammation. Inflammation resolution is the return of tissues to normal equilibrium and function, a process that is as complicated as inflammation initiation, but is not as thoroughly understood. Critical steps in resolution performed by eicosanoids are propagation of leukocyte apoptosis, limitation of the synthesis of cellular adhesion molecules, recruitment and activation of macrophages for phagocytosis, and modulation of pro-resolving mediators.<sup>11</sup>

### *Discovery of Eicosanoids and Early Research*

Eicosanoids have been a focus of scientific research since their discovery, and the knowledge base for the full range of their impact on biological functions remains incomplete. The importance of these signaling molecules was initially discovered by George and Mildred Burr in 1930 when they observed that rats with fat-free diets experienced reproductive disturbances,

growth hindrance, scaly skin, kidney lesions, and excess water consumption. The Burrs were the first to coin the term “essential fatty acids” and published their results stating that fats were not just necessary for calorie consumption, as previously thought, but for a variety of biological pathways.<sup>12,13</sup> Around the same period, two other research groups discovered that lipid extracts from seminal plasma and sheep’s vesicular glands had vasodepressor and smooth muscle-stimulation effects.<sup>14,15</sup> The identified lipids were called prostaglandins. It took another 30 years before the implications of these individual observations were integrated by Bergström and Samuelsson.<sup>16</sup> They demonstrated the chemical structure of “classic” prostaglandins and that prostaglandins were biosynthesized from the essential fatty acids, arachidonic acid (AA) and dihomo- $\gamma$ -linolenic acid. Today the members of the eicosanoid family include virtually all long-chain oxygenated products from AA, whether formed enzymatically or nonenzymatically.<sup>17</sup> Humans ingest/synthesize over 7 fatty acids that are substrates for human lipoxygenases (LOX), cyclooxygenases (COX), and cytochrome P450 (CYP). These 7 fatty acids are enzymatically converted to oxylipins. Eicosanoid is derived from the Greek word for twenty, *eikosi*, since their first identified precursor lipid, AA, has a 20-carbon chain.

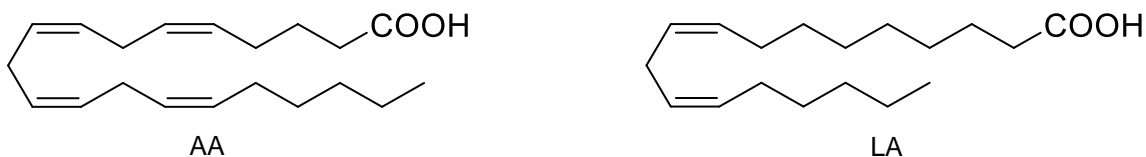


**Figure 1. Polyunsaturated fatty acid (PUFA) chemical structures.** Chemical structure of the most common PUFAs converted to oxylipins in mammals (AA) and in plants (linoleic acid (LA)). AA is an omega-6 fatty acid with a 20-carbon chain and four *cis* double bonds. LA is also an omega-6 fatty acid with an 18-carbon chain and two *cis* double bonds.

## *Eicosanoid Biosynthesis*

Eicosanoids behave similarly to hormones in terms of their ability to initiate and resolve cellular functions at nanomolar concentrations. However, unlike hormones, eicosanoids are not transported by the circulatory system for distal effects.<sup>17</sup> Therefore, physiology utilizes eicosanoids for potent, local effects on signaling pathways rather than as an inter-systemic messenger.

Hundreds of structurally and stereochemically unique eicosanoids can be generated by the metabolism of LA, AA, and other less abundant essential fatty acids such as dihomo- $\gamma$ -linolenic acid, which is derived from LA, and eicosapentaenoic acids (EPA), which are derived from  $\alpha$ -linolenic acid.<sup>18,19</sup> Some of the more commonly investigated types of eicosanoids are prostaglandins and thromboxanes, formed by COX superfamily members, leukotrienes (LTs) and lipoxins (LXs) formed by LOX superfamily, and epoxyeicosatrienoic acids which are formed by the CYP superfamily.<sup>20</sup>

Relatively few of the eicosanoids have their physiological role identified, but some have been observed to play a role in vasodilation, muscle contraction, inflammation propagation and resolution, and pain response.<sup>2</sup> The type and concentration of eicosanoids biosynthesized by tissue is dependent on the type of cell, the tissue location, and the activation state of the cell. Some eicosanoids, such as prostaglandins, are synthesized in most cell types and in most tissues, but the identity and degree of prostaglandins produced varies depending on local conditions. For example, in macrophages, the type of specific prostaglandin as well as their concentration after cell stimulation show significant differences based upon the progenitor tissue. Differences in prostaglandin production also exist between primary macrophages and transformed macrophages.<sup>21</sup> A further wrinkle in the differing processes is observed by intra-cellular alterations of eicosanoid type produced depending on the activation state. For example, resting macrophages

synthesize thromboxanes over classic prostaglandins. This changes after cellular activation by bacterial lipopolysaccharide (LPS) or complement cleavage product C3b.<sup>22,23</sup> These observations indicate a high level of eicosanoid regulation. This is hypothesized to be a necessary cellular function as over expression of eicosanoids can cause damage to their surrounding tissue.

Given their clinically relevant inflammatory properties, eicosanoids are pharmaceutical targets. Currently the most prevalent therapeutic on the market for regulation of eicosanoids is for inhibition of prostaglandin synthesis by nonsteroidal anti-inflammatory drugs (NSAIDs). NSAIDs non-selectively bind to COX isoform-1 (COX-1) and COX isoform-2 (COX-2) to prevent oxygenation of AA. Limiting prostaglandin biosynthesis is problematic as prostaglandins are important signaling molecules in several physiological pathways. In addition, NSAIDs can have adverse gastrointestinal effects.<sup>24</sup> These treatments, however, are only one approach to eicosanoid regulation, prompting further research to form a complete understanding of the inflammatory process and the mechanisms by which it can be regulated. This literature review will focus on the eicosanoids, LTs, LXs, and resolvins (Rv), and the enzymes involved with their biosynthesis and regulation. These specific eicosanoids are identified to have essential pro- and anti-inflammatory properties, and thus are of particular note.

### Leukotrienes

LTs are primarily synthesized in inflammatory cells such as polymorphonuclear (PMN) leukocytes, macrophages, MCs, and dendritic cells (DC).<sup>11</sup> These cells can be activated by a variety of stimuli such as IgE-antigen complexes, TNF- $\alpha$ , and increased concentration of ionophores.<sup>25</sup> Cellular activation most notably results in an increase in Ca<sup>2+</sup> concentrations in the cytosol. The increase in Ca<sup>2+</sup> directly initiates the biosynthesis of LTs. The correlation between

LTs biosynthesis and  $\text{Ca}^{2+}$  concentration was first demonstrated in the 1970s in rabbit PMNs and mouse mastocytoma cells.<sup>26,27,28</sup>  $\text{Ca}^{2+}$ -stimulation of LT biosynthesis was also described in rat basophilic leukemia (RBL) cells when an increase in ionophore A23187 (a mobile divalent ion carrier) resulted in increased production of 5-hydroxyeicosatetraenoic acid (5-HETE).<sup>29</sup> 5-HETE is a metabolized product of 5-hydroperoxyeicosatetraenoic acid (5-HpETE), which is the precursor molecule for LT synthesis.

### *LT Biosynthesis*

$\text{Ca}^{2+}$  ions will bind to both cytosolic phospholipase A<sub>2</sub> (cPLA<sub>2</sub>) and 5-LOX causing them to translocate from the cytosol to the nuclear membrane.<sup>30,31</sup> Two or three  $\text{Ca}^{2+}$  ions bind to the C2 domain in cPLA<sub>2</sub> and to the polycystin-1, lipoxygenase,  $\alpha$ -toxin (PLAT) domain in LOXs.  $\text{Ca}^{2+}$  concentrations between 4-10  $\mu\text{M}$  are required for full activation of 5-LOX in intact cells.<sup>32</sup> When transported to the nuclear membrane, cPLA<sub>2</sub> catalyzes the hydrolysis of the sn-2 acyl bond in phospholipids to generate free AA.<sup>33</sup> 5-LOX will form a protein complex with 5-lipoxygenase activating protein (FLAP) at the membrane when it translocates to the nuclear membrane.<sup>34</sup> It is hypothesized that free AA generated by cPLA<sub>2</sub> is facilitated from the membrane to 5-LOX by FLAP. AA is oxygenated at the C-5 position by 5-LOX to generate 5-HpETE. 5-HpETE is either enzymatically reduced to form 5-HETE or 5-LOX will convert 5-HpETE to LTA<sub>4</sub>, an unstable epoxide intermediate.<sup>35</sup>

LTA<sub>4</sub> can be metabolized by two pathways. It can be hydrolyzed by LTA<sub>4</sub> hydrolase (LTA<sub>4</sub>H) to form LTB<sub>4</sub> or it can be conjugated to glutathione by LTC<sub>4</sub> synthase (LTC<sub>4</sub>S) to form LTC<sub>4</sub>.<sup>2</sup> LTA<sub>4</sub>H is distributed in the cytosol of almost all mammalian cells. LTC<sub>4</sub>S is an integral membrane protein expressed in eosinophils, MCs, and monocytes.<sup>36</sup> The tripeptide moiety of LTC<sub>4</sub>

can be hydrolyzed to generate LTD<sub>4</sub> by  $\gamma$ -glutamyl transpeptidase (GGT) and then LTD<sub>4</sub> can be hydrolyzed by several dipeptidases to form LTE<sub>4</sub> (Figure 2).<sup>37</sup> These LTs are called cysteinyl-leukotrienes (cys-LT) and are identified as slow-reacting molecules of anaphylaxis.

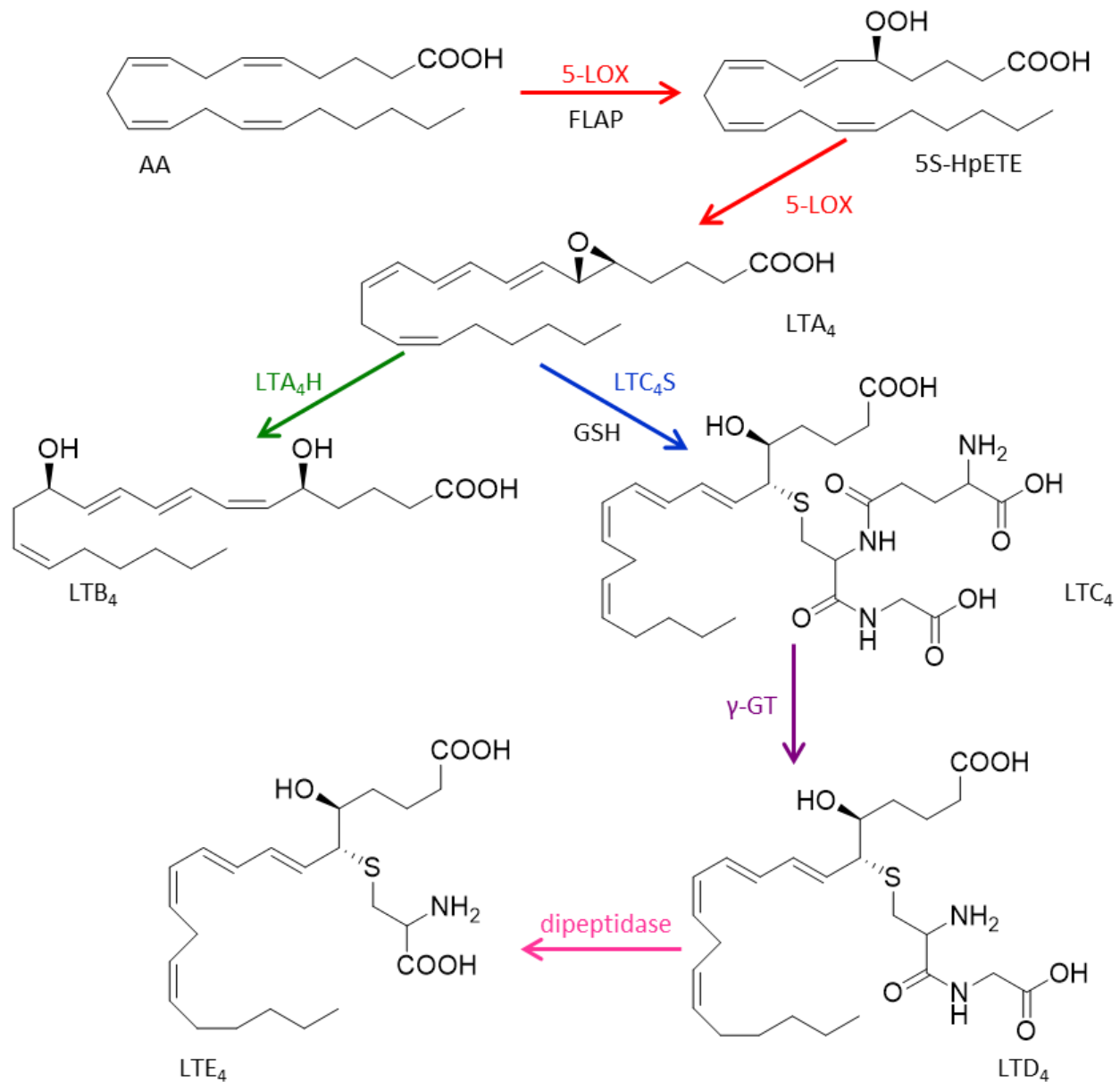


**Figure 2. LT biosynthesis.** Free AA is oxygenated and subsequently hydrolyzed by 5-LOX in complex with FLAP to form LTA<sub>4</sub>. LTA<sub>4</sub> is either hydrolyzed by LTA<sub>4</sub>H to generate LTB<sub>4</sub> or conjugated to GSH to form LTC<sub>4</sub>. LTC<sub>4</sub> is further metabolized to form the additional cys-LTs, LTD<sub>4</sub> and LTE<sub>4</sub>.

### *Biological Mechanisms of LTs*

LTs are identified as pro-inflammatory mediators that act by binding to four different G-protein-coupled receptors (GPCR).<sup>11</sup> LTB<sub>4</sub> has a high affinity for leukocyte LTB receptor-1 (BLT1). This receptor is coupled to G<sub>q</sub> protein which has an  $\alpha$ -subunit that binds and induces activity of phospholipase C. Phospholipase C cleaves phosphatidylinositol 4,5-bisphosphate (PIP<sub>2</sub>) to form D-myo-inositol-1,4,5-trisphosphate (IP<sub>3</sub>) and diacylglycerol (DAG) both of which are potent signaling molecules in inflammation.<sup>38</sup> High concentrations of LTB<sub>4</sub> are required for LTB<sub>4</sub> to bind to LTB receptor-2 (BLT2), which signals through similar pathways to BLT1. The remaining GPCRs are the cys-leukotriene receptors, CysLT1, CysLT2, and CysLT3.<sup>39,40</sup>

LTs have differing effects on inflammatory cells depending on LT type and cellular stimuli. In DCs, increased concentration of LTC<sub>4</sub> results in increased C-C chemokine receptor type 7, a chemokine that promotes DC migration through extracellular matrix to sites of injury.<sup>41</sup> In lymphocytes, responses to LT are dependent on the type and amount of lymphocytes present. For example, in lymphocyte cell cultures infected with Epstein-Barr virus LTB<sub>4</sub> inhibited B-cell proliferation. *In vivo* experiments indicated LTB<sub>4</sub> played a role in directing T-cell migration.<sup>42</sup>

LTs are associated with the pathogenesis of several inflammatory or autoimmune diseases. RA is caused by severe inflammation of joints that eventually leads to destruction of bone and cartilage. Inhibiting the synthesis of LTB<sub>4</sub> protected mouse models of RA from erosion of bone and influx of inflammatory cells.<sup>43</sup> Cys-LTs were originally called “slow reacting substance of anaphylaxis” due to their potent bronchoconstrictor activity.<sup>28</sup> Excess Cys-LTs results in the clinical manifestation of asthma and allergic responses, bronchial spasms, diarrhea, and blood pressure variations.<sup>3</sup>

## Lipoxins

Resolution of inflammation has historically been viewed as a passive process, occurring as a result of the withdrawal of pro-inflammatory signals, such as LTs and prostaglandins. LXs were the first eicosanoid subgroup that were shown to actively resolve inflammation.<sup>11</sup> The resolution of acute inflammation is complex, as it involves several cellular pathways occasionally acting simultaneously. One crucial step in resolution is cell clearance, which is accomplished by apoptosis of leukocytes and limiting cell adhesion. The regulation of the resolution rate is also an indispensable process. Inflammation resolution is mediated by recruitment of macrophages that complete phagocytosis of the microbes and apoptotic cells.<sup>44</sup> Without this process the accumulation of cells results in tissue and organ damage. LXs have been observed to play important roles in all of these pathways, the details of which will be discussed below.

### *LX Biosynthesis*

LX biosynthesis requires interacting LOXs and the proximity of specific cells. Moreover, in some occurrences the metabolites are transferred to another cell for metabolism. There are two main pathways for LX synthesis. In the first pathway, 5-LOX catalyzes the conversion of AA to LTA<sub>4</sub> similar to the first step in LT synthesis. LTA<sub>4</sub> is then transferred to adjacent platelets and is converted to LXA<sub>4</sub> or LXB<sub>4</sub> by the oxygenation from 12-LOX.<sup>45</sup> In the second pathway, AA is converted to 15-HpETE in the endothelium by 15-LOX. 15-HpETE is subsequently taken up by PMN cells or monocytes and oxygenated by 5-LOX to form the 5,6-epoxytetraene intermediate. This short lived intermediate is hydrolyzed to generate LXA<sub>4</sub> or LXB<sub>4</sub>.<sup>46</sup> Alternatively, there is a pathway to produce 15-epimer-LXs that is triggered by acetylated COX-2. When COX-2 is acetylated by acetylsalicylic acid (aspirin) the catalytic product is altered to 15(R)-HpETE as



opposed to the 15(S)-HpETE product formed by 15-LOX. 15(R)-HpETE is oxygenated by 5-LOX to form 15(R)-LXA<sub>4</sub>.<sup>47</sup> Aspirin triggered LXs are twofold more potent than the 15(S)-LXs formed by the classic pathway.<sup>44</sup>

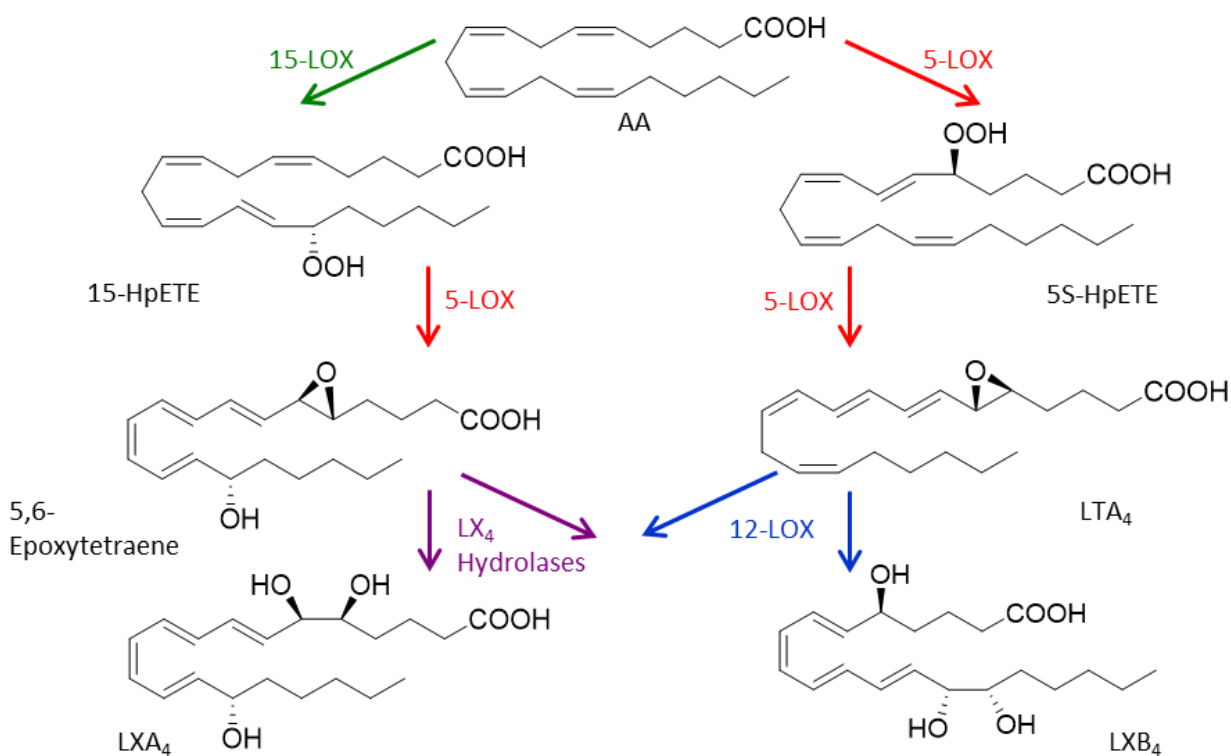


**Figure 3. LXs Biosynthesis.** LXs are synthesized through 2 main pathways by LOX oxygenation and sequential hydrolase activity. LX are the first eicosanoids identified to play a role in resolution of inflammation.

### *Biological Pathways of LXs*

LX research has so far yielded conflicting results. The variances in experimental conclusions are proposed to be due to a lack of positive control for LXA-induced responses.<sup>48</sup> Research suggests that LXs resolve inflammation through several pathways. LXs biological effects are produced by binding to formyl-peptide receptor-2, also referred to as FPR2/ALX due to its

interaction with LXs.<sup>49</sup> In DCs, LXs inhibit the productions of IL-2, an important cytokine in the immune response.<sup>50</sup> In addition, LXA<sub>4</sub> has been identified to resolve bronchial constriction in murine models of asthma. Administration of a stable analog agonist for LXA<sub>4</sub> receptors resulted in decreased leukocyte recruitment and a decrease in the pro-inflammatory mediators, IL-5, IL-13, prostanoids, and cys-LTs. Transgenic expression of human LXA<sub>4</sub> receptors in murine leukocytes resulted in inhibition of pulmonary inflammation and eicosanoid-initiated eosinophil tissue infiltration.<sup>51</sup> LXA<sub>4</sub> has also been observed to increase natural killer cell mediated eosinophil apoptosis and decreased IL-13 release by type 2 innate lymphoid cells.<sup>52</sup> Combining these observations leads to the overall conclusion that LXs initiate the resolution of inflammation. However, additional studies are needed to clarify the cellular pathways directly affected.

### Resolvins

Rv are another class of anti-inflammatory mediators that have recently been identified. Rv names are derived from their identification as “inflammation resolution interaction products”.<sup>19</sup> They can be classified as either a D-series, meaning the Rv was derived from docosahexaenoic acid (DHA)<sup>19</sup>, or E-series, which are derived from EPA.<sup>18</sup> Both DHA and EPA are naturally occurring omega-3 fatty acids. The biosynthesis of Rv E-series is initiated by the conversion of EPA by CYP. The resulting intermediate is then either oxidized by 5-LOX in leukocytes to form RvE1, or can be reduced to form RvE2.<sup>53</sup> Similarly to LXs, an aspirin triggered epimer has been identified with EPA initially transformed by acetylated COX-2.

Biosynthesis of D-series of Rv is similar to the E-series in which DHA is converted by either acetylated COX-2 or CYP to a stereoselective intermediate. This intermediate is enzymatically converted by 15-LOX to form either RvD1-4 or (R)-RvD1-4 depending on which

intermediate is utilized.<sup>54</sup> Knowledge on Rvs biological function and receptors is in the early stages of development. Currently, RvE1 is known to interact with either receptor Chem R23 or BLT1 to mediate cell-type specific effects.<sup>55,56</sup> Protein-ligand interaction screening also revealed FPR2/ALX and orphan receptor GPR32 as potential receptors for RvE1.<sup>57</sup> The receptor for RvE2 has not been characterized, but its pro-resolving actions are mediated by a GPCR in leukocytes. RvE series has been shown to be a potent mediator in regulating chemotaxis of human neutrophils, enhancing phagocytosis, and increasing anti-inflammatory cytokine production.<sup>58</sup> RvD series has been observed to limit PMN infiltration in a dose-dependent manner.<sup>59</sup> The continued discoveries of new eicosanoids and their roles in cellular pathways indicate a continued need for research on these signaling molecules and the enzymes that complete their metabolism.

### The Lipoxygenase Superfamily

The enzymatic products of LOXs are crucial in both the propagation and resolution of inflammation, a process which brands LOXs as therapeutic targets by pharmaceutical companies. The only drug in active use that targets LOXs is Zileuton. Zileuton is an inhibitor of 5-LOX that regulates leukotriene biosynthesis. However, Zileuton currently suffers from clinical limitations such as short half-life and potential liver toxicity. These complications have necessitated that patients take several daily dosages rather single daily supplements. They also have to complete frequent liver-function tests.<sup>60</sup> Atreuloton is a 5-LOX reversible inhibitor that is currently under clinical trials. However, it is currently unavailable for patients and must be researched further once clinical trials are completed.<sup>61</sup> Alternative pharmaceuticals for regulating LT and LX biosynthesis need to be investigated. An essential step in this investigation could be the development of an extensive knowledge base on LOX structure and function.

LOXs are a superfamily of non-heme iron-containing dioxygenases that catalyzed the oxygenation of PUFAs that contain a series of *cis*-double bonds.<sup>62</sup> LOXs are expressed in a variety of cells among animals, plants, and fungi.<sup>63</sup> Until recently, LOXs were thought to be found only in eukaryotes, however, LOX sequences have now been detected in prokaryotic organisms, mainly in gram-negative bacteria. Their biological function in bacteria has yet to be identified.<sup>64</sup> The expression levels of LOXs significantly vary depending on the organism and the LOX homolog. For example, 12- and 15-LOX have relatively low expression in mammalian skin<sup>65</sup> and relatively high expression in rabbit reticulocytes.<sup>66</sup> The biological importance of their enzymatic products (LTs, LXs, and Rvs) have already been discussed.

In addition, some homologs of LOXs are believed to play supplementary roles in cells. A precursor screen of lipids extracted from ionophore-treated IL-4-induced human monocytes identified four intact phospholipids that were oxidized by 15-LOX.<sup>67</sup> Clustering of oxidized phospholipids is thought to result in a “hydrophilic pore” that disrupts the barrier function of the cellular membrane. The lipid hydroperoxides (LOOH) produced by LOX catalysis have also been implicated in regulating the cellular redox state, which may lead to increased or decreased expression of redox sensitive genes.<sup>62</sup>

### *LOX Nomenclature*

Historically LOXs are named according to the specific position of oxygenation of their most common substrate (AA in mammals and LA in plants) as counted from the carboxyl of the fatty acid (Figure 4). For example, human 15-LOX oxygenates the fifteenth carbon on AA to produce 15-HpETE. If the LOX is stereochemistry-specific the name will also identify the stereospecific product (e.g. 12S-LOX or 12R-LOX). This naming system can lead to some

confusion due to the differing lengths of the common substrates across species. The plant LOX corresponding to human 15-LOX is 13-LOX due to the shorter carbon chain in LA compared to AA. Additional confusion arises when there are multiple LOXs in the same species with differing primary sequences that yield the same enzymatic products. For example, mammalian 12-LOXs are named for the prototypical tissues in which they are expressed, such as platelet 12-LOX and leukocyte 12-LOX. In addition, some LOXs form more than one HpETE isomer, leading a mixture of products. This results in names such as 12/15-LOX (also called 15-LOX-1).

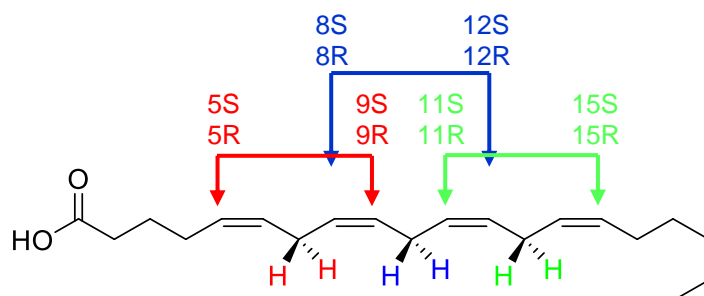


**Figure 4. LOXs oxygenation sites on AA.** AA has three pentadiene moieties creating six possible hydrogens for abstraction. The hydrogens are labeled different colors with the corresponding oxygenation products in the same color.

#### *LOX catalytic mechanism and product specificity*

All LOXs initiate, control, and terminate a free radical reaction between a substrate fatty acid and molecular oxygen (Figure 5). The catalytic cycle begins by activation of the enzyme through oxidation of the catalytic iron in the active site ( $\text{Fe}^{2+}$  to  $\text{Fe}^{3+}$ ). This oxidation is proposed to be completed by discrete concentrations of LOOHs in the cell. *In vitro* assays show a decrease in the lag phase of LOX enzyme kinetics, corresponding to increased concentrations of LOOHs.<sup>68</sup> The active state of the catalytic iron is coordinated with a hydroxide ion. After iron activation, the substrate enters the active site and is positioned in a regio- and stereo- specific orientation by

hydrophobic amino acids side chains. In the active site, a proton-coupled electron transfer takes place on the allylic carbon in the pentadiene moiety with an electron from the substrate's hydrogen entering the d-orbital of the iron and the proton from the hydrogen transferred to the hydroxide ion coordinated to the iron to form water. From there, the substrate becomes a lipid radical that will undergo delocalization and allow molecular oxygen to attack on the substrate face opposing the proton-coupled electron transfer.<sup>69</sup> The iron then donates an electron to the O<sub>2</sub> on the substrate. The O<sub>2</sub> will abstract the hydrogen from the iron-water complex allowing the HpETE product to form and restoring the iron's active state.

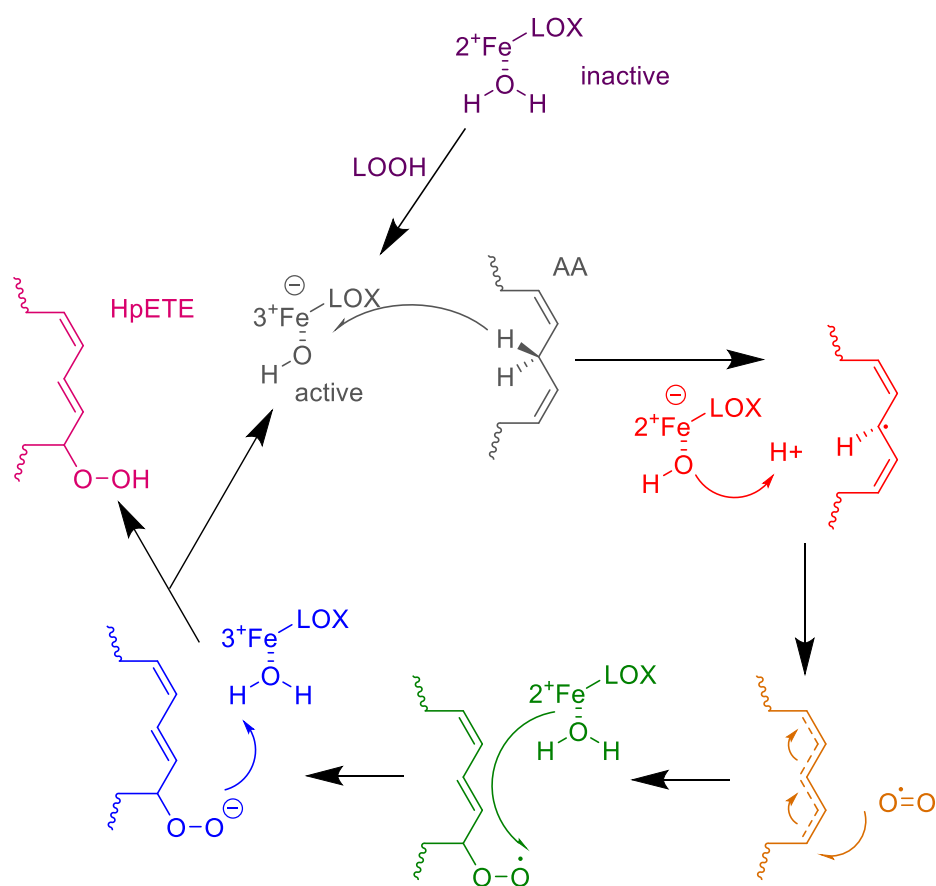


**Figure 5. The catalytic cycle of LOXs.** The catalytic iron is activated by LOOHs. A proton-coupled electron transport forms a lipid radical that is attacked by molecular oxygen. Catalysis by LOXs requires the iron to switch redox states multiple times.

There are three possible pentadiene moieties on AA for LOX oxygenation leading to six possible reaction sites and two possible stereospecific conformers per site. Therefore, twelve unique products can be produced from AA by different LOXs oxygenation. In nature, there are enzymes specific for 10 of the 12 available sites on AA (5R, 5S, 8R, 8S, 9R, 11R, 11S, 12R, 12S, and 15S).<sup>70</sup> While the enzymatic mechanism for LOXs is well understood, the structural basis for product specificity remains complicated and ambiguous. The current understanding of product specificity involves three different aspects: (1) channel depth that positions the fatty acid; (2) the head-to-tail orientation of the fatty acid; and (3) the access site of molecular oxygen. Channel depth involves shifting the fatty acid so that a different pentadiene moiety has the allylic hydrogen abstracted (a frameshift). The impact of channel depth in LOXs was first observed when a M419V site mutation in 15-LOX-1 changed the ratios of HpETE products.<sup>71</sup> Site mutagenesis studies that reduce the substrate channel depth in 11R-LOX revealed no change in substrate affinity, but did result in product variation and decreased turnover rate.<sup>72</sup> The alteration between head-to-tail orientation was first contemplated when it was observed that plant 9S-LOX and 13S-LOX abstracted the pro-R and pro-S hydrogen from the same carbon on LA.<sup>73</sup> The 9S- and 13S-positions on LA are on opposite faces of LA, which indicates that the substrate was simply in the opposite head to tail orientation in the active site. The molecular oxygen channel to the active site is hypothesized to be controlled by a single amino acid in the active site. Mutagenesis studies indicate that an alanine conserved in most S-LOXs and a glycine conserved in most R-LOXs are important in directing the molecular oxygen to the pentadiene on the substrate.<sup>74</sup> Mutation of alanine to glycine in S-LOX resulted in generation of R-HpETE product.

## *Structural Analysis of Lipoxygenases*

In addition to sharing catalytic mechanisms, LOXs share many structural features. The first LOX structure, LOX-1 isoform from soybean, was identified in 1993.<sup>75</sup> The structure established common elements that have been observed in all subsequent LOX structures, even though plant LOXs generally have a longer primary sequence (approximately 900 amino acids, while mammalian have approximately 650 amino acids). LOXs have two domains, the catalytic domain and the PLAT domain, with the exception of a recently published structure from *P. aeruginosa*.<sup>76</sup> Bacterial LOXs appear to lack the PLAT domain and have additional helices that cap the catalytic subunit in its place.

In all mammalian LOXs, the catalytic domain is composed of approximately 17  $\alpha$ -helices and crystal structures indicate a roughly parallel orientation for the majority of the helices.<sup>77</sup> At the center of the catalytic domain is the active site which houses the catalytic iron. This iron is coordinated by invariant histidines, the C-terminal carboxyl group, and a water molecule.<sup>78</sup> Use of the C-terminal carboxyl group as part of the active site is an uncommon and quite remarkable feature in LOXs. The terminus is allowed to enter the protein core by irregularities in helices structures. The C-terminus is frequently a conserved isoleucine, but the role of the isoleucine side chain is unknown. The nonpolar bonds in the side chain have limited van der Waals interactions with the helices that form the active site. However, a crystal structure of 8R-LOX from *Pseudomonas aeruginosa* suggest this area of the active site is highly solvated due to an intricate network of water molecules leading to the active site, indicating there is not a tight association between the helices and the side chain of isoleucine.<sup>76</sup>

A high degree of flexibility in the tether linking the catalytic and PLAT domain was indicated by small angle x-ray scattering experiments, however, to date every LOX crystal



structure has conformed to the same domain orientations suggesting an extensive domain interface.<sup>79</sup> The PLAT domain was originally known as a “C2-like” domain due to its structural and functional similarity to the Ca<sup>2+</sup>-dependent, membrane-binding domains in phospholipases. The domain has a high degree of structural conservation amongst LOXs, but the sequence similarity is low. A <sup>45</sup>Ca<sup>2+</sup> overlay binding assay in 5-LOX originally indicated the PLAT to be the Ca<sup>2+</sup> binding domain.<sup>80</sup> The amino acids identified to coordinate the binding of Ca<sup>2+</sup> are not conserved throughout the superfamily. The PLAT domain is also identified to be essential for membrane association. However, studies indicate the PLAT domains in different LOXs isoforms may have differences in phospholipid preference upon membrane association.<sup>81,82</sup> The PLAT domain was previously thought to play a role only in membrane association, although recent evidence indicates this domain may play several roles in LOX function. Eek et al. have suggested a  $\pi$ -cation interaction between an invariant tryptophan on the PLAT domain, and a lysine or arginine in the catalytic domain.<sup>72</sup> This interaction would constitute a connecting site between the Ca<sup>2+</sup> binding loops and  $\alpha$ -helix 2, which is part of the external side of the active site. Currently, there is no structural evidence for a connection between the PLAT domain and substrate binding. However, a crystal structure of truncated 12S-LOX (lacking PLAT domain) revealed significant positional shifts in  $\alpha$ -helix 2 upon removal of the PLAT domain, implying that a physical restraint imposed by the domain may play a role in positioning  $\alpha$ -helix 2.<sup>83</sup> In addition, mutations involved in inter-domain interactions in rabbit 12/15-LOX resulted in a decrease in both catalytic activity and protein stability.<sup>84</sup>

## 5-Lipoxygenase

A significant amount of research has been focused on 5-LOX due to its role in LT biosynthesis. In this work preliminary steps in identifying 5-LOX protein and ligand interactions are completed. 5-LOX is primarily expressed in cells of myeloid origin such as neutrophils, eosinophils, MCs, basophils, and monocytes. To ensure the inflammatory response is appropriately matched to the cellular threat, cells have evolved a complex series of cellular and molecular controls to regulate 5-LOX enzymatic activity. Optimal activity of 5-LOX *in vivo* requires metal binding, translocation from the cytosol to the nuclear membrane, protein-complex formation with FLAP (a membrane scaffolding protein), and regulation by phosphorylation and additional allosteric regulators. 5-LOX is also regulated through autoinactivation.<sup>85</sup>

It is hypothesized that the non-turnover dependent autoinactivation mechanism is due to oxidative inactivation of the catalytic iron or loss of iron coordination. *In vitro* incubation of 5-LOX with reducing agents such as glutathione increases the enzymatic half-life of 5-LOX, indicating either reactive oxygen species or hydrogen peroxides could play a role in *in vivo* 5-LOX loss of activity. Autoinactivation of 5-LOX is believed to be important to organism health by limiting LT production. However, this native lack of structural stability creates obstacles during *in vitro* studies. The turnover rate for purified wild type (WT) 5-LOX decreases by approximately 50% when stored at 4 °C for 20 hours.<sup>86</sup> Common methods for improving protein stability have been tested, such as adjusting buffers to increase viscosity, addition of chelating or reducing reagents, and addition of co-factors or analogs. However, these methods did not increase the enzymatic half-life. To obtain a crystal structure of 5-LOX, a mutated version of 5-LOX had to be created with eight different site mutations. This mutated 5-LOX is called “Stable 5-LOX”. The

mutations increased the enzymatic half-life from approximately 7 hours to 16 hours at 37 °C, and increased the melting temperature for the enzyme by 3 °C.<sup>87</sup>

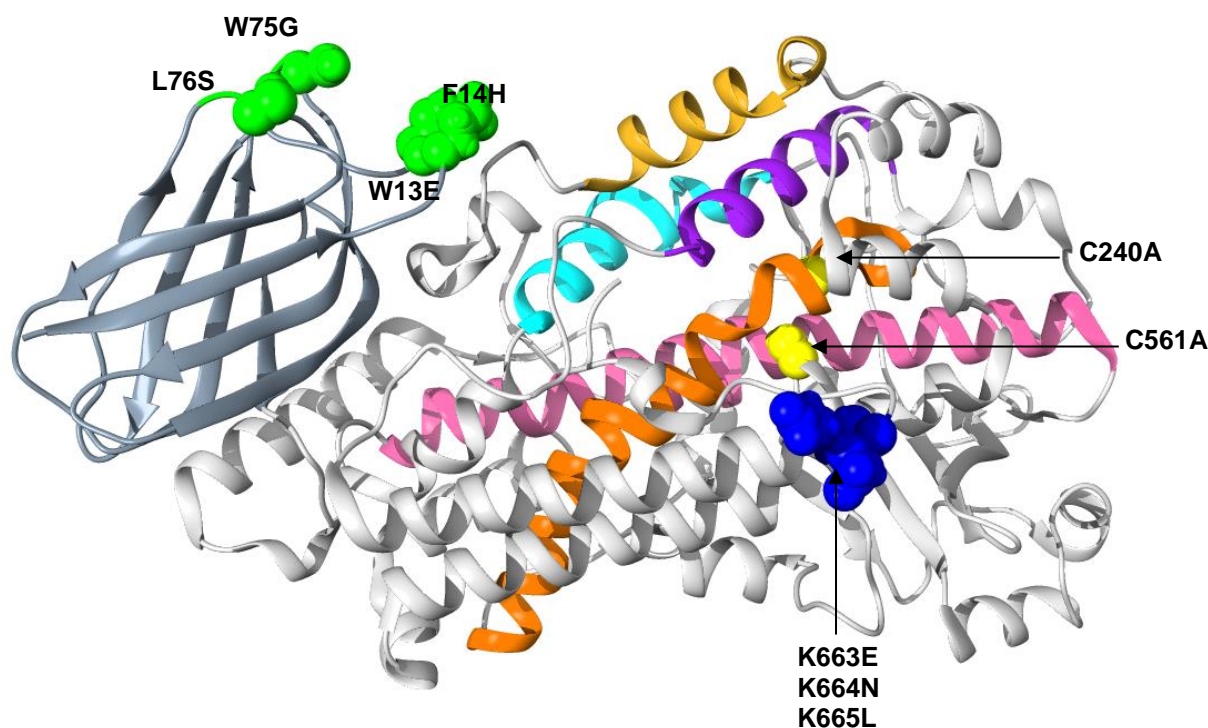


**Figure 6. Crystal structure of Stable 5-LOX.** The PLAT domain is dark gray while the catalytic domain is light gray. Site mutations are represented by spheres, with green representing membrane associating amino acids ( $\Delta$ 40-44GS, W13E, F14H, W75G, and L76S), yellow representing the cysteines (C240 and C561A), and blue the destabilizing sequence (K663E, K664N, K665L). Key helices are also labeled with  $\alpha$ -2 in tan,  $\alpha$ -7 in pink,  $\alpha$ -8 in purple,  $\alpha$ -14 in orange, and  $\alpha$ -16 in cyan.

#### *Structural analysis of Stable 5-LOX*

Stable 5-LOX is mutated in the proposed membrane-associating amino acids ( $\Delta$ 40-44GS, W13E, F14H, W75G, and L76S), and a pair of cysteines (C240A and C561A) that are able to form disulfide bonds are mutated to alanines. In addition, a triple lysine sequence (K663-K665) located on the turn before the terminal helix was mutated to ENL (E663-L665). The triple lysine sequence was identified as a “destabilizing sequence” as it projected K665 towards R651, resulting in

repulsion between side chains and creating structural strain on the terminal helix. The triple-K sequence was mutated to the motif found conserved to other LOX sequences (ENL).

The crystal structure of Stable 5-LOX at 2.4 angstrom resolution was determined in 2011.<sup>88</sup> There are several features of the structure that are conserved in other LOX crystal structures. The catalytic iron is coordinated by 3 histidines (H367, H372, and H550) and the carboxyl group on the C-terminus. The active site is structured by four main  $\alpha$ -helices ( $\alpha$ -helix 7,  $\alpha$ -helix 8,  $\alpha$ -helix 14, and  $\alpha$ -helix 16). Analysis of other mammalian LOX crystal structures revealed that these helices have similar positions and orientations in all LOXs.<sup>87</sup> The Stable 5-LOX structure differs significantly from the majority of other LOXs by the structure of its  $\alpha$ -helix 2. In most LOX crystal structures,  $\alpha$ -helix 2 consist of 6 to 7 turns where as in 5-LOX and 11R-LOX from *Gersemia fruticose*, the helix consists of 3 turns and two unstructured loops (Figure 7).<sup>72</sup> This configuration greatly limits accessibility to the active site. Specifically, the positions of F177 and Y181 on  $\alpha$ -helix 2 obstruct access to a hydrophobic channel in the active site. In other LOX structures this channel is open and allows substrate entry without structural changes. 5-LOX  $\alpha$ -helix 2 has no consequential differences when compared to the primary sequences of other LOXs with the exception of an alanine (A606 in 5-LOX and A612 in 11R-LOX) and its role in the different helix formation remains inconclusive. F177 and Y181 in 5-LOX are conserved in other LOX primary sequences, indicating that the blocking of the active site in 5-LOX and 11R-LOX is most likely due to  $\alpha$ -helix 2 distinctive bent shape and the positioning of the bulky side chains in these LOX isozymes.

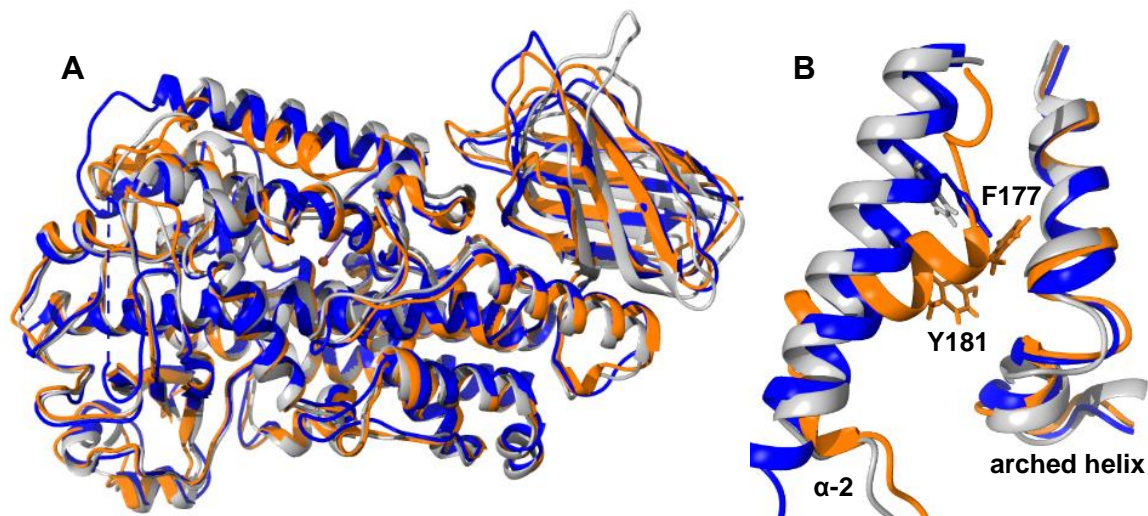


**Figure 7. Similarities of LOX crystal structures.** (A) Alignment of LOX structures with 5-LOX in orange, 8R-LOX in blue, and 15-LOX-2 in gray. (B) Differences in  $\alpha$ -2 between conserved helices seen in 8R-LOX and 15-LOX-2 and bent helix in 5-LOX.

The active site of 5-LOX is lined with conserved hydrophobic leucines (L368, L373, L414, and L607). These leucines are observed in all AA metabolizing LOXs. The closed cavity has a volume of  $663 \text{ \AA}^3$  which allows space for AA binding in several different orientations.<sup>87</sup> However, the structural changes required for substrate entry into the active site are inconclusive. Currently, there are two proposed routes. The first proposal is that the phenylalanine and tyrosine that block the channel are removed from the opening through local structure fluctuations that allow substrate entry. The second proposal is a rotamer shift in the side chain of W147 that allows AA to complete a “back-entry”. Both mechanisms would result in the substrate ending in the proper active site regio- and stereo- position. However, the latter model would require significantly fewer conformational changes.

The PLAT domain of Stable 5-LOX has the putative membrane associating amino acids mutated, therefore, limiting structural information on 5-LOX membrane association.  $\text{Ca}^{2+}$  is known to reversibly bind to the PLAT domain of 5-LOX with a  $K_d$  of  $6 \mu\text{M}$  and equilibrium

dialysis experiments indicate that two  $\text{Ca}^{2+}$  bind to a single enzyme molecule. The PLAT domain consists of a conserved set of eight  $\beta$ -strands forming a  $\beta$ -barrel-like structure. Structural analysis of 5-LOX upon membrane association is currently lacking, however, computational modeling predicts that W75 will insert approximately 9 Å into the membrane. Experiments measuring fluorescence energy transfer between tryptophans in the 5-LOX PLAT domain and 1,2-dioleoyl-sn-glycero-3-phosphoethanolamine-N-(1-pyreneslfonyl) in lipid vesicles indicate that 5-LOX forms a tighter association with the membrane as membrane fluidity increases and in the presence of zwitterionic phospholipids.<sup>89,90</sup> This corresponds to *in vivo* studies that demonstrate 5-LOX associates to the nuclear membrane, as phosphatidylcholine with AA esterified in the sn2-position is the predominant phospholipid in the nuclear membrane.

#### *Allosteric regulation of 5-LOX*

5-LOX enzymatic activity is allosterically regulated by selective phosphorylation and binding of adenosine triphosphate (ATP). ATP stimulation of 5-LOX activity was first observed when ATP that was added to crude cell lysates of peritoneal PMN leukocytes increased 5-LOX activity.<sup>91</sup> The allosteric mechanism for ATP modulation of 5-LOX does not involve ATP hydrolysis as it is also activated by ADP and AMP.<sup>91</sup> The ATP binding effect is only observed when  $\text{Ca}^{2+}$  is present, indicating the importance of membrane association in ATP allosteric regulation. The molecular mechanism of allosteric regulation by ATP is not elucidated despite the finding that bound ATP acts to stabilize 5-LOX.

5-LOX is also allosterically regulated by phosphorylation. 5-LOX has been reported to phosphorylate three different amino acids, S271, S523, and S663. Phosphorylation of 5-LOX was first identified in HL60 cells that were ionophore stimulated. When tyrosine kinase inhibitors were

added to cell cultures, 5-LOX did not translocate to the membrane efficiently and exhibited decreased leukotriene synthesis, demonstrating tyrosine kinase phosphorylated 5-LOX.<sup>92</sup> In addition, later experiments identified an inhibitor of mitogen-activated protein kinase-activated protein kinase (MAPKAP) that prevented 5-LOX translocation and limited leukotriene production in fMLP-challenged neutrophils.<sup>93</sup> MAPKAP is phosphorylated by p38 mitogen-activated protein kinase, which is activated by increased  $\text{Ca}^{2+}$  concentrations. This indicates that  $\text{Ca}^{2+}$  not only promotes 5-LOX activity via membrane association but also promotes 5-LOX phosphorylation by MAPKAP. Mutation of S217 to an alanine abolished MAPKAP phosphorylation of 5-LOX and reduced LT biosynthesis, demonstrating that MAPKAP phosphorylates S217.<sup>94</sup>

Another MAP kinase (MAPK1) phosphorylates 5-LOX *in vitro* on S663. This phosphorylation event increases leukotriene production in PMN leukocytes.<sup>95</sup> Phosphorylation at S523 by protein kinase A, unlike phosphorylation at S217 and S663, directly suppresses LT biosynthesis *in vitro* and *in vivo*. S523 phosphorylation also prevents 5-LOX translocation to the nuclear membrane.<sup>96</sup> It was previously known that cyclic adenosine monophosphate and exogenous adenosine inhibited 5-LOX catalytic activity.<sup>91</sup> These molecules activate protein kinase A providing a connection for their 5-LOX catalytic suppression.

The phosphorylation of 5-LOX at S663 was further investigated and provided surprising results. *In vitro* experiments showed an increase in HpETE products formed by 5-LOX upon phosphorylation by ERK2. However, this data is contradicted by *in vivo* experiments which showed a decrease in leukotriene production in cells with increased ERK2 expression. Stable-5-LOX was mutated at S663 to aspartic acid to mimic phosphorylation at this site. This mutated 5-LOX enabled connection of the two observations. S663D-Stable 5-LOX demonstrated robust 15-HpETE formation in place of 5-HpETE formation. In addition, discrete amounts of LXA<sub>4</sub> were

also detected. A crystal structure of the S663D mutant was determined with AA bound to the active site. Upon AA binding,  $\alpha$ -helix 2 and the arched helix that structure the exterior of the active site become displaced, resulting in the alignment with the open configuration observed in the crystal structure of human 15-LOX-2. The orientation of AA in the active site results in C-13 positioning over the catalytic iron for hydrogen abstraction. However, the carbon chain adopts an orientation that significantly differs from the orientation observed by the substrate mimic in the crystal structure of human 15-LOX-2.<sup>97</sup> Therefore, structural changes required for substrate entry and substrate binding orientation require further investigation. Current structural data of 5-LOX provides putative models for 5-LOX enzymatic and regulatory mechanisms, however, additional investigations on substrate binding and protein complex formations will assist in the full elucidation of these mechanisms.

### 15-Lipoxygenase

15-LOX has been observed to possess both pro- and anti-inflammatory properties. In mouse models, analogs of LXs, downstream products of 15-LOX oxygenation of AA, were tested to investigate the effect on PMN infiltration and vascular permeability. A LXA<sub>4</sub> analog was able to inhibit PMN migration and tissue biopsies, indicating that the LX analog was able to inhibit inflammation as efficiently as the LTB<sub>4</sub> receptor antagonist.<sup>98</sup> 15-LOX has also been implicated to propagate inflammation by increasing the formation of atherosclerotic plaques.<sup>99</sup> In addition, 15-LOX and 15-HpETE have an elevated presence in carotid lesions.<sup>100</sup> In mouse models of hyperlipidemia and in atherosclerosis-induced mammalian models, increased 15-LOX expression results in an increase in low density lipoprotein oxidation.<sup>101</sup> An increase in lipid oxidation results



in a release of pro-inflammatory mediators and promotes the transformation of macrophages to foam cells, an important step in the formation of atherosclerotic plaques.

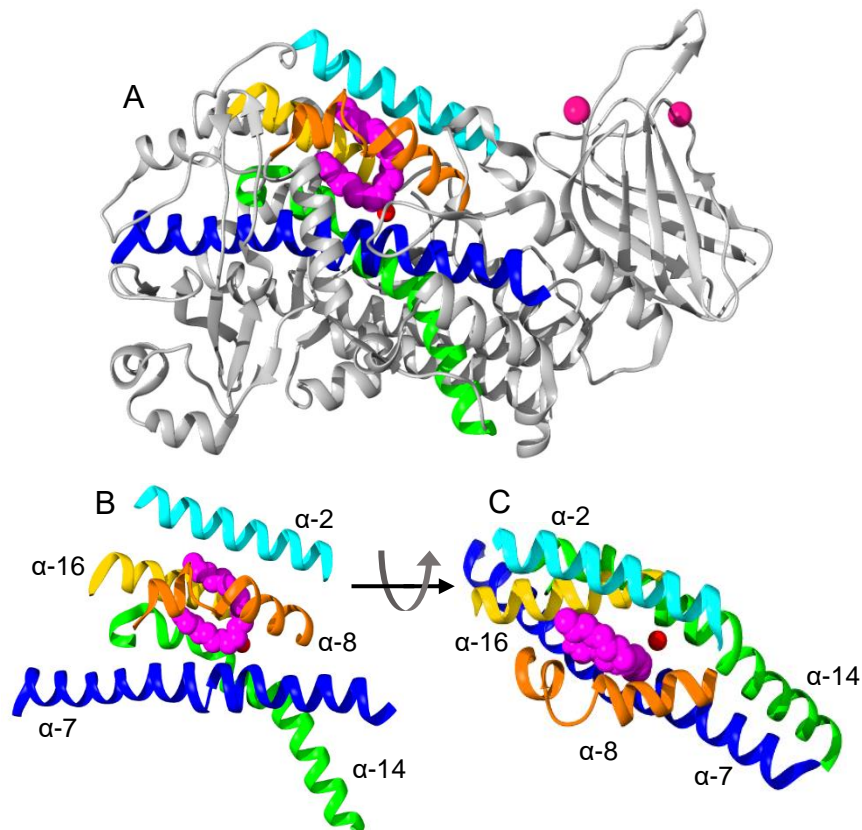


**Figure 8. Crystal structure of 15-LOX-2.** (A) Overall structure of 15-LOX-2 with  $\text{Ca}^{2+}$  bound to the PLAT domain and a substrate mimic, C8E4, bound to the active site. Conserved  $\alpha$ -helices that define the active site are highlighted by varying colors. (B)  $\alpha$ -helices involved in the active site are highlighted to clarify substrate binding. (C) Rotation of the active site, reveals an open channel that allows substrate to slide into the active site.

#### *15-LOX isoforms and their crystal structures*

In humans, two isoforms of 15-LOX are expressed, 15-LOX-1 and 15-LOX-2. The isoforms have a modest degree of sequence similarity (37%), and their substrate specificity and cellular distribution are significantly different.<sup>102</sup> 15-LOX-2 has the highest degree of similarity with 5-LOX (42%) and less than 38% similarity with other LOX that have been crystalized. 15-

LOX is primarily expressed in human (and rabbit) airway epithelial cells, eosinophils, reticulocytes, macrophages, and MCs.<sup>103</sup> Human 15-LOX-1 mainly synthesizes 15-HpETE with a small amount of 12-HpETE. Therefore, this 15-LOX isoform is also called 12/15-LOX.<sup>104</sup> Human 15-LOX-2 solely produces 15-HpETE when oxygenating AA.<sup>105</sup>

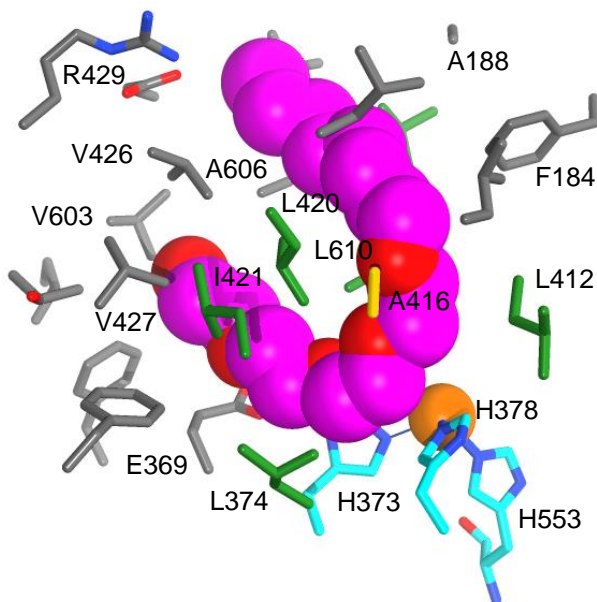


**Figure 9. 15-LOX-2 active site.** Amino acids that line the active site of 15-LOX-2 with C8E4 bound. Residues that define the active site shape are in gray with invariant leucines and isoleucines in green. A416, which is responsible for directing oxygen direction is in yellow and histidines that coordinate the catalytic iron are in blue.

The crystal structures of rabbit 15-LOX-1<sup>106</sup> and human 15-LOX-2<sup>107</sup> have been determined. The 2.4 Å crystal structure for rabbit 15-LOX-1 was the first mammalian LOX to be crystallized and the crystal structure had an aryl carboxylate inhibitor bound in the active site. This structure was the first to reveal the structural features that are now associated with mammalian LOXs. The 2.65 Å structure for human 15-LOX-2 was determined in 2014 by Dr. Marcia Newcomer's lab (Figure 8). The crystal structure displayed the typical LOX fold with an N-terminal PLAT domain and catalytic domain composed of  $\alpha$ -helices.<sup>107</sup> The catalytic iron is

positioned by the side chains of conserved histidines (H373, H378, and H553), the main chain carboxyl of the C-terminal (I676), and a water molecule. The core of the catalytic domain is composed of the same helices that are observed in other crystalized LOXs ( $\alpha$ -helix 7,  $\alpha$ -helix 8,  $\alpha$ -helix 14, and  $\alpha$ -helix 16).

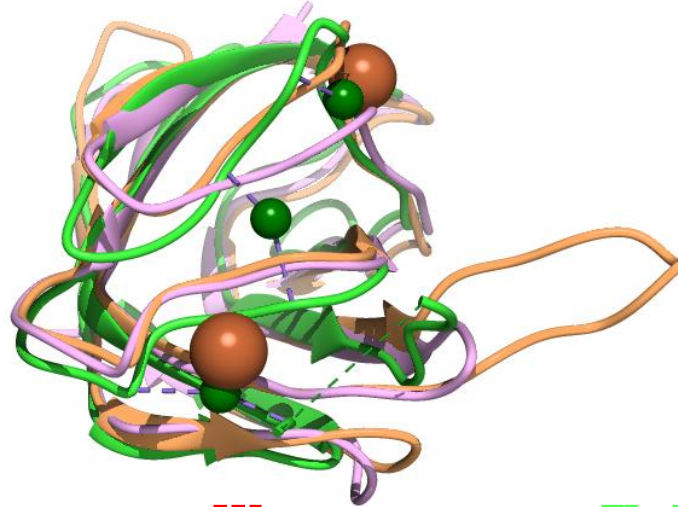
In the active site of the 15-LOX-2 crystal structure, electron density for a ligand was seen to be positioned above the catalytic iron. The most likely identity was a polyoxyethylene detergent, tetraethylene glycol monoethyl ether (C8E4), which was added to obtain diffraction-quality crystals. C8E4 is bound in a U-shaped conformation (Figure 9). Moreover, AA is superimposed over C8E4, carbon-13 is positioned above the catalytic iron for the hydrogen abstraction step in the catalytic mechanism. This suggest the orientation and conformation adopted by C8E4 reflects those of AA. In addition, C8E4 was identified as a competitive inhibitor for 15-LOX-2.<sup>107</sup>

As discussed previously,  $\alpha$ -helix 2 has two distinct conformations observed in LOX crystal structures. The  $\alpha$ -helix 2 in 15-LOX-2 is straight and consists of 6 turns. This allows an opening that would permit AA to slide into the active site through interactions with hydrophobic side chains (Figure 8). Several amino acids are conserved throughout LOX active sites. Conserved leucines and isoleucines are hypothesized to position the substrate in the U-conformation. In 15-LOX-2, these amino acids are L374, I412, L420, and L610 (Figure 9). In addition, several hydrophobic side chains are believed to grease the active site and allow hydrophobic interactions to stabilize the substrate. If AA is positioned to overlay with C8E4 in the active site, R429 would be able to stabilize the polar head group of AA. Another conserved amino acid is A416 in 15-LOX-2, which is observed in the active site of S-LOXs and has been shown to direct stereo-specificity of the molecular oxygen attack on AA (Figure 9).<sup>74</sup>

### *15-LOX-2 membrane association*

In intact mammalian cells, 15-LOX-2 translocates to the plasma membrane where it oxygenates AA to initiate eicosanoid synthesis. In addition, 15-LOX-2 is observed to oxygenate AA-bearing phospholipids without the need for a lipase or for re-esterification of the product.<sup>74</sup> Membrane association in 15-LOX-2 is Ca<sup>2+</sup> dependent and in intact cells is necessary for substrate acquisition. The PLAT domain of 15-LOX-2 has two apparent Ca<sup>2+</sup> binding sites. This differs from other reported structures (11R-LOX and 8R-LOX) which have three binding sites (Figure 10). In 15-LOX-2, Ca<sup>2+</sup> binding site 1 is located at a turn containing amino acids 39-44. The site is coordinated by D39 and E44 side chains and main chains from N39 and G42, and the fifth site is coordinated by a water molecule (Figure 10).

The second Ca<sup>2+</sup> binding site is stabilized by a hydrophobic loop between P74 and A86. This loop is projected approximately 20 Å from the PLAT domain (Figure 10). The loop's position is restrained by a crystal-packing contact, with the loop nestled into the active site entrance of an adjacent protein. This loop is composed of a unique sequence when compared to other human LOXs as seen by the sequence alignment in Figure 10. Other human LOXs are believed to associate to the membrane by conserved hydrophobic amino acids located on one face of the PLAT domain. The evolutionary need for an additional hydrophobic loop in 15-LOX-2 is currently not well understood. It is hypothesized that this loop may be stabilized in an extended position by Ca<sup>2+</sup> binding, which allows it to be buried into the membrane to serve as a hydrophobic anchor. *In vitro* assays with nanodiscs used as a membrane mimic indicated that when both Ca<sup>2+</sup> binding sites were mutated (D39A/E44A/D85A), 15-LOX-2 will not associate to the nanodiscs but does retain its enzymatic activity.<sup>107</sup>



15S-LOX-2	1	MAEFRVRVSTGEAF	GAGTWDKVS	SVSIVGTRGES	PPPLIDN	-	LGKEFTAGAEED	FQVTL	PE	
5S-LOX	1	MPSYTVTVATGSQW	FAGTDDYI	YLSLVGSAGC	SEKHLID	KPFYND	FERGAVDSY	DVTVD	E	
12S-LOX	1	MGRYRIRVATGAWL	ESGSYNRVQ	LWLVGTRGE	AELQLR	-	-	-	PARGEEEEFDH	VAE

15S-LOX-2	60	DVGRVLLLRVHK	APPVPL	LLGPIA	EDAWFCRWF	QLTTPRG	-	GHLLFPCYQ	WLEGAGT	LVL			
5S-LOX	61	ELGEIQLVRIE	KRKY	-----	WINDDWY	LKYITL	KTPHG	-	DYIEFPCYR	WITG			
12S-LOX	56	DLGLLQFVRL	RKH	HW	-----	LVD	AWFC	DRITV	QGGACAE	VAFPCYR	WVQGED	IL	SL

**Figure 10. Alignments of LOX PLAT domains.** PLAT domains of LOXs are aligned to show structural differences (green is 8R-LOX, purple is 11R-LOX, and tan is 15S-LOX). These alignments highlight amino acids involved in Ca<sup>2+</sup> binding. Site 1 is boxed in red, and site 2 in green. Amino acids that interact with Ca<sup>2+</sup> ions through side chains are in solid lines, while amino acids main chains that interact with Ca<sup>2+</sup> ions are in dashed lines. The hydrophobic loop that protrudes from the PLAT domain in 15-LOX-2 is boxed in blue.

Some LOXs are known to interact with preferred phospholipids upon membrane association. 15-LOX-1 primarily targets the plasma membrane in human DCs. In addition, *in vitro* membrane association studies utilizing lipid vesicles with AA that are composed of phosphatidylcholine (PC), phosphatidylinositol-4,5-bisphosphate (PI-4,5-BP) and PI-3,4-BP increased 15-LOX-1 activity relative to lipid vesicles containing solely zwitterionic phospholipids.<sup>108</sup> This result agrees with *in vitro* FRET studies that utilized small unilamellar vesicles (SUV) with varying phospholipid content to identify that 11R-LOX prefers association with vesicles containing phosphatidylethanolamine and anionic phospholipids.<sup>82</sup>

### *Allosteric regulation of 15-LOX*

LOXs can be allosterically regulated by their enzymatic products. This process was first identified in soybean LOX-1 and human 15-LOX-1. A synthetic fatty sulfate, oleyl sulfate, was found to increase the kinetic isotope effect in both enzymes and stopped-flow experiments further demonstrated that the allosteric binding site differed from the substrate binding site.<sup>109</sup> 15-LOX-2 has been extensively investigated for allosteric regulation by oxygenated fatty acids. These studies demonstrated an increase in the enzymatic turnover for AA metabolism from binding of 13(*S*)-hydroxy-9*Z*,11*E*-octadecadienoic acid (13-HODE). This allosteric effect was not repeated for AA oxygenated product 15-HpETE or 12-HpETE, indicating the allosteric site is specific. The site was also found to be pH dependent as increased pH correlated with increased allosteric effect. In addition, a deletion of the PLAT domain alters the degree of allostery but did not eliminate the allosteric effect, indicating that the allosteric ligand binding site is most likely on the catalytic domain.<sup>110</sup> As this literature review on 15-LOX-2 demonstrates further investigations of the structural dynamics involved with 15-LOX-2 enzymatic and allosteric mechanisms, in addition to membrane association are needed to fully understand how 15-LOX-2 functions.

### 5-Lipoxygenase Activating Protein (FLAP)

Generation of free AA by the hydrolysis of phospholipids by cPLA<sub>2</sub> is not sufficient to properly initiate the biosynthesis of LTs in intact cells. 5-LOX activity requires the expression of an integral membrane protein for the oxygenation of AA. This protein was identified by Merck-Frosst while testing newly developed therapeutics for inflammation.<sup>111</sup> Compounds MK-886 (from Merck) and Bay X1005 (from Bayer) are able to inhibit 5-HpETE synthesis without affecting the enzymatic activity of either 5-LOX or cPLA<sub>2</sub>.<sup>112,113</sup> The mechanism of these pharmaceuticals was

unidentified until a photoaffinity labeling analog of MK-886 and a MK-886 affinity gel was used to identify an 18 kDa integral membrane protein that was essential for the biosynthesis of LTs in intact cells.<sup>111</sup> The protein was called FLAP as it was hypothesized to initiate 5-LOX activity by acting as a scaffold protein. FLAP appears to have no catalytic activity and its role in LT biosynthesis is not fully understood, however, it is shown to directly bind AA.<sup>114</sup>

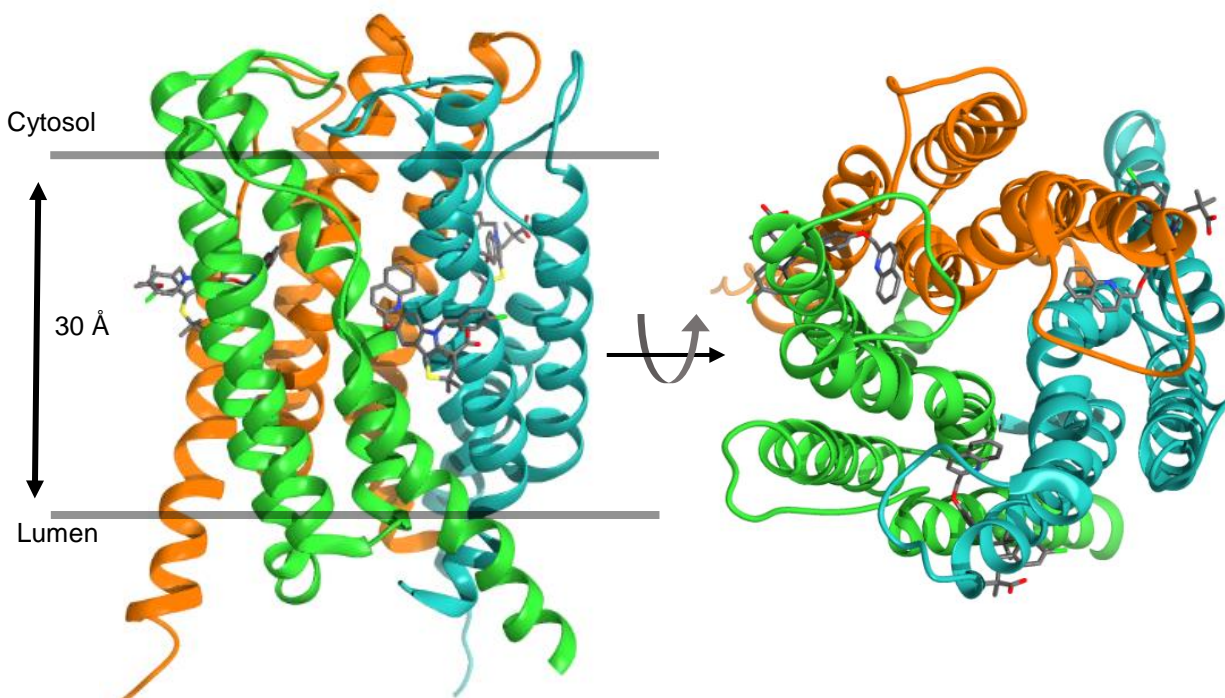


**Figure 11. The 4.0 resolution crystal structure of FLAP.** (A) The FLAP homotrimer with each monomer a unique color and the iodinated analog of MK-591 in gray. (B) Rotated (cytosolic) view of FLAP crystal structure. FLAP contains a large hydrophobic cavity accessible via an opening at the lumen/membrane interface.

Studies utilizing fluorescence lifetime imaging microscopy (FLIM) demonstrated 5-LOX translocates to the nuclear membrane to form a protein complex with FLAP in  $\text{Ca}^{2+}$  stimulated cells.<sup>115</sup> Direct interaction between 5-LOX and FLAP led to the current hypothesis for FLAP's role in LT biosynthesis. FLAP is proposed to be a membrane scaffolding protein that facilitates

the transfer of AA from the membrane to 5-LOX. This hypothesis is supported by the identification of FLAP as an AA binding protein through photoaffinity studies.<sup>114</sup> In addition, FLIM studies indicate that AA binding to FLAP alters the conformation of the protein to promote a tighter association between FLAP and 5-LOX.<sup>34</sup>

### *Structural analysis of FLAP*

FLAP is a member of the membrane-associated protein in eicosanoid and glutathione metabolism (MAPEG) superfamily. It is the only superfamily member that does not bind glutathione or have an identified enzymatic activity. Sequence alignment of superfamily members shows FLAP lacks the conserved amino acids that bind glutathione and are present in all other MAPEG members. A 4.0 Å crystal structure of FLAP was determined in 2007 with MK-591 bound, a LT biosynthesis inhibitor (Figure 11).<sup>116</sup> FLAP crystallized as a homotrimer with MK-591 bound in small openings located in the middle of the transmembrane (TM) helices. Each monomer of FLAP contains four TM helices with the N- and C-termini located on the luminal end and projected into the perinuclear space. The helices are connected by two elongated cytosolic loops (CL1 and CL2) and a shorter luminal loop (L1). The unstructured cytosolic surface loops connecting  $\alpha$ -helix 1 to  $\alpha$ -helix 2 (CL1) and  $\alpha$ -helix 3 to  $\alpha$ -helix 4 (CL2) in FLAP are highly conserved in different species, indicating a possible role in protein or ligand binding.

The orientation of FLAP helices and loops has a high degree of consistency with LTC<sub>4</sub>S, another member of the MAPEG family for which a structure has been determined.<sup>117</sup> LTC<sub>4</sub>S binds LTA<sub>4</sub> and glutathione to synthesize LTC<sub>4</sub>. When the structure of FLAP is compared to another family member, microsomal prostaglandin E1 Synthase (MPGES-1), there are significant differences in conformation and in the orientation of helices. The MPGES-1 structure contains a



small helical domain between  $\alpha$ -helix 1 and  $\alpha$ -helix 2 that contains the site for glutathione binding and the active site.<sup>118</sup> The structural differences between MPGES-1 and FLAP explain FLAP's lack of glutathione binding and enzymatic activity.

Surface maps of the FLAP homotrimer reveal a flattened cytosolic top and a pointed luminal base. Hydrophobic residues line the TM helices to form nonpolar contacts with the membrane and the cytosolic end contains positively and negatively charged residues. Several parts of the cytosolic end are charged and may be involved in interactions with 5-LOX. There are several inter-subunit contacts distributed throughout  $\alpha$ -helices 1, 2, and 4 in FLAP monomers. There is also an approximately 3200 Å<sup>3</sup> hydrophobic pocket in the center of the trimer. This pocket can be accessed by a 6 Å entrance opening to the lumen or laterally in through small openings between the TM helices. This central cavity extends to the middle of the trimer and is constricted by a bend in TM helix-2 due to P65 in FLAP. Proline induced distortions of  $\alpha$ -helices can act as a molecular hinge and are observed in TM proteins involved in signal transduction and solute transport.<sup>119</sup> Interestingly, while this pocket is mainly hydrophobic, the entrance and ending point are negatively charged.

The LT biosynthesis inhibitor MK-591 is bound to a small cavity found in the membrane spanning region between  $\alpha$ -helix 2 and  $\alpha$ -helix 4. This may help illuminate an AA transfer mechanism. One proposal is that AA may diffuse through the nuclear membrane after phospholipid hydrolysis, enter into the hydrophobic cavity of FLAP through the small opening between the helices and then eventually diffuse through the luminal cavity out of the membrane into the 5-LOX active site for oxygenation. Another model is based on the notion MK-591 can inhibit a FLAP conformational change that takes place upon AA binding, which allows the substrate to be transferred to the 5-LOX active site.

### *FLAP as a pharmaceutical target*

FLAP has received significant attention from pharmaceutical companies due to its essential role in LT biosynthesis and its limited involvement with other cellular pathways. The most prevalent drugs for regulating LT biosynthesis are three Cys-LT receptor antagonists: Zafirlukast, Pranlukast, and Montelukast. However, in addition to Cys-LTs, 5-HpETE and LTB<sub>4</sub> propagate inflammation making FLAP a promising alternative for regulating LT mediated inflammation.<sup>11,120</sup> The modest resolution of the FLAP crystal structure and inadequate information on the FLAP molecular mechanism of AA transfer prevents rational structure based drug design. The FLAP inhibitor MK-591 binds to FLAP with high affinity (IC<sub>50</sub> of 36 nM) *in vitro*, however, *in vivo*, low solubility and unspecific interactions of MK-591 leads to lower affinity and adverse reactions in the form of skin rashes. Similar limitations were observed for another FLAP inhibitor, MK-886.<sup>121</sup> However, no drugs have currently passed phase 1 clinical trials. Additional information on the mechanism of AA transfer from FLAP and 5-LOX association may be beneficial in the development of novel inhibitors.

### Hydrogen/deuterium exchange mass spectrometry

The elucidation of the function of a protein on a molecular level can be assisted by determining the three-dimensional structure of the protein. Commonly used techniques in structural biology are nuclear magnetic resonance (NMR) spectroscopy and X-ray crystallography.<sup>122</sup> Both methods provide vital information on protein-ligand interaction and protein-protein interactions. However, both are compromised by obstacles that limit their practical utility. X-ray crystallography requires collection of structural data using non-native solid-state samples and provide little insight into native protein motions. Crystal packing may also alter the

native conformational state. In addition, proteins with high intrinsic disorder will not readily form well-diffracting crystals. On the other hand structure determination by NMR spectroscopy can be completed at ambient temperatures in solution. This technique can also provide information on structural dynamics. However, this technique requires high concentrations of protein and is limited to smaller proteins (usually less than 150 amino acids).<sup>123</sup> Backbone amide hydrogen/deuterium (H/D) exchange mass spectrometry (MS) provides a complementary method to X-ray crystallography and NMR spectroscopy to investigate protein structure and conformational dynamics.

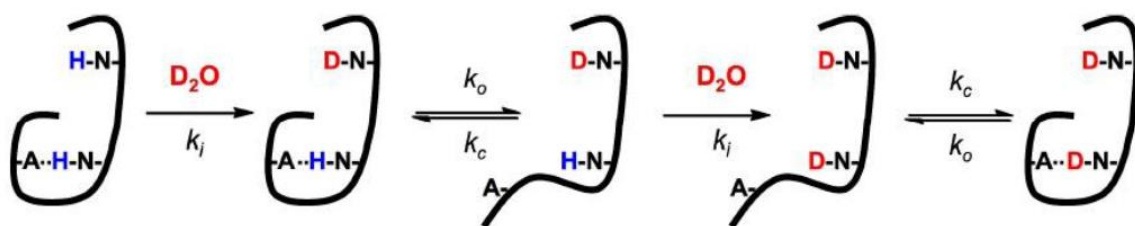


**Figure 12. The Linderstrøm-Lang model of H/D exchange.** Amide protons that are solvent exposed exchange with deuterons in the solvent within milliseconds. Amide protons that are buried within the protein or involved in hydrogen bonding exchange only when structural fluctuations ( $k_o$  and  $k_c$ ) allow solvent exposure, which may span any length of time between seconds and years. This allows analysis of observed exchange kinetics to provide insight into structural dynamics and protein conformations.

### *H/D exchange theory*

H/D exchange was first described in the 1950s by Kaj Ulrik Linderstrøm-Lang when the extent of deuterium incorporation on insulin solubilized in  $D_2O$  was calculated via density gradient ultracentrifugation.<sup>124</sup> The first experiment of H/D exchange MS was completed with horse cytochrome c incubated in  $D_2O$  at varying time points, then proteolyzed by pepsin, and analyzed using fast atom bombardment MS.<sup>125</sup> The advent of electrospray ionization (ESI) and matrix-

assisted laser desorption/ionization (MALDI) in the 1980s allowed H/D exchange analysis of intact proteins. Coupling of protein digest with liquid chromatography (LC) to separate generated peptides and ESI ionization to obtain H/D exchange data at a peptide resolution of a whole, intact protein was first completed with apo- and holo-myoglobin in 1994.<sup>126</sup>

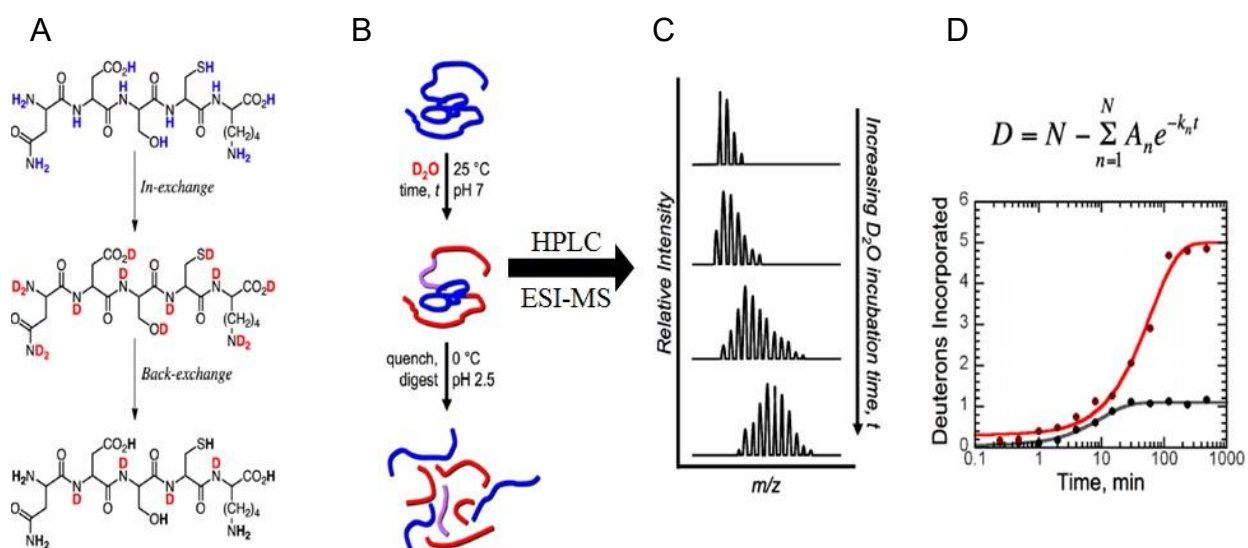


**Figure 13. H/D exchange-MS experimental method.** (A) “In-exchange” and “back-exchange” of deuterium during the D<sub>2</sub>O incubation and quenching steps of H/D exchange is depicted (B) The conditions used for D<sub>2</sub>O incubation and the quenching/ protein digestion steps in H/D exchange MS are shown. (C) Increases in m/z of isotopic envelopes are measured for each peptide to calculate the average mass. (D) Plotting the number of deuterons verse time for each peptide in different protein states allows for a comparison of exchange kinetics for individual peptides that reports on the final state of the intact protein.

Hydrogen exchange is both acid- and base-catalyzed. At physiological pH, which is used in the majority of H/D exchange studies involving intact proteins, the hydrogen exchange is primarily base-catalyzed. In a base-catalyzed hydrogen exchange, the hydrogen is abstracted from the amide nitrogen by a hydroxide ion and protonated by a solvent hydrogen. The intrinsic rate of

hydrogen exchange is effected by various conditions such as pH, adjacent amino acids, solvent exposure, and chemical interactions.<sup>127</sup> The rate of backbone amide hydrogen exchange is primarily dependent upon the rate of structure unfolding ( $k_o$ ) and refolding ( $k_c$ ), which is mediated by local structural dynamics that disrupt the hydrogen bonds and results in temporary solvent access (Figure 12).<sup>123</sup> Therefore, protein conformation and conformational changes between different states of a protein can be identified by measuring the rate of deuterium incorporation as a function of time.

#### *H/D exchange methodology*

H/D exchange occurs at ambient temperature and at a neutral pH, with continuous labeling being the most common analysis technique. In this method purified protein, in an aqueous buffer, is diluted with deuterated solvent and incubated at approximately 25 °C and neutral pH. The incubation time ranges from 15 seconds to hours or days. This is identified as the “in-exchange” process. The “in-exchange” is quenched by lowering the pH to 2.3 and the temperature to 0 °C by the addition of quenching buffer that has been cooled in an ice-bath (usually an acidic aqueous buffer). This quenching reduces hydrogen exchange of backbone amides by several magnitudes, but hydrogens on the amino acid’s side chain will “back-exchange” for hydrogen in the quenching buffer. Therefore, deuterium incorporated in H/D exchange experiments during the D<sub>2</sub>O incubation is trapped on the amides on the peptide backbone only (Figures 13A and 13B).

The sample is then digested by an acidic protease and analyzed by MS. Peptide resolution is achieved by coupling reverse-phase LC with ESI-MS in positive mode. The mass to charge ratio (m/z) for desired time points is analyzed for the individual peptides. Peptides are identified prior to H/D exchange experiments by tandem mass spectrometry (MS/MS). The number of deuterons

incorporated on the backbone is calculated for each time point using the centroid of the individual peptide isotopic envelope (Figure 13C). The number of deuterons incorporated into the peptide back-bone can be plotted as a function of time and fit to a sum of first-order exponential rate terms (Figure 13D). The determined kinetic rates are classified as fast, intermediate, and slow. This data can provide information on peptide solvent exposure, hydrogen bonding, or local structural fluctuations. Changes in the exchange rates between different protein states (e.g. apo protein verses ligand bound) indicate alterations in hydrogen bonding due to ligand interaction or conformational changes that alter solvent exposure.

#### Purpose of these studies

Historically, inflammation was considered to be most closely associated with pathogenesis in autoimmune and chronic inflammatory diseases. However, current research has shown increasing connections between inflammation and a variety of other diseases such as several cardiovascular diseases, forms of cancer, and even Alzheimer's disease.<sup>4</sup> An extraordinary effort has been dedicated to the studies of inflammatory mediating molecules and the enzymes that synthesize them. LOXs are known to play a role in the initiation and resolution of inflammation through signaling pathways associated with their enzymatic products.<sup>11</sup> While 70 years of LOX research has developed a strong knowledge base on the superfamily, ongoing investigations on LOX protein structure, biological functions, and cellular regulation will continue to extend our understanding of inflammation.

Of particular interest, the regulation of LOX activity has been identified as a key area for pharmaceutical development.<sup>2</sup> Historically, drug discovery frequently began with identification of a lead compound. In this approach, the lead compound is identified either by characterizing a

natural ligand of the protein or by completing *in vitro* assays involving screening of compounds from libraries. The lead compound is then systematically modified and tested for biological activity to extract structure-activity relationships between the protein and drug. Currently, high through-put screening leverages automation to assay the impact of a large number of drug-like compounds on a biological or biochemical activity associated with the target protein.<sup>128</sup> High through-put screening allows researchers to quickly test and detect possible protein-drug interactions. This approach is extensively used today.<sup>129</sup> However, high through-put methods are often limited by their cost and oversimplification of cell-drug interactions.

Another method for drug discovery is structure-based drug design, or rational drug design, which has been used since the late 1980s. This method begins by identifying a target protein involved in disease pathogenesis or critical cellular functions. The target protein undergoes structural analysis most commonly through crystallography or NMR methods. The protein binding site is revealed by analysis of the structural data combined with methods such as protein mutagenesis, binding assays, and reaction kinetic assays. Structural information regarding the protein-ligand complex is used to rationally modify the ligand to produce novel analogs that are more potent or specific for the protein active site.

Due to the limited number of pharmaceuticals on the market that target proteins involved in LT, and LX biosynthesis, further research focusing on the structural analysis of these proteins can be expected to provide essential information for the development of novel drugs through structure-based drug design techniques. While the available structures for human FLAP, 15-LOX-2, and Stable 5-LOX are indispensable, they provide only a static structural depiction of protein conformation.<sup>107,87,116</sup> In addition, technical difficulties involved in obtaining LOX or FLAP crystal structures limit the ease of obtaining structures that include bound substrates or inhibitors.

The aim of this dissertation is to elucidate the role of structural dynamics and conformations in the LOX catalytic and regulatory mechanisms. Backbone amide H/D exchange MS was employed as a route to complement the current structural information on these proteins.

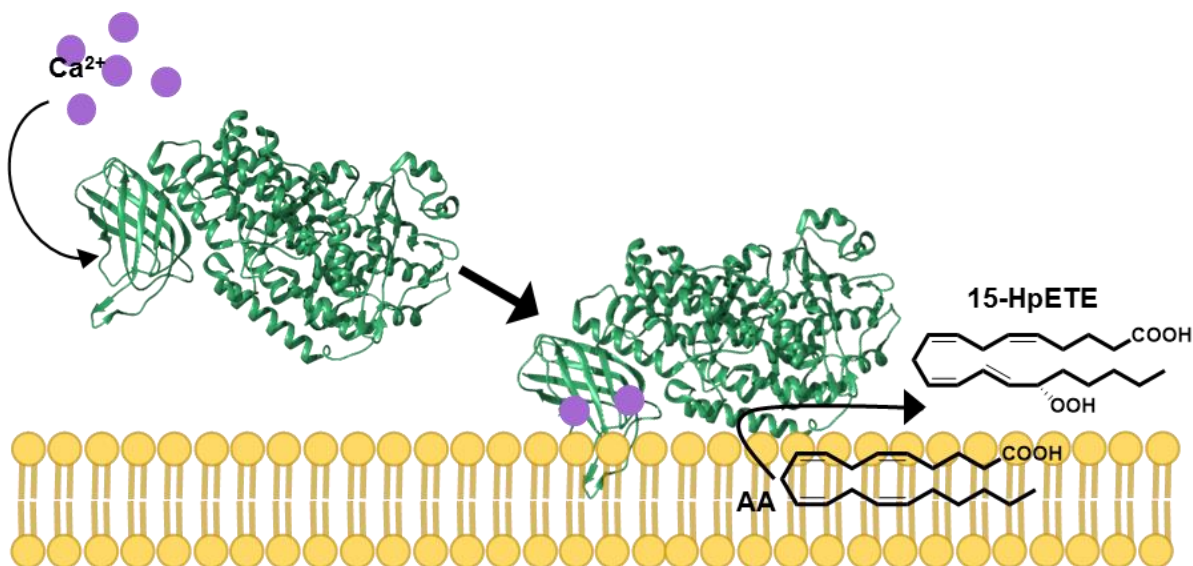


**Figure 14. 15-LOX-2 reaction in intact cells.**  $\text{Ca}^{2+}$  concentrations are increased in the cell in response to stress.  $\text{Ca}^{2+}$  ions bind to the PLAT domain of 15-LOX-2, resulting in a translocation from the cytosol to the membrane. 15-LOX-2 then binds its substrate, AA, and oxygenates it to form 15-HpETE. 15-HpETE is further metabolized by downstream enzymes to form LXs, which initiate the resolution of inflammation.

This study focuses on the 15-LOX-2 reaction mechanism in intact cells, in which 15-LOX-2 binds  $\text{Ca}^{2+}$  ions to the PLAT domain, promoting translocation to the cellular membrane for acquisition of substrate (Figure 14). The crystal structure suggests that changes in PLAT conformation may promote this translocation. However, the work presented in this dissertation suggests an alternative model in which binding of  $\text{Ca}^{2+}$  changes the electrostatic potential of the PLAT domain to promote interaction with the negatively charged head group of phosphatidylserine (PS). This work also supports the hypothesis of inter-domain communication playing a role in



LOX catalytic activity by identifying changes in structural dynamics in the PLAT domain upon AA binding in 15-LOX-2. The observed structural dynamics offer an explanation for 15-LOX-2 ability to oxygenate substrates with bulky head groups and also suggests a structural mechanism for 13-HODE positive allostery in 15-LOX-2. In the cases of 5-LOX and FLAP, our results provide a basis for future studies. However, experimental limitations prevented the ultimate goal of identifying the FLAP and 5-LOX interaction site. Nevertheless, the limited H/D exchange data obtained did provide interesting information on the effects of AA binding to the FLAP homotrimer.

## CHAPTER II

### MATERIALS AND METHODS

#### Materials

Buffer salts and common chemicals were purchased in high quality forms from commercial vendors. Fatty acids and their oxygenated derivatives including, AA, 15-HpETE, and 13-HODE, were purchased from Cayman Chemical Company, Ann Arbor, MI. Phospholipids, such as PS and PC, were purchased from Avanti Polar Lipids, Alabaster, AL. Competent cells used in transformations were obtained from Merck Millipore, Billerica, MA. PIP and Spingo-Strips were ordered from Thermo Fisher Scientific. 15-LOX-2 and MSP1e3d1 expression plasmids were generous gifts from Dr. Marcia Newcomer, Department of Biological Sciences, Louisiana State University.

#### Methods

##### *Expression of LOX*

The expression methods for 15-LOX-2 and 5-LOX were adapted from protocols developed by Dr. Marcia Newcomer's lab.<sup>107,87</sup> The Stable 5-LOX gene with N-terminal hexa-histidine tag was subcloned into pET-14b vector. 15-LOX-2 was subcloned into the pET-Duet-1 vector with a N-terminal hexa-histidine tag and co-expressed with *E. coli* YjgD protein. Rosetta-2(DE3) *E. coli* competent cells were transformed with the LOX expression vectors and grown in 5 mL of Luria-Bertani (LB) broth with the appropriate antibiotic (100 µg/mL of ampicillin for 5-LOX and 30 µg/mL kanamycin for 15-LOX-2) for approximately 14 hours. The LB cultures were then diluted (1:200 dilution for 15-LOX-2 and 1:100 dilution for 5-LOX) with Terrific Broth (TB)

supplemented with 0.4% glycerol and antibiotic (100 µg/mL of ampicillin for 5-LOX and 30 µg/mL of kanamycin for 15-LOX-2). The cells were grown in 2 L Erlenmeyer flasks at 37 °C. The cultures were incubated at 200 rpm until an OD<sub>600</sub> of between 1.0 and 1.2 was reached. The temperature was then dropped to 18 °C and the shaker decreased to 160 rpm for leaky protein expression. The cultures were grown between 18-24 hours. The cells were harvested by centrifugation at 6500 x g and 4 °C for 10 minutes. The resulting cell pellets were stored at -80 °C until they were used in later experiments.

### *Purification of 5-LOX*

Frozen cell pellets were resuspended in Bugbuster 10x protein extraction reagent (Novagen) with 2 mL of solution per 1 gram of cell pellet. In addition, 60 µg/mL of lysozyme, and 2 Complete Mini Protease Cocktail Inhibitor tablets (Sigma Aldrich) were added to the resuspension solution. Resuspended cells were stirred at 4 °C for approximately 30 minutes to promote cell lysis. Cells were further lysed by sonication on ice with 1 second pulses (50% power, 60% duty cycle, and 2 min on, 3 min off). Cellular debris was cleared by centrifugation at 30,000 x g for 30 minutes at 4 °C. The cleared lysate was incubated with 10 mL of Ni<sup>2+</sup>-NTA agarose resin (approximately 5 mL per 25 g of cell pellet) that was pre-equilibrated with 10 x resin volume of column buffer (20 mM Tris, 500 mM NaCl, 20 mM imidazole, pH 7.6). The resin-lysate slurry was then applied to a gravity column and washed with column buffer containing 35 mM imidazole to elute impurities. 5-LOX was eluted with column buffer containing 200 mM imidazole and then concentrated to 2 mL using Amicon centrifugal filters (MilliporeSigma) with a molecular weight cut off (MWCO) of 30 kDa. Concentrated 5-LOX was dialyzed using Slide-A-Lyzer dialysis cassettes (Thermo Fisher Scientific) against 500 mL of sample buffer (20 mM Tris, 150 mM KCl,

5 mM TCEP, pH 7.5). 5-LOX was then applied to a HiLoad 16/60 Superdex 200 pg column with bed dimensions of 16 x 600 mm, equilibrated with sample buffer. Fractions (3 mL) were collected as the column was eluted with sample buffer. Fractions were analyzed for protein identification and extent of purification by SDS-PAGE and western blotting techniques. 5-LOX eluted from the column between 70-80 mL. Fractions containing isolated 5-LOX were concentrated using Amicon centrifugal filters. The protein was either tested for enzymatic activity or frozen at -20 °C for further use. Enzymatic activity of 5-LOX was monitored after thawing of the protein and before all H/D exchange experiments.

#### *Purification of 15-LOX-2*

Cell pellets with overexpressed 15-LOX-2 were lysed in B-PER Bacterial Protein Extraction buffer (Thermo Fisher Scientific) (2 mL solution per 1 gram cell pellet). The buffer was supplemented with 200 µL of DNase 1 (Sigma Aldrich) and 10 µL per 1 mL lysis solution of Problock 2D protease inhibitor cocktail (Gold Biotechnology). Cells were lysed by stirring in extraction buffer for approximately 30 minutes at 4 °C followed by probe sonication (1 second pulse, 2 minutes on, 3 minutes off) on ice, until no longer viscous. Cellular debris was cleared by centrifugation (approximately 17,500 x g) for 30 minutes at 4 °C. Imidazole was added to the supernatant to a final concentration of 10 mM. Supernatant was incubated for 30 minutes at 4 °C with approximately 10 mL of Co<sup>2+</sup>-NTA resin (Thermo Fisher Scientific) equilibrated with column buffer (50 mM Tris, 500 mM KCl, 10 mM imidazole, pH 8.0). Resin was applied to a gravity column and washed with column buffer containing 20 mM imidazole (10 x resin volume). 15-LOX-2 was eluted with column buffer containing 200 mM imidazole (3 x resin volume) and then concentrated to approximately 2 mL using Amicon centrifugal filters with a MWCO of 30 kDa.

15-LOX-2 was then applied to a HiLoad 16/60 Superdex 200 pg column with bed dimensions of 16 x 600 mm equilibrated with sample buffer. Fractions (3 mL) were collected as the column was eluted with sample buffer. Fractions were analyzed for protein identification and extent of purification by SDS-PAGE and western blotting techniques. 15-LOX-2 eluted from the column between 70-80 mL. Fractions containing isolated 15-LOX-2 were concentrated using Amicon centrifugal filter with MWCO of 30 kDa. The protein was either tested for enzymatic activity or frozen at -20 °C for further use. Enzymatic activity of 15-LOX-2 was monitored after thawing of the protein and before all H/D exchange experiments.

#### *Expression of 5-lipoxygenase activating protein*

The human FLAP gene with a C-terminal hexa-histidine tag was subcloned into a pET-21b vector. C43(DE3) competent cells (Lucigen) were transformed with the expression vector and grown in 7 mL of LB media between 14-18 hours. The small cultures were diluted 200-fold with minimal media (20 mM Na<sub>2</sub>HPO<sub>4</sub>, 20 mM KHPO<sub>4</sub>, 90 mM NaCl, 200 mM NH<sub>4</sub>Cl, 130 μM CaCl<sub>2</sub>, 1 mM MgSO<sub>4</sub>, 0.4% glucose, 0.3% casamino acids) and grown at 37 °C and 250 rpm until an OD<sub>600</sub> of 0.4 was reached. FLAP expression was induced by the addition of isopropyl β-D-1-thiogalactopyranoside (IPTG) to a final concentration of 1 mM. The cells were cultured further at 18 °C and 200 rpm for 20 to 24 hours. Cells were harvested by centrifugation at 6,500 x g for 10 minutes at 4 °C and stored at -80 °C.

#### *Purification of 5-lipoxygenase activating protein*

Frozen cell pellets were resuspended in cold lysis buffer (50 mM KH<sub>2</sub>PO<sub>4</sub>, 300 mM KCl, 1 mM DTT, 1 MM EDTA, 10% glycerol, pH 8.0). Lysozyme was added at 0.2 mg per mL of lysis

buffer and stirred for 2 hours at 4 °C. Cells were lysed further by sonication (60% power, 50% duty cycle, 2 minutes on, 3 minutes off, 1 second pulses) on ice, until no longer viscous. Cellular debris was removed by centrifugation at 10,000 x *g* at 4 °C for 30 minutes. Then the membrane fraction was collected from the supernatant using ultracentrifugation at 100,000 x *g* for 2 hours and 4 °C. The membrane pellets were washed with 50 mM Tris, pH 8.0 and resuspended in cold extraction buffer (50 mM KH<sub>2</sub>PO<sub>4</sub>, 300 mM KCl, 10% glycerol, 10 mM imidazole, 0.5% dodecyl- $\beta$ -maltoside (DDM), pH 8.0). The membrane pellet was solubilized by stirring at 4 °C for approximately 18 hours. The membrane extract was then added to 10 mL of Ni<sup>2+</sup>-NTA agarose resin that was pre-equilibrated with 10 x resin volume of the extraction buffer. The membrane extract and resin were incubated for 1 hour at 4 °C with gentle mixing. Resin was applied to a gravity column and washed with the extraction buffer containing 35 mM imidazole. FLAP was eluted from the resin with 3 x resin volume of 50 mM KH<sub>2</sub>PO<sub>4</sub>, 300 mM KCL, 10 glycerol, 0.2% DDM, 200 mM imidazole, pH 8.0. FLAP was concentrated to approximately 2 mL using Amicon centrifugal filters with a MWCO of 10 kDa and dialyzed in sample buffer (20 mM Tris, 300 mM KCl, 2.5% glycerol, 1 mM DDT, 0.1% DDM, pH 7.5). FLAP was applied to a HiLoad 16/60 Superdex 200 pg column (GE Healthcare) equilibrated with sample buffer. The 2 mL fractions were tested for protein identity and purification extent by SDS-PAGE and western blotting. Protein eluted from the column, using the sample buffer, between 40-50 mL. Fractions containing FLAP were concentrated using Amicon centrifugal filters (MWCO of 10 kDa). The protein was frozen at -20 °C for further use. Solubility trials using DDM (from 0.01% to 0.2% w/v) and 3-((3-cholamidopropyl) dimethylammonio)-1-propanesulfonate (CHAPS) (from 0.5-1% w/v) were completed to determine buffer conditions that prevented protein aggregation.

### *LOX Activity Assay*

The oxygenation of AA by LOXs can be monitored by measuring the increase in absorbance at 238 nm, which arises from the conjugated double bonds found in the LOX reaction product HpETE. Stable 5-LOX and 15-LOX-2 enzymatic activities were assayed by measuring the product formation with a Perkin Elmer Lambda 45 UV/VIS Spectrometer at 25 °C. Enzymes were incubated at 25 °C in 20 mM Tris, 150 mM KCl, pH 7.8 (in addition to 5 mM TCEP for Stable 5-LOX). Assays were performed in activity assay buffer (20 mM Tris, 150 mM KCl, 0.5 mM CaCl<sub>2</sub>, pH 7.8). LOXs were added to activity assay buffer to a final concentration between 0.5 μM and 1 μM. The reaction was initiated by the addition of AA between 80 μM-160 μM (from 28 mM AA in 100% ethanol stock solution) at 25 °C. The assay components were added so that the total assay volume was 1 mL in a quartz cuvette. Absorbance at 238 nm was recorded. Non-enzymatic oxygenation of AA was also measured under the same conditions to ensure increases in absorbance were produced from LOX enzymatic activity. Specific activity was calculated using the following equations, where  $\epsilon$  is the molar absorptivity (27,000 L·mol<sup>-1</sup>·cm<sup>-1</sup> for HpETE),  $b$  is the path length (1 cm), and  $c$  is the concentration of HpETE.

$$\text{Equation 1.} \quad \text{Absorbance}_{(\text{at } 238 \text{ nm})} = \epsilon \cdot b \cdot c$$

$$\text{Equation 2.} \quad \text{Specific Activity} = \frac{\text{mg of product}}{\mu\text{mol of enzyme} \cdot \text{minutes}}$$

The specific activity for 15-LOX-2 was similar to the published activity, however, the specific activity for 5-LOX was significantly less than reported.<sup>107,88</sup> One experimental attempt to increase 5-LOX specific activity consisted of adding oxygenated product to the assay, as these lipids have been shown to increase 5-LOX activity by oxidizing the catalytic iron in previous

studies.<sup>130</sup> In this experiment either 10  $\mu\text{M}$  of 13-HpODE or 10  $\mu\text{M}$  of 15-HpETE was added to the activity assay (5  $\mu\text{L}$  of 2 mM stock solution in 100% ethanol). The assay had a total volume of 1 mL and used 1  $\mu\text{M}$  of Stable 5-LOX. 13-HODE or 15-HpETE was added to the protein approximately 5 minutes before the reaction initiation. The reaction was initiated by the addition of 160  $\mu\text{M}$  of AA (as previously described). The absorbance at 238 nm was monitored for 4 minutes at 25 °C.

#### *LOX Product Assay*

To identify the regio-specific HpETE being synthesized by 15-LOX-2 and 5-LOX, the products were extracted from the activity assays previously described. The activity assay was quenched after approximately 10 minutes by acidifying the reaction buffer to pH 4.0 with 5  $\mu\text{L}$  of 6N HCl. Then 1 x reaction volume of dichloromethane was added to the assay and the mixture was shaken vigorously. The organic and aqueous phases were allowed time to fully separate and the lower organic layer was extracted. The organic layer was washed with 1 mL of water twice to remove remaining acid, salts, and enzyme. A stream of nitrogen was used to evaporate the dichloromethane and the remaining product was dissolved in a small volume of 1:1 methanol/water. Reverse-phase HPLC was performed on the products using a Varian ProStar HPLC system with a Kinetex 5 $\mu$  C18 100A column (30 x 2.1 mm) (Phenomenex) using a mobile phase of acetonitrile/water/formic acid (70:30:0.4, v/v/v) at a flow rate of 0.5 mL/min. Elution times of the products were observed by monitoring the absorbance at 238 nm and then were compared to elution times determined for a HETE standard mixture containing 15-, 12-, 11-, 9-, and 5-HETE.



### *Expression and Purification of Membrane Scaffolding Protein 1E3D1*

The membrane scaffolding protein (MSP) 1E3D1 gene in a pET-28 vector was provided by Dr. Marcia Newcomer's lab. pMSP1E3D1 was transformed into Rosetta 2 (DE3) competent cells and grown in 5 mL LB cultures for 14-18 hours. The small cultures were added to 1 L of TB with 30 µg/mL kanamycin. MSP1E3D1 protein expression was induced with 1 mM IPTG when OD<sub>600</sub> of 1.0 was reached. The cells were grown for an additional 4 hours at 37 °C. Cells were harvested by centrifugation at 6,500 rpm for 10 minutes and frozen at -80 °C.

Frozen cell pellets were resuspended in lysis buffer with 5 mL per 1 gram cell pellet (50 mM Tris, 300 mM NaCl, 1% Triton X-100, pH 8.0) supplemented with 2 Complete Mini Protease Cocktail Inhibitor tablets and 200 µL of 10 mg/mL DNaseI. Lysozyme (0.2 mg/mL) was added to the cell lysate and stirred at 4 °C for 1.5 hours. The cells were further lysed by sonication (60% power, 50% duty cycles, 1 sec pulses, 2 min on, 3 min off) on ice. Cellular debris was cleared from the lysate by centrifugation at 10,000 x g for 30 minutes and the resulting supernatant was applied to 15 mL of Ni<sup>2+</sup>-NTA agarose resin that was equilibrated with 50 mM Tris, 300 mM NaCl, pH 8.0. Resin was applied to a gravity column and washed with 10 x resin volume of equilibration buffer. Resin was further washed with 10 x resin volume of equilibration buffer containing 50 mM imidazole. MSP1E3D1 was eluted from the resin with 5 x resin volume of equilibration buffer with 250 mM imidazole. MSP1E3D1 was concentrated to approximately 10 mL using Amicon centrifugal filters with MWCO of 10 kDa and dialyzed against 1 L of nanodisc buffer (20 mM Tris, 150 mM KCl, pH 8.0).

### *Nanodiscs Preparation*

Nanodiscs formation was initiated by the addition of 100 mM cholate to MSP1E3D1 stock (at 6.5 mg/mL) in nanodisc buffer. A 3:1 powder mixture phosphatidylcholine (PC) and phosphatidylserine (PS) was added to the solution at a 160:1 lipid:MSP1E3D1 molar ratio. The solution was shaken for 1 hour at 4 °C until all phospholipids and cholate were solubilized. Nanodiscs buffer was added until cholate concentration was lowered to 25 mM. To remove the cholate nanodisc buffer-washed Biobeads (Bio-Rad) were then added to a 0.1 g/mL, and the solution was shaken for 1 hour at 4 °C. The mixture was shaken at 4 °C for 2 hours, followed by addition of more (0.2 g/mL) Biobeads. The shaking of the mixture continued at 4 °C for another 4 hours and yet another 0.2 g/mL of Biobeads were added. The mixture was shaken at 4 °C for an additional 4 hours and then filtered to remove Biobeads. The spontaneous formation of nanodiscs was verified by SECC using a Superose-12 column connected to UV-detector monitoring at 280 nm. The column was eluted with nanodisc buffer containing 0.5 mM CaCl<sub>2</sub>. Fractions (1 mL) were collected and analyzed by SDS-PAGE, and subsequent western-blotting.

The complex of 15-LOX-2 associated with nanodiscs was prepared by, first, estimating the nanodisc concentration by measuring the band volumes of MSP1E3D1 from the nanodiscs sample and MSP1E3D1 stock standards on an SDS-PAGE gel. 15-LOX-2 concentration was determined by UV-vis absorbance at 280 nm. 15-LOX-2 that had been dialyzed in nanodisc buffer was added to nanodisc stock and association was promoted by the addition of 0.5 mM CaCl<sub>2</sub>. Different ratios of 15-LOX-2 molecules and nanodiscs were tested with 4 nanodiscs for each 15-LOX-2 molecule used in the majority of nanodiscs studies in this work. 15-LOX-2 was incubated with nanodiscs in 20 mM Tris, 150 mM NaCl, and 0.5 mM CaCl<sub>2</sub> for 1 hour at 4 °C and then concentrated to 0.5 mL using Amicon centrifugal filters with a MWCO of 30 kDa. 15-LOX-2 association was confirmed

by SEC using Superose-12 column (GE Healthcare) that was equilibrated with nanodisc buffer. Fractions (1 mL) collected from the observed peaks were analyzed with SDS-PAGE gels and western blots to confirm that 15-LOX-2 was associated with the nanodiscs.

### *PIP and SphingoStrips*

PIP and Sphingo Strips were used to identify the phospholipid that 15-LOX-2 prefers for membrane association. The strips were used according to the manufacturer's instructions. Briefly, the membranes were blocked with 3% bovine-serum albumin (BSA) in TBS-T buffer (20 mM Tris-HCl, 150 mM NaCl, 0.1% Tween-20, pH 8.0) and gently rocked for 1 hour at approximately 25 °C. Then the membranes were incubated with 1 µg/mL of 15-LOX-2 in TBS-T buffer with 3% BSA and 0.5 mM CaCl<sub>2</sub> for 2 hours at approximately 25 °C. The membranes were rinsed thoroughly three times by gently rocking in TBS-T buffer for 10 minutes, followed by incubation with a monoclonal mouse anti-penta-histidine antibody (1:3000 dilution) in TBS-T buffer containing 3% BSA for 2 hours. The membranes were rinsed four times with TBS-T as described before and incubated with an AP-conjugated anti-mouse secondary antibody (1:10,000 dilution) in TBS-T buffer containing 3% BSA for 2 hours. The membranes were washed four times with TBS-T buffer by gentle rocking for 10 minutes. Protein binding was visualized by incubating the strips in alkaline phosphatase staining solution for approximately 20 minutes.

### *Peptide Mapping by MS/MS*

Prior to H/D exchange MS analyses, all of the proteins analyzed in this work (5-LOX, 15-LOX, and FLAP) were peptide mapped by LC-MS/MS. The proteins were brought to a concentration of 5 µM (5 µL from 50 µM protein stock solution) in cold H<sub>2</sub>O to a final volume of

50  $\mu$ L. Then 50  $\mu$ L of quenching buffer was added to the sample. For Stable 5-LOX and 15-LOX-2 the quenching buffer was 100 mM  $\text{KH}_2\text{PO}_4$ , 10 mM TCEP, pH 2.4 and for FLAP the quenching buffer was 100 mM  $\text{KH}_2\text{PO}_4$ , 10 mM TCEP, 4 M urea, pH 2.4. Protein digestion was initiated with the addition of an acidic protease. Digestion was performed on ice, with pepsin in  $\text{H}_2\text{O}$  providing the highest sequence coverage for all proteins. 15-LOX-2 optimal digestion was completed by addition of 2  $\mu$ L of 20 mg/mL of pepsin (final sample concentration of 0.4 mg/mL) and incubating for 7 minutes. FLAP digestion underwent digestion trials and optimal digestion was found when 2  $\mu$ L of 10 mg/mL pepsin (final sample concentration of 0.2 mg/mL) was added and incubated for 7 minutes. 5-LOX optimal digestion was performed with 2  $\mu$ L of 10 mg/mL pepsin (final sample concentration of 0.2 mg/mL) and a 9 minute digestion time. The resulting peptides were separated by reverse-phase HPLC utilizing an Aeris PEPTIDE 3.6  $\mu$  XB-C18 column (50 x 2.6 mm, Phenomenex) on ice and connected to ThermoFinnigan LTQ Linear Ion Trap with an ESI ionization source set in positive mode. Peptides were eluted with a flow rate of 0.1 mL/min with a 30 minute gradient (5-50% acetonitrile/ $\text{H}_2\text{O}$  containing 0.4% formic acid for 15-LOX-2 and 5-LOX and 5-75% acetonitrile/ $\text{H}_2\text{O}$  containing 0.4% formic acid for FLAP). A column washing step was added after each sample (95% acetonitrile/ $\text{H}_2\text{O}$  with 0.4% formic acid at 0.1 mL/min for 10 minutes). An additional washing step was added to samples containing detergents, phospholipids, or fatty acids (50:40:10 propan-2-ol/acetonitrile/ $\text{H}_2\text{O}$  containing 0.4% formic acid at 0.1 mL/min for 10 minutes). Scans of  $m/z$  from 300 to 2000 were utilized for peptide detection.

Peptides were sequenced by data-dependent tandem MS/MS by CID. Collision voltage was set to 15V, 25V, and 35V. The putative identity of each peptide was determined by the computation program PEAKS Client 6 (Bioinformatics Solutions Inc.). This program determines the identity

of the peptide from the experimental parent mass and the raw fragmentation data. PEAKS creates theoretical peptide fragmentation patterns based on the type of protease used, the FASTA sequence for the protein, MS instrument used, and the parameters for MS. Experimental fragmentation is matched with the theoretical fragmentation and a false discovery rate (FDR) is calculated for the match. The FDR is calculated using matches for decoy sequences and is reported as a  $-10\log(p)$  value, where  $p$  is the probability of a false identification. All peptides with a  $-10\log(p)$  value greater than 20 (equal to a  $p$  value of 0.01) were selected and further verified. MassXpert MS analysis software presents all possible peptides in the protein with the same parent mass as the experimental parent mass. Then the theoretical fragmentation of the peptide is generated by ProteinProspector program MS-product and compared to the experimental data. Verified peptides are combined to create the peptide coverage map.

#### *Sample Preparation of 15-LOX-2 for H/D Exchange Ligand Binding Experiments*

Several kinetic analyses of backbone amide H/D exchange were performed on 15-LOX-2. All samples contained 5  $\mu$ L of 50  $\mu$ M 15-LOX-2 in sample buffer (20 mM Tris, 150 mM KCl, pH 7.8) or sample buffer supplemented with ligands and metals. The metals and ligands were added to the sample through the following methods. Purified 15-LOX-2 in sample buffer is called native 15-LOX-2. In this state, the 15-LOX-2 catalytic iron is coordinated in the active site, but  $\text{Ca}^{2+}$  is removed by chelation with 5 mM EGTA or EDTA. Samples with EGTA or EDTA were dialyzed in sample buffer containing 5 mM of the chelating agent at 4 °C for 20-28 hours. Samples containing  $\text{Ca}^{2+}$  had 0.5 mM  $\text{CaCl}_2$  (2  $\mu$ L of 12.5 mM  $\text{CaCl}_2$  in  $\text{H}_2\text{O}$ ) added to the protein stock 2 minutes before  $\text{D}_2\text{O}$  incubation in H/D exchange experiments. 13-HODE, 15-HpETE, and AA were added from 100% ethanol to the protein stock 30 seconds before  $\text{D}_2\text{O}$  incubation.

Complication of data interpretation due to ethanol affecting 15-LOX-2 structure was avoided by varying the concentrations of the ligand stock solutions so only 1  $\mu\text{L}$  of ligand was added to the samples to achieve the desired concentrations. The sample concentrations of ligands tested ranged from 10  $\mu\text{M}$  to 500  $\mu\text{M}$ .

#### *Sample Preparation of 15-LOX-2 for H/D Exchange Membrane Association Experiments*

For analyzing 15-LOX-2 membrane association four different conditions were tested. Native 15-LOX-2 and  $\text{Ca}^{2+}$  bound 15-LOX-2 samples for H/D exchange were prepared as previously described. 15-LOX-2 that was associated to nanodiscs or DDM (at concentrations ranging from 0.02% to 0.2%) in the presence of 0.5 mM  $\text{CaCl}_2$  was also tested. 15-LOX-2 associated to nanodiscs was prepared as described in the Nanodiscs Preparation section. 15-LOX-2 associated with DDM micelles was prepared by adding DDM to the desired concentration (between 0.02%-0.2% w/v) to the  $\text{Co}^{2+}$ -NTA resin elution buffer as described in the 15-LOX-2 purification section. In the 15-LOX-2-DDM complex samples,  $\text{CaCl}_2$  was added (to a final sample concentration of 0.5 mM) 2 minutes before  $\text{D}_2\text{O}$  incubation.

#### *FLAP Sample Preparation for Hydrogen/Deuterium Exchange*

FLAP stored in sample buffer (20 mM Tris, 300 mM KCL, 2.5% glycerol, 1 mM DDT, 0.02% DDM, pH 7.8) was used in H/D exchange experiments. To investigate ligand binding H/D exchange experiments were conducted on native FLAP unbound to any ligands and compared to FLAP with bound AA and FLAP with bound MK-886. FLAP samples with AA had 1  $\mu\text{L}$  of 12.5 mM AA added (to a sample concentration of 250  $\mu\text{M}$ ) 2 minutes before  $\text{D}_2\text{O}$  addition. For samples involving the binding of MK-886, overnight pre-incubation at 4  $^\circ\text{C}$  was initiated by the addition

of 1  $\mu\text{L}$  of 5 mM MK-886 in 100% ethanol to 50  $\mu\text{L}$  of 50  $\mu\text{M}$  FLAP to a final MK-886 sample concentration of 100  $\mu\text{M}$ .

#### *H/D Exchange MS*

H/D exchange was initiated by the addition of 45  $\mu\text{L}$  of  $\text{D}_2\text{O}$  to the sample (prepared by methods previously described) (1:10 dilution with  $\text{D}_2\text{O}$ ) at 24  $^\circ\text{C}$ . The deuterium-protein solution was incubated for time points ranging from 15 seconds to 8 hours at approximately 24  $^\circ\text{C}$ . H/D exchange was quenched with the addition of 50  $\mu\text{L}$  of quench buffer (identified during peptide mapping) and dropping the temperature to 0  $^\circ\text{C}$  by putting the sample on ice. Pepsin (2  $\mu\text{L}$  of 20 mg/mL in  $\text{H}_2\text{O}$  for 15-LOX and 2  $\mu\text{L}$  of 10 mg/mL for FLAP) was added immediately after quenching and incubated on ice for 7 minutes. All samples were prepared individually and analyzed on the mass spectrometer on the same day. The resulting peptides were separated by reverse-phase HPLC on an ice-cold Phenomenex Aeris Peptide 3.6  $\mu\text{m}$  XB-C18 50 x 21 mm column and eluted at a flow rate of 0.1 mL/min with a 15-minute gradient of 5-50% acetonitrile/ $\text{H}_2\text{O}$  with 0.4% formic acid for 15-LOX-2 and a 15-minute gradient of 5-75% acetonitrile/ $\text{H}_2\text{O}$  with 0.4% formic acid for FLAP. Scans of  $m/z$  from 300 to 2000 were utilized for peptide detection on a ThermoFinnigan LTQ Linear Ion Trap with an ESI ionization source set in positive mode. Deuterium incorporation was observed as a shift in the centroid of the ion envelope for each peptide at varying time points.

In order to correct for loss of deuterium that occurs during the chromatography step (back-exchange) a 100% control was completed. This control was created by digesting 15-LOX-2 using the same conditions used for peptide identification and H/D exchange. The resulting peptides were repeatedly lyophilized and subsequently incubated in  $\text{D}_2\text{O}$  to ensure 100% deuteration of the

peptides, after which the peptides were frozen at -80 °C until analysis by MS. Peptides were injected onto the mass spectrometer using the same method utilized for time-point samples. In this control the back-exchange was calculated to be between 15-35% depending on peptide's innate exchange rates, elution time, and length.

The spectra from each H/D exchange sample were analyzed using the program HDExaminer (Sierra Analytics). This program determines the centroids of the isotope envelope for each peptide, at each time point, using a program-specific algorithm. HDExaminer identifies the peptide ion envelope using the parent mass, charge, and retention time of the peptide. After HDExaminer analysis, the peptide ion envelope identified by HDExaminer were manually confirmed by comparing the spectra to the peptide sequencing spectra generated during the peptide mapping. HDExaminer determines the number of deuterons incorporated onto each peptide using Equation 3, where  $D$  is the number of deuterons incorporated,  $N$  is the total number of exchangeable backbone amides,  $m_t$  is the average mass of the peptide at the given time point,  $m_{0\%}$  is the mass of the non-deuterated peptide, and  $m_{100\%}$  is the mass of the fully deuterated peptide (back-exchange control).

$$\text{Equation 3.} \quad D = N - \left( \frac{m_t - m_{0\%}}{m_{100\%} - m_{0\%}} \right)$$

Each sample was tested 2-3 times and deuterium incorporation for that peptide was averaged. The total number of deuterium incorporated was plotted verses time and fit to the sum of first-order rate terms as seen in Equation 4, in which  $D$  is the number of deuterons incorporated,  $N$  is the number of exchangeable sites,  $A$  and  $k$  are the amplitude and rate constants of the  $n$ th phase of exchange.



Equation 4. 
$$D = N - A_1 e^{-k_1 t} - A_2 e^{-k_2 t} - A_3 e^{-k_3 t} \dots - A_n e^{-k_n t}$$

The exchange amplitude at time zero ( $A_{\text{fast}}$ ) represents the number of hydrogens that exchange within the first 15 seconds. The value of  $A_{\text{fast}}$  is calculated by taking the differences between the sum of the fitted amplitudes in the intermediate kinetic phases (> 15 s) and the total number of exchangeable sites in the peptide. Inasmuch as  $A_{\text{fast}}$  is an extrapolated value and not a fitted parameter, no errors are reported. Given that the errors in the fitted amplitudes  $A_1$ ,  $A_2$ , and  $A_3$  are typically less than 10% the errors in  $A_{\text{fast}}$  are estimated to be less than 20-30%. The calculated rates for H/D exchange will be classified into rapid, intermediate, and slow exchange categories. Peptides identified as displaying significant changes in deuterium incorporation between states were those that displayed a 10% or greater change in  $A_{\text{fast}}$  or slow exchange rates. Due to the large number of identified peptides and different states tested, only the kinetic profiles for peptides that are important in understanding data interpretation are shown herein. The remaining kinetic profiles are shown in Figures 38-41 of the Appendix.

## CHAPTER III

### EXAMINATION OF 15-LIPOXYGENASE-2 STRUCTURAL DYNAMICS IN SOLUBLE AND MEMBRANE ASSOCIATED STATES

A crystal structure of 15-LOX-2 revealed that a  $\text{Ca}^{2+}$  binding site stabilized a hydrophobic loop between P74 and A86.<sup>107</sup> This loop projects from the PLAT domain and is composed of a unique primary sequence when compared to other human LOXs (Figure 10). Dr. Marcia Newcomer's laboratory suggested that  $\text{Ca}^{2+}$  binding may stabilize the loop in a position that allows it to be buried into the membrane upon 15-LOX-2 membrane association, however, this putative membrane association model required further studies to determine its validity.<sup>107</sup> In this work, the structural dynamics of 15-LOX-2 in both soluble and membrane associated states were investigated to determine the impact of  $\text{Ca}^{2+}$  binding and membrane association on 15-LOX-2 structure.

#### Results

##### *Peptide mapping of 15-LOX-2*

Our optimization of the digestion procedure for 15-LOX-2 (protocol in Chapter 2) included testing different proteases at varying molar ratios, the addition of denaturants to the quenching buffer, and varying protein-protease incubation times. A pepsin digest with a 7 min digestion period, analyzed by tandem MS, created a peptide map providing 72% sequence coverage and 68 measurable peptides ranging from 5 to 20 residues for the native 15-LOX-2 enzyme (Figure 15).

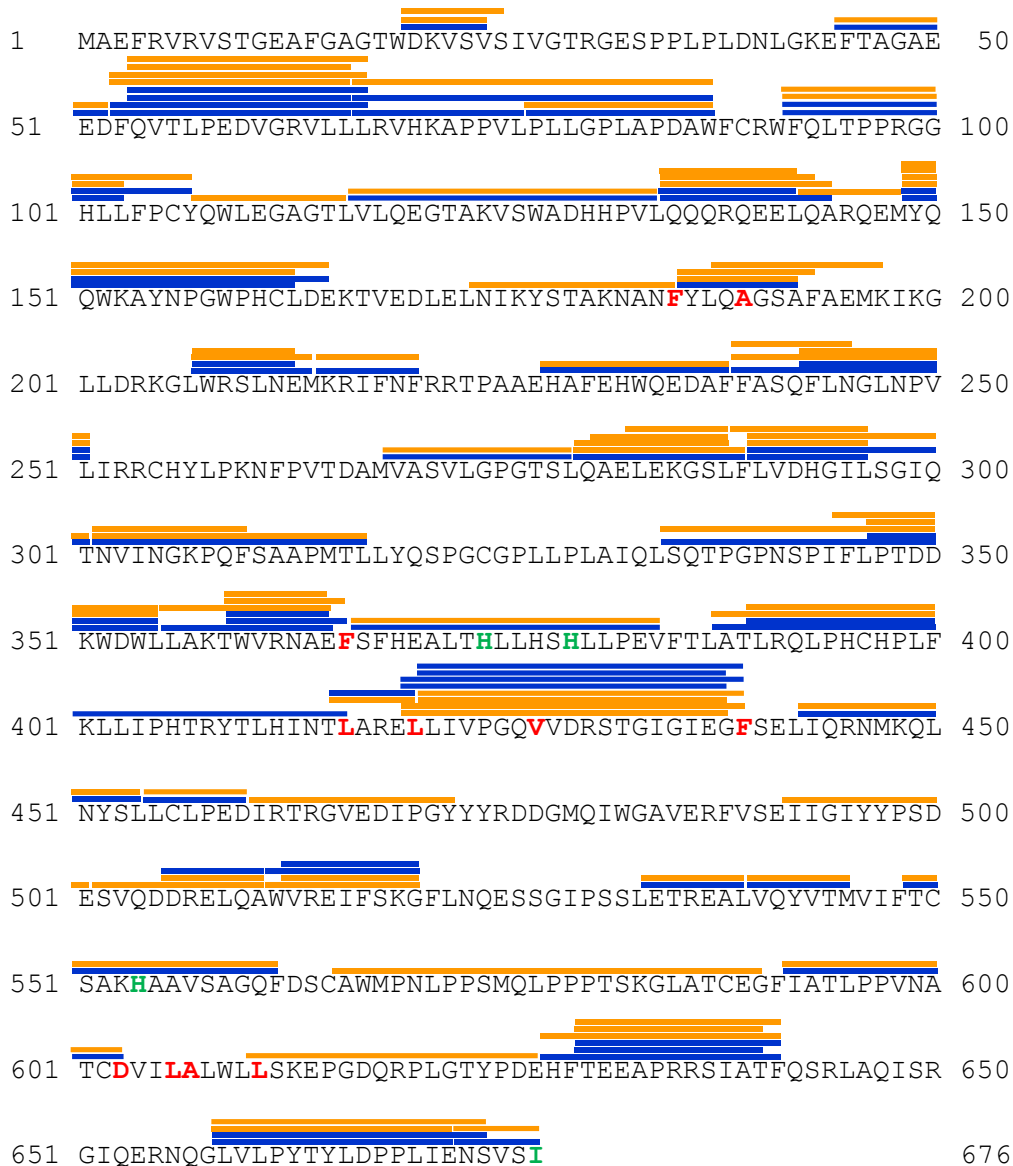


**Figure 15. Peptide Map of 15-LOX-2.** Peptides from 15-LOX-2 were generated by a pepsin digest, analyzed by tandem MS, and identified by the PEAKS computation program. Peptides with measurable ion envelopes in soluble 15-LOX-2 are shown by orange lines above the sequence and measurable peptides in nanodisc-associated 15-LOX-2 are shown by blue lines. Residues that are conserved in mammalian LOXs and thought to be part of substrate binding are in red while residues that coordinate the catalytic iron are in green.

Addition of AA and nanodiscs decreased MS signals due to charge competition in ESI and also the competition of 15-LOX-2 peptides with peptides derived from the MSP component of the nanodiscs. Therefore, sequence coverage slightly decreased in samples containing these additives. Results for the most pertinent peptides for illuminating the roles of structural dynamics in 15-LOX-2 regulation and function are presented herein. More of the H/D exchange kinetics data, not specifically discussed throughout this work, are shown in the Appendix to provide the overall view of 15-LOX-2 H/D exchange profile (Figures 38-41). The following nomenclatures were used in the description of our research: “peptide” being used when referring to an actual peptide identified in the protein digestion and “region” being used to refer at an area of the protein that may or may not correspond to an actual peptide.

#### *Spatial resolution of 15-LOX-2 structural dynamics*

The peptide backbone stability of partially water-exposed secondary structural elements that undergo local unfolding can be investigated by measuring deuterium incorporation onto the peptide backbone of 15-LOX-2 after 1 hour of H/D exchange. The level of deuteration of 15-LOX-2 with no bound  $\text{Ca}^{2+}$  or AA after 1 hour of H/D exchange was mapped onto the crystal structure of human 15-LOX-2 (PDB entry 4NRE, which has  $\text{Ca}^{2+}$  bound to the PLAT domain and a substrate mimic, the detergent C8E4, bound to the active site in the catalytic domain) (Figure 16A).<sup>107</sup> A wide range (from 5% to 90%) of levels of deuterium incorporation were observed for peptides from 15-LOX-2 following 1 hour of H/D exchange. This data indicates the two domains of 15-LOX-2 exhibit significant differences in deuterium incorporation. In general, peptides derived from the PLAT domain, such as peptide 45-52 and 67-87, exhibit a high incorporation of deuterium ranging from 60% to 90%, indicating relatively high solvent exposure and flexibility, whereas

many peptides in the catalytic domain exhibit low incorporation of only 0%-20%, indicating limited solvent exposure and less flexibility (Figure 16A). Part of the PLAT domain that exhibited the highest deuterium incorporation (85%) was peptide 67-87, which is part of a hydrophobic loop that is projected from the PLAT domain in the 15-LOX-2 crystal structure.<sup>107</sup> This loop is hypothesized to act as a hydrophobic anchor in 15-LOX-2 membrane association. Another interesting result is the high deuterium incorporation observed in peptide 117-134, indicating that the linker between the PLAT and catalytic domain is both flexible and solvent-exposed.

There are regions in the catalytic domain that exhibit high H/D exchange. The highest deuterium incorporation in the catalytic domain involves  $\alpha$ -helix 2 (peptide 185-192) which is known to be flexible so that the active site can accommodate different substrates such as phospholipid-esterified AA (Figure 16B).<sup>131,132</sup> The entrance of the active site in 15-LOX-2 displays higher deuterium incorporation (peptide 419-438), indicating this region is flexible and also can play a role in 15-LOX-2 ability to bind ligands with bulky head groups. As anticipated, peptides that are involved in coordination of the catalytic iron, such as peptide 366-383 and 548-558, exhibit a low deuterium incorporation of only 5%, indicating that the region is highly protected from solvent exposure. The only iron-coordinating peptide that showed a higher deuterium incorporation level was the peptide that contains the C-terminal end of 15-LOX-2 (peptide 671-676) (Figure 16B).

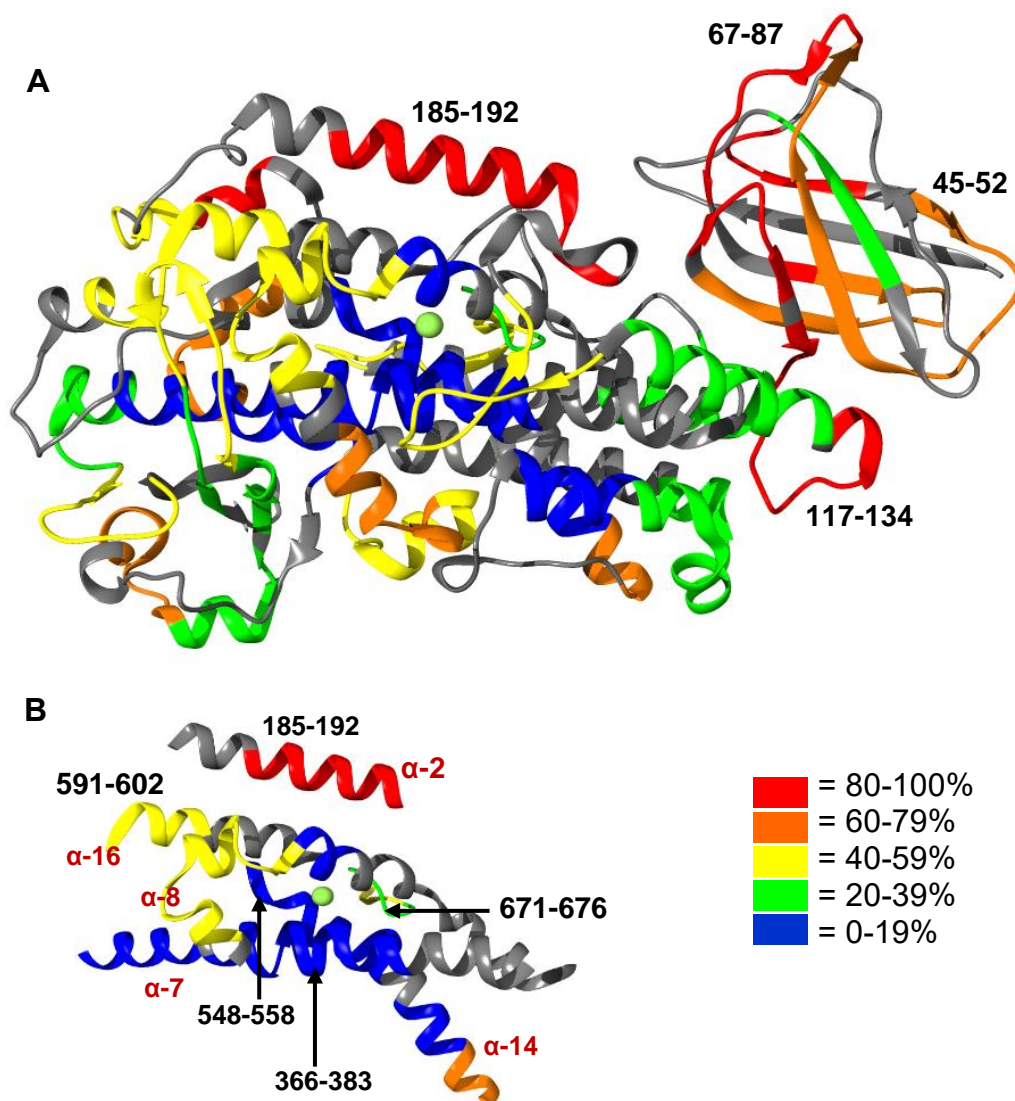


**Figure 16. Structural dynamics of ligand- and substrate-free 15-LOX-2.** (A) Backbone amide deuteration levels of 15-LOX-2 peptides following 1 hour of H/D exchange were mapped onto the 15-LOX-2 crystal structure (PDB entry 4NRE)(11) to identify general flexibility and solvent exposure. Gray indicates regions that could not be identified. Peptides referred to in this work are designated by their sequence range. (B) Deuterium levels of the 5 helices that form the active site and coordinate the catalytic iron are shown. Helices are labeled by their numerical order in LOXs.

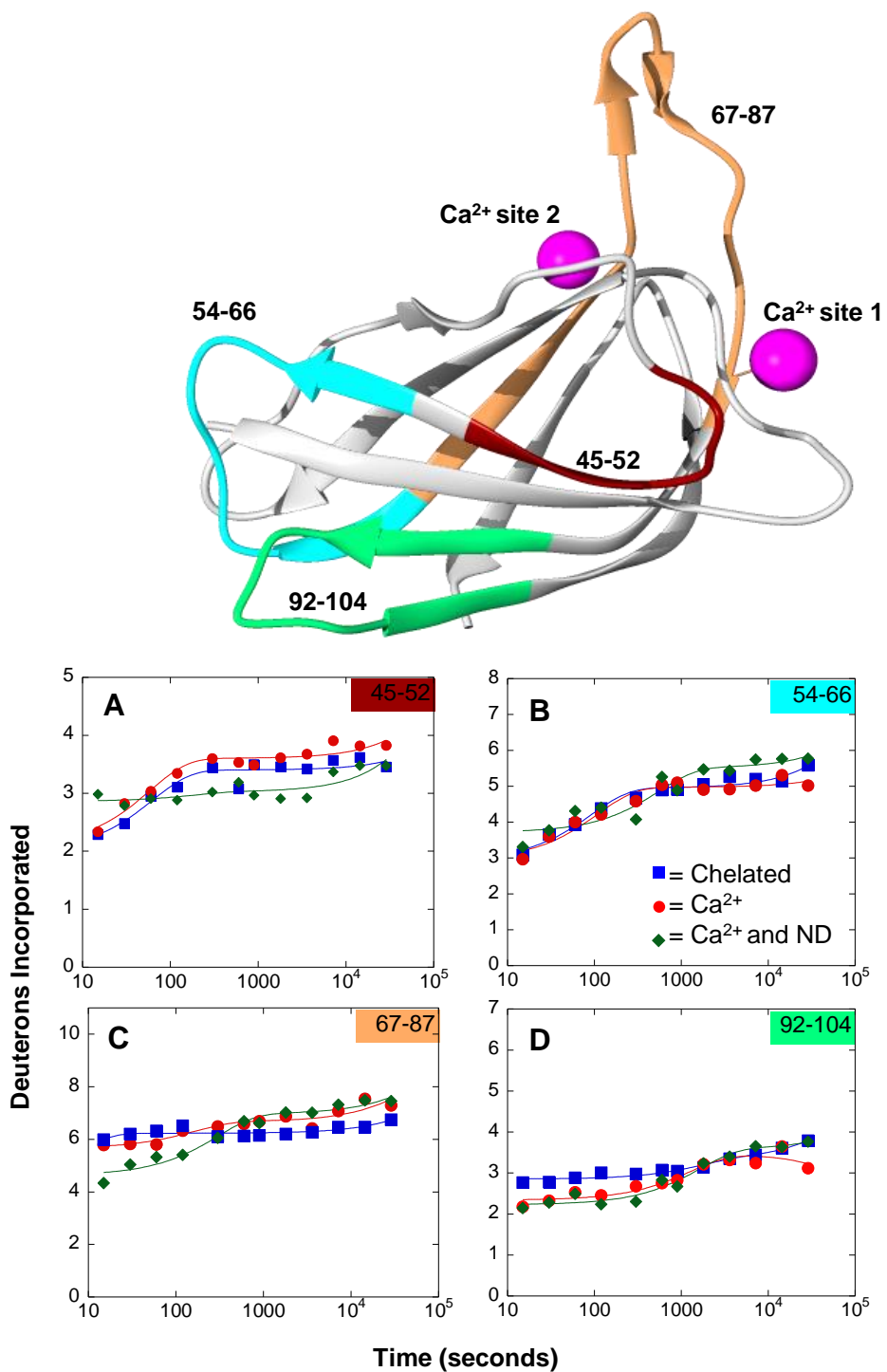


**Figure 17. Impact of Ca<sup>2+</sup> binding and membrane association on H/D exchange for the PLAT domain of 15-LOX-2.** The number of deuterons incorporated into peptides vs time was plotted to obtain H/D exchange kinetics for 15-LOX-2 peptides in a Ca<sup>2+</sup> free state (blue squares), Ca<sup>2+</sup> bound state (red circle), and nanodisc-associated state (green triangle). Peptides are labeled by their sequence range and mapped onto the PLAT domain of 15-LOX-2 by color.

### *Structural dynamics in 15-LOX-2 upon binding $Ca^{2+}$*

15-LOX-2 is a peripheral protein that translocates from the cytosol to the membrane upon binding  $Ca^{2+}$ . There are two  $Ca^{2+}$  binding sites located on one face of the PLAT domain in 15-LOX-2. To investigate how the binding of  $Ca^{2+}$  might affect 15-LOX-2 structural dynamics and promote membrane association, full backbone H/D exchange kinetics of 15-LOX-2 were performed in the presence and absence of  $Ca^{2+}$ . Due to low ion envelope resolution, peptides that contain residues of  $Ca^{2+}$  binding site 1 could not be analyzed. However, peptide 67-87, which had high ion envelope resolution and could be analyzed, is important in structuring  $Ca^{2+}$  binding site 2 (Figure 17, panel C). Surprisingly, there are no significant changes in the H/D exchange kinetic profiles in this peptide upon  $Ca^{2+}$  binding. In fact, the only peptide to show a change in deuterium incorporation due to  $Ca^{2+}$  binding was peptide 92-104, which exhibited a small 8% reduction in deuterium incorporation during the first 5 minutes of H/D exchange (Figure 17, panel B). Comparison of H/D exchange for 15-LOX-2 and 15-LOX-2 with bound  $Ca^{2+}$  indicates there are no significant changes in the structural dynamics of the PLAT domain upon binding  $Ca^{2+}$ . These results raise questions on how  $Ca^{2+}$  binding promotes membrane association in 15-LOX-2.

### *Association of 15-LOX-2 with nanodiscs*

In addition to investigating how  $Ca^{2+}$  binding may affect the structural dynamics of soluble 15-LOX-2, H/D exchange kinetics of 15-LOX-2 associated to a membrane substitute were collected to identify regions involved in membrane association or that undergo conformational changes upon membrane association. Dr. Marcia Newcomer's lab demonstrated that 15-LOX-2 associates to nanodiscs in a  $Ca^{2+}$  dependent manner.<sup>107</sup>



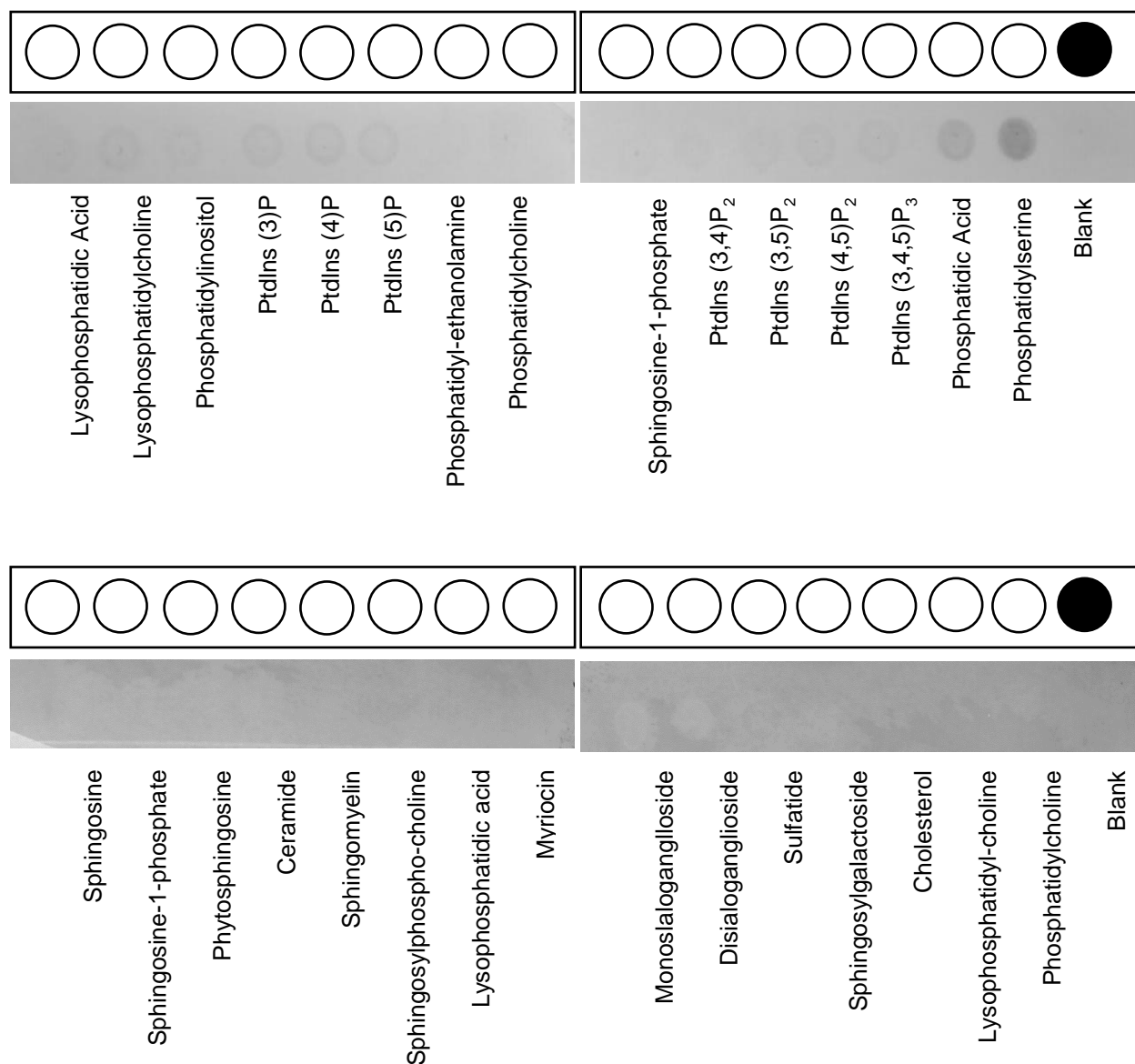


**Figure 18. 15-LOX-2 binding to lipids on “strips” to screen for the lipid binding preference of this enzyme.** PIP and SpingoStrips were used to identify the phospholipid 15-LOX-2 prefers to associate with. Detection of protein was completed with an alkaline phosphatase staining solution. The strips demonstrated that of the lipids represented in this experiment 15-LOX-2 associates with the highest affinity to PS.

Nanodiscs are model membrane systems that are believed to have a number of native membrane-like properties. They are formed by discoidal phospholipid bilayers that are encircled

by an amphipathic helical protein called the MSP and create ideal conditions for analyzing protein interactions with membranes. Therefore, 15-LOX-2 associated with nanodiscs was used to model 15-LOX-2 associated to the cellular membrane in H/D exchange experiments. Preliminary experiments with PIP and SphingoStrips indicate that 15-LOX-2 preferably associates with PS over other phospholipids (Figure 18) and so this lipid was included as one of the lipid components of the nanodiscs used in this study.

Prior to H/D exchange, 15-LOX-2 association to PS-containing nanodiscs was verified using SEC as monitored by a 280 nm UV-detector. An elution peak was observed at approximately 8.8 mL when isolated nanodiscs were run on a Superose-12 10/300 GL column. Purified 15-LOX-2 eluted at 13.7 mL, while the peak for 15-LOX-2 associated with nanodiscs in the presence of  $\text{Ca}^{2+}$  eluted at approximately 8.5 mL (Figure 19). Peak identities were confirmed using SDS-PAGE (Appendix, Figure 42). These results confirm that 15-LOX-2 associates with nanodiscs in the presence of  $\text{Ca}^{2+}$ .

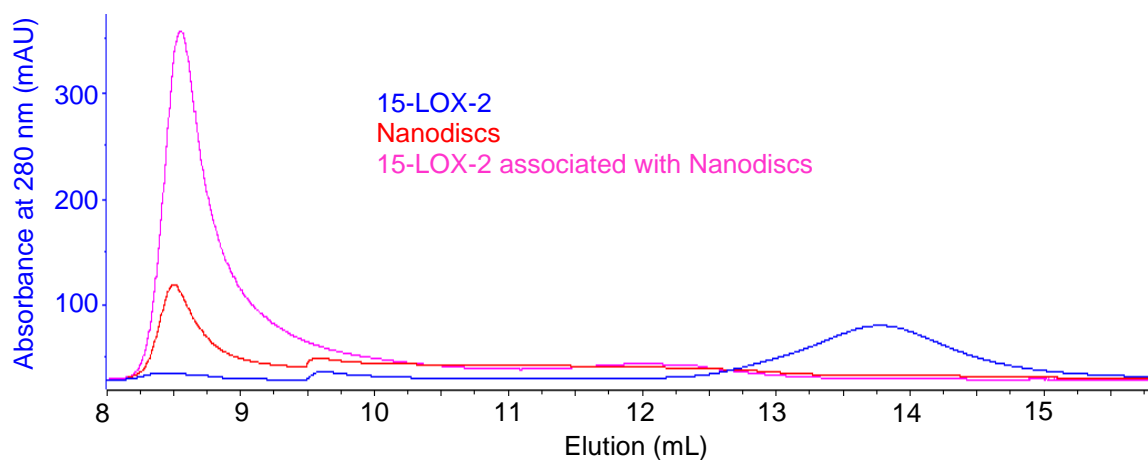


**Figure 19. Association of 15-LOX-2 with nanodiscs.** SEC chromatography profiles showing 15-LOX-2 association to nanodiscs. Free 15-LOX-2 eluted at 13.7 mL, but shifted to elution at 8.5 mL when associated with nanodiscs.

### *H/D exchange of 15-LOX-2 associated with nanodiscs*

H/D exchange of  $\text{Ca}^{2+}$ -15-LOX-2 in solution and associated with nanodiscs was compared, revealing only slight changes in H/D exchange kinetics when 15-LOX-2 is membrane-associated (Figure 17). Peptide 67-87, which is part of the hydrophobic loop proposed to act as a membrane anchor, showed a slight reduction in deuterium incorporation (12%) during the first 2 minutes of exchange for nanodisc-associated  $\text{Ca}^{2+}$ -15-LOX-2 compared to  $\text{Ca}^{2+}$ -15-LOX-2 in solution (Figure 17, panel C). Peptide 45-52 also experienced a slight change upon membrane association of  $\text{Ca}^{2+}$ -15-LOX-2, its rapid exchange increased by only one deuterium when compared to  $\text{Ca}^{2+}$ -15-LOX-2 in solution. However, over long exchange times the deuteration level of nanodisc-associated 15-LOX-2 remained constant, ending with only a slightly lower deuterium incorporation (Figure 17, panel D). No other peptides in 15-LOX-2 exhibited differences in their H/D exchange kinetic profiles when comparing soluble and nanodisc-associated  $\text{Ca}^{2+}$ -15-LOX-2. These results indicate that membrane association has only a minimal effect on the structural dynamics of 15-LOX-2 and that no region of 15-LOX-2 is stably buried in the membrane.

Alterations in the type of model membrane used for these experiments were investigated to try and promote a tighter association between 15-LOX-2 and the membrane substitute. Substituting DDM for nanodiscs as a membrane model and varying  $\text{Ca}^{2+}$  concentration yielded similar H/D exchange as for nanodisc-associated 15-LOX-2 (Figure 20). Addition of AA to the nanodiscs resulted in the same levels of deuterium incorporation (Appendix, Figure 43), indicating that the presence of substrate does not increase 15-LOX-2 association.

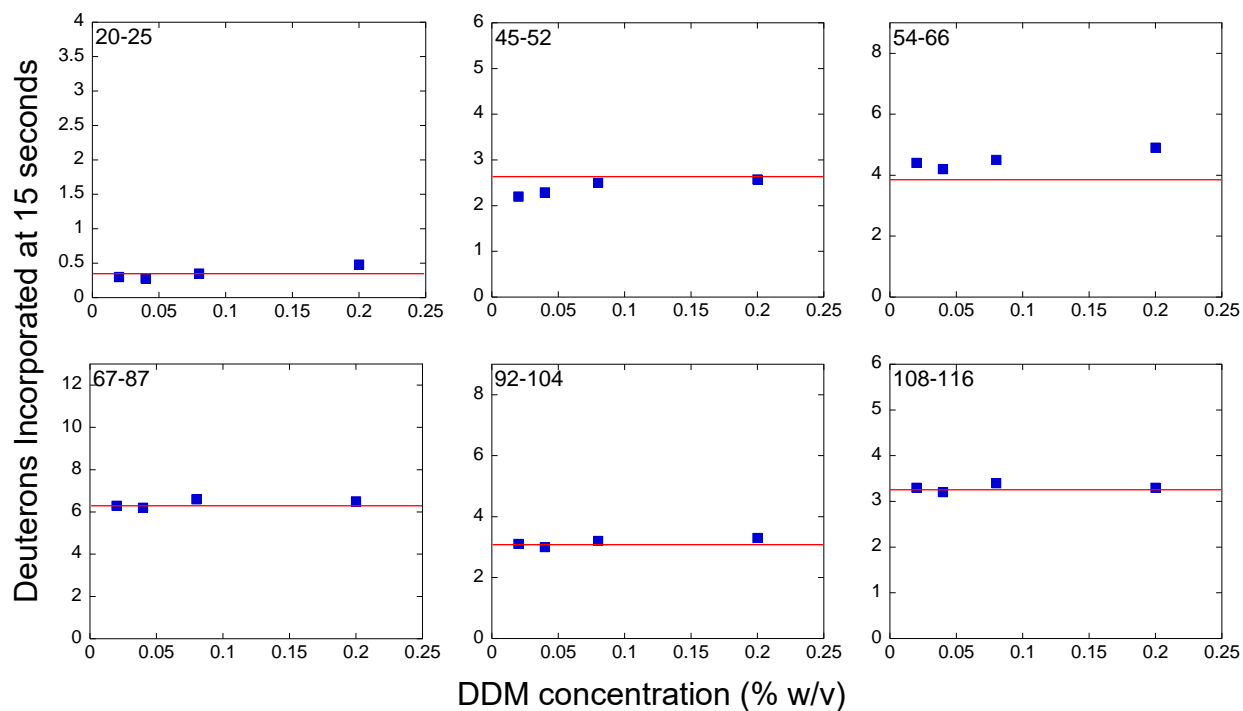


**Figure 20. Effect of DDM micelles effect on deuterium incorporation.** Deuterium incorporation was measured at 15 seconds for  $\text{Ca}^{2+}$ -15-LOX-2 and at varying DDM concentrations to analyze whether the protein associates to DDM micelles. The blue squares represent the amount of deuterons incorporated at 15 seconds. The red line represents the deuterium incorporation at 15 seconds for  $\text{Ca}^{2+}$ -15-LOX-2. There are no significant differences in deuterium incorporation between  $\text{Ca}^{2+}$ -15-LOX-2 in solution and  $\text{Ca}^{2+}$ -15-LOX-2 in the presence of DDM.

## Discussion

### *Conformational Dynamics of native 15-LOX-2*

Data on protein structural dynamics provided by H/D exchange MS is particularly useful when mapped onto 3D crystal structures. A crystal structure provides an indispensable “snapshot” of the protein conformation in a static state. Experimental data from H/D exchange MS can be used to characterize the local dynamics and motions of the protein of interest in solution at ambient temperature. Currently, there is only one crystal structure of 15-LOX-2.<sup>107</sup> This structure has a

substrate mimic C8E4 bound to the active site. The PLAT and catalytic domains are dominated by stable secondary structures. The PLAT domain is composed of eight  $\beta$ -sheets in a barrel-like conformation, and the catalytic domain is composed of  $\alpha$ -helical bundles (see Figure 16).<sup>133</sup> H/D exchange data after 1 hour of deuterium incubation indicated the two domains in native 15-LOX-2 in solution exhibited significantly different degrees of flexibility. The peptides derived from the PLAT domain exhibited relatively high levels of deuterium incorporation indicating that the PLAT domain is globally dynamic to the extent that the  $\beta$ -strands of the barrel become transiently free from their normal  $\beta$ -sheet hydrogen bonding patterns enabling facile H/D exchange (Figure 16). The interior region of the catalytic domain was very stable and protected from solvent exposure.

One interesting observation is that the long loop that connects the PLAT domain and the catalytic domain exhibited high deuterium incorporation after 1 hour of H/D exchange (Figure 16). In all crystal structures of mammalian LOXs, the domains adopt a similar overall arrangement with the PLAT domain resting atop the catalytic domain, giving the LOXs a 100 Å long cylindrical topology.<sup>88,107,134</sup> The two domains share a large interdomain interface and are interconnected by non-covalent interactions. This suggests the possibility of an extensive interaction interface between the two domains in solution. However, in this work, the peptide backbone on the loop (peptide 117-134) and peptides involved in the domain interface (peptide 92-104) exhibit a high deuterium incorporation level. This implies that they are both solvent exposed and highly dynamic, contrary to what might be supposed from the crystal structures, suggesting few or weak interactions between these domains in solution. This conclusion concurs with small angle X-ray scattering experiments, which suggested the PLAT domain can swing away from the catalytic domain while in solution.<sup>79</sup>

The H/D exchange after 1 hour observed in the 15-LOX-2 active site region revealed low exchange on the active site interior ( $\alpha$ -helix 7 and  $\alpha$ -helix 14) indicating well-ordered structures with few local structural fluctuations (Figure 16B). The higher levels of deuterium incorporation at the active site entrance and exterior ( $\alpha$ -helix 2; peptide 185-191,  $\alpha$ -helix 8; peptide 419-438 and  $\alpha$ -helix 16; peptide 591-602) indicate moderate to high degrees of flexibility. This flexibility very likely allows for inhibitors such as RS7, observed in the crystal structure of rabbit 15-LOX-1 (PDB entry 1LOX), to access the active site<sup>106</sup>. In addition, 15-LOX-2 is able to oxygenate intact phospholipids and cholesteryl esters.<sup>132</sup> The flexibility of the active site is needed to accommodate the bulky head groups of the fatty acids.

*Significant structural changes are not required for 15-LOX-2 to associate to the membrane*

15-LOX-2 is located in the cytosol until binding of  $\text{Ca}^{2+}$  to the PLAT domain results in translocation to the membrane.<sup>135</sup> This cellular compartmentalization is an important regulatory feature observed in LOXs. The nature of any structural changes that occur upon  $\text{Ca}^{2+}$  binding that promote LOX membrane association have yet to be identified. Previous H/D exchange studies with cytosolic phospholipase A<sub>2</sub> (cPLA<sub>2</sub>) suggested that binding of  $\text{Ca}^{2+}$  to the cPLA<sub>2</sub> C2 domain resulted in an overall decrease in the domain flexibility in a manner that promotes translocation to the nuclear membrane.<sup>136</sup> However, in this work, we found that the addition of  $\text{Ca}^{2+}$  to 15-LOX-2 PLAT domain did not result in significant changes in the rate of deuterium incorporation into any part of the protein that we were able to analyze (Figure 17).

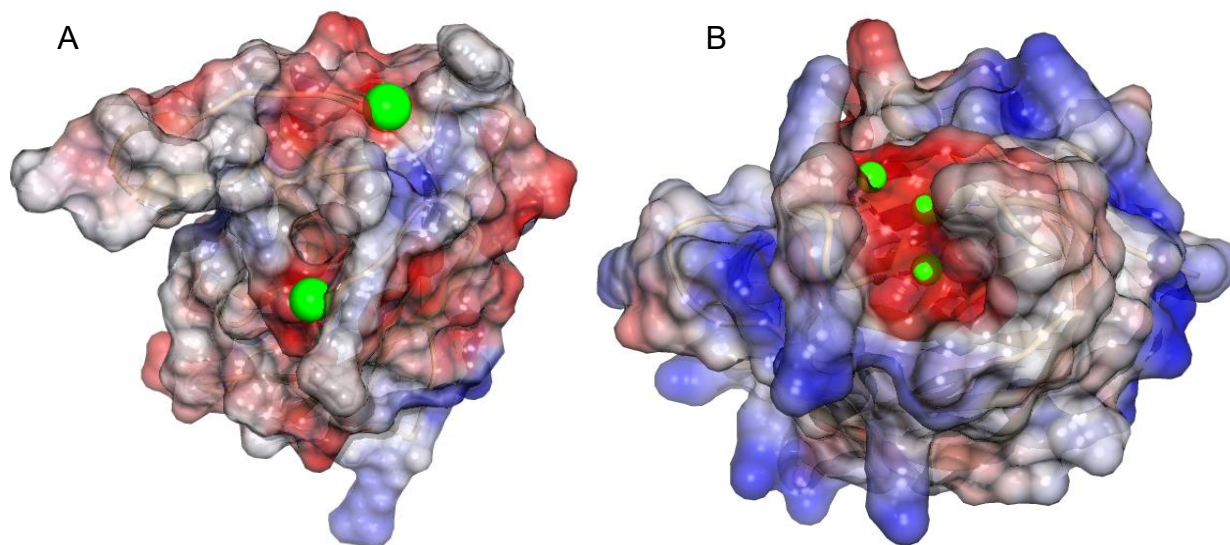
In previous H/D exchange experiments with peripheral membrane proteins, such as cPLA<sub>2</sub>, regions of the protein that are stably buried in the phospholipid bilayer are shielded from H/D exchange.<sup>137</sup> However, nanodisc-associated 15-LOX-2 did not exhibit significant differences in

H/D exchange kinetics compared to  $\text{Ca}^{2+}$ -15-LOX-2 in solution (Figure 17). In fact, the only peptide to show a slight decrease in deuterium incorporation in nanodisc-associated 15-LOX-2 was peptide 67-87 (Figure 17, panel B). This peptide spans the unique hydrophobic loop (P73-A86) that protrudes from the PLAT domain and is proposed to act as a membrane anchor. The H/D exchange kinetics obtained in this study for nanodisc-associated 15-LOX-2 eliminates the possibility of the hydrophobic PLAT loop inserting deeply and stably into the membrane. The data leaves open the possibility of the loop being involved in membrane surface binding in a manner that still allows transient water accessibility and H/D exchange.

#### *15-LOX-2 preferentially associates with PS relative to other phospholipids*

An alternative explanation for how  $\text{Ca}^{2+}$  binding promotes 15-LOX-2 membrane association can be proposed based on our observation that  $\text{Ca}^{2+}$ -15-LOX-2 preferentially associates with the anionic phospholipid PS over other phospholipids, including a number of others that also are anionic (Figure 18). It is plausible that binding of  $\text{Ca}^{2+}$  to the PLAT domain adds positive charge for association with PS, without changing the structure and dynamics of the protein. However, because 15-LOX-2 binds PS specifically over other anionic lipids, this electrostatic effect is also complemented by headgroup-specific recognition of the PS moiety. This proposed membrane-associating mechanism is similar to that proposed for select peripheral proteins with C2 domains such as protein kinase C. Structural comparison of the C2 domains of protein kinase C (PKC) in  $\text{Ca}^{2+}$ -free and  $\text{Ca}^{2+}$ -bound states lacked conformation changes upon  $\text{Ca}^{2+}$  binding. A crystal structure of PKC $\alpha$  in complex with  $\text{Ca}^{2+}$  and phosphatidylserine revealed that phosphatidylserine filled the incomplete coordination sphere of the  $\text{Ca}^{2+}$  and  $\text{Ca}^{2+}$  acted as a bridge between the C2 domain and the membrane.<sup>138</sup> The C2 domain of PKC $\alpha$  has large negatively

charged regions, similar to the PLAT domain in 15-LOX-2. It is possible that binding  $\text{Ca}^{2+}$  to the anionic regions of 15-LOX-2 PLAT domain switches the electrostatic potential to promote interactions with the negatively charged head groups of PS.

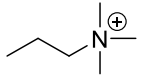
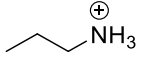
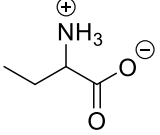


**Figure 21. Comparison of membrane association domains in 15-LOX-2 and PKC $\alpha$ .** Electrostatic maps of the (A) PLAT domain in 15-LOX-2 and (B) the C2 domain in PKC $\alpha$  show anionic regions in the domains that promote binding of  $\text{Ca}^{2+}$ . It is plausible that binding calcium switches the electrostatic potential to promote membrane association to anionic phospholipids.

The 15-LOX-2 preference for PS has several interesting biological implications. First, its preference for PS differs from previous LOX membrane association studies. To date the PLAT domain of 11R-LOX from *Gersemia fruticosa* is the only LOX for which the mechanism of membrane association has been extensively studied. That study used fluorescence resonance energy transfer (FRET) and surface plasmon resonance to monitor interfacial binding of 11R-LOX to and SUV composed of varying molar ratios of lipids.<sup>82</sup> These studies showed that 11R-LOX



associated with vesicles containing phosphatidylethanolamine and anionic phospholipids. 5-LOX membrane association was also investigated by monitoring *in vivo* membrane association, which showed that 5-LOX primarily translocates to nuclear membranes rich with PC, a zwitterionic phospholipid.<sup>139</sup> In addition, 5-LOX activity was monitored with AA present in PC vesicles. Addition of 10-20% PS resulted in decreased 5-LOX activity, which was interpreted to indicate the PS decreased 5-LOX membrane association as this is required for 5-LOX to acquire AA in intact cells.<sup>89</sup> The differences in preferred membrane compositions for association of various LOX suggest different mechanisms for membrane binding throughout enzyme superfamilies that have PLAT domains. This is likely reflected by a comparison of the 15-LOX-2 primary sequence with sequences of other LOX. 15-LOX-2 has a unique sequence from A74 to P84, which forms a hydrophobic loop, mainly composed of leucines and prolines, which protrudes from the PLAT domain. Other LOXs have conserved tryptophans in their corresponding primary sequence that are identified to be essential in membrane association.<sup>87,107,78</sup>

Phospholipid	Head Group	Net Charge (pH 7.0)
Phosphatidylcholine (PC)		0
Phosphatidylethanolamine (PE)		0
Phosphatidylserine (PS)		-1
Phosphatidic Acid (PA)	—H	-1

**Table 1. Preferred phospholipids of LOX upon membrane association.** Common phospholipids that are connected with LOX membrane association are presented here to highlight the different charges of their head groups. In this work 15-LOX-2 was found to prefer PS upon membrane association. PS is the most prevalent anionic phospholipid in the plasma membrane.

Another interesting implication of the 15-LOX-2 preference for PS upon membrane association is that PS is known to initiate several important cellular pathways. PS enriched membranes recruit proteins, such as kinases, small GTPases and fusogenic proteins, to the membrane for initiation of enzymatic activity.<sup>140</sup> This regulatory mechanism is observed for conventional C2 domains, which are structurally and functionally similar to the PLAT domain. However, most C2 domains show broad preference for anionic phospholipids and not specifically PS.<sup>141</sup> Previous studies imply that LOX recruitment to the membrane and enzymatic activity may be regulated by the lipids present.<sup>72,139</sup> Therefore, it is plausible that increased presence of PS increases 15-LOX-2 activity in intact cells. This observation could also provide a connection between PS and its observed anti-inflammatory properties. Previous studies demonstrated that the addition of PS to IL-1 $\beta$  stimulated synoviocytes reduced production of inflammatory mediators, such as IL-6, IL-8 and PGE<sub>2</sub>.<sup>142</sup> *In vivo* studies using RA-induced murine models demonstrated that injections of PS containing liposomes reduced inflammatory responses.<sup>143</sup> While part of the anti-inflammatory mechanism in this mouse model appears to be dependent on activation of peroxisome proliferator-activated receptors the full cellular pathway is unknown. If PS promotes 15-LOX-2 membrane association, it is plausible that increased PS may promote 15-LOX-2 association to the membrane, therefore increasing LX biosynthesis and promoting resolution of inflammation.

### *Conclusions*

Backbone amide H/D exchange is an excellent tool for identifying flexible regions of proteins. For 15-LOX-2 in both cytosolic and membrane associated states, the PLAT domain is more flexible and solvent exposed than the catalytic domain. Moreover, the linker between the

domains is highly flexible, implying the PLAT domain may be able to swing away from the catalytic domain in solution. In addition, the lack of substrate specificity observed for 15-LOX-2 can be explained by the flexibility of the active site exterior. The H/D exchange data presented in this study suggest a mechanism for 15-LOX-2 membrane association that depends on  $\text{Ca}^{2+}$  binding. The mechanistic model can be derived by combining insight from the 15-LOX-2 crystal structure, its preference for PS, and similarities in H/D exchange kinetics for  $\text{Ca}^{2+}$ -15-LOX-2 compared to  $\text{Ca}^{2+}$  free 15-LOX-2. As  $\text{Ca}^{2+}$  binding does not change the structural dynamics of the PLAT domain it is plausible that its role is primarily electrostatic, adding positive charge to anionic regions of the PLAT domain, which potentiates interactions with the negatively charge head group of PS. The membrane interaction may be stabilized by the hydrophobic loop interacting with the membrane surface in a way that still allows transient water accessibility to the peptide backbone in the loop. Overall, our results provide a detailed insight in 15-LOX-2 structural dynamics and challenge the previous hypothesis that conformational changes of the PLAT domain upon  $\text{Ca}^{2+}$  binding are responsible for membrane association.<sup>107</sup>

## CHAPTER IV

### ANALYSIS OF 15-LIPOXYGENASE-2 CONFORMATIONAL CHANGES UPON LIGAND BINDING

Knowledge regarding modes of substrate binding and related structural effects in LOX is limited. There have been significant difficulties obtaining a crystal structure of 15-LOX-2 with bound AA. AA is proposed to slide into the active site through hydrophobic interactions with  $\alpha$ -helix 2 and  $\alpha$ -helix 8 (Figure 8). It is believed to adopt a U-shape conformation in the active site, as AA adopts this conformation in a mutated version of 5-LOX (PDB entry 3V99), whereas C8E4, a substrate mimic, also adopts a similar conformation in 15-LOX-2 although the position in the active site is different between the structures (PDB entry 4NRE).<sup>107,97</sup> Our research focused on identifying areas of the active site that interact with 15-LOX-2 ligands and resulting structural effects in LOXs upon ligand binding.

#### Results

##### *Structural dynamics of substrate binding in 15-LOX-2*

To map conformational changes that potentially occur upon substrate binding, H/D exchange experiments were performed with  $\text{Ca}^{2+}$ -15-LOX-2 in the presence of AA. As  $\text{Ca}^{2+}$ -15-LOX-2 is active throughout the H/D exchange incubation times, the production of product (15-HpETE) as a complication to interpretation of the data was a concern. Therefore, activity assays were conducted using the same buffer and protein-substrate molar ratio as in the H/D exchange samples. The activity assays revealed that only 10% of AA is converted to 15-HpETE by 15-LOX-2 after 200 seconds. Therefore, we focused only on H/D exchange data collected during the first

120 seconds of deuterium incubation in 15-LOX-2 in the presence of AA. As an additional control, H/D exchange was performed for  $\text{Ca}^{2+}$ -15-LOX-2 with bound 15-HpETE.

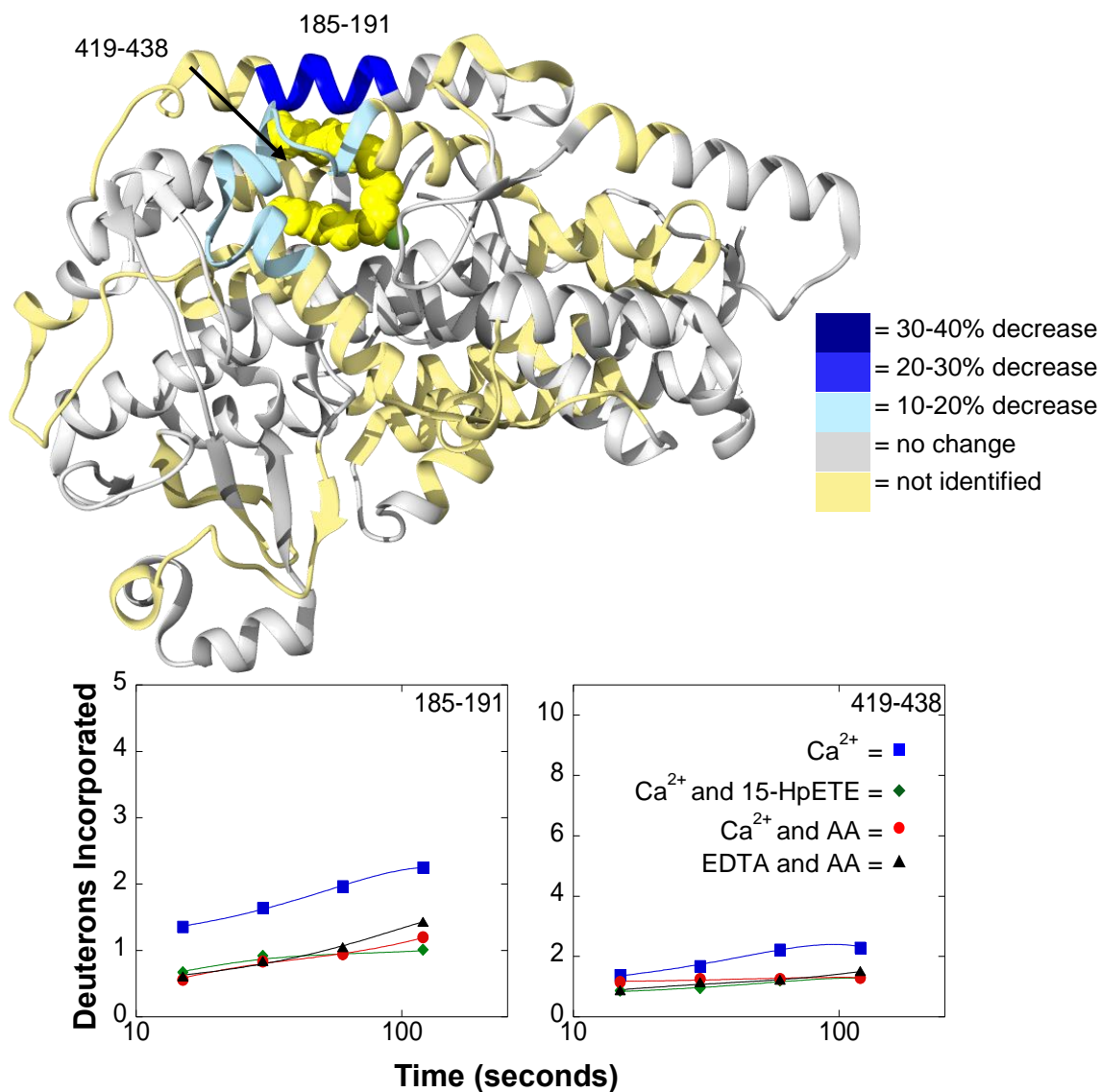


**Figure 22. Deuterium exchange in the catalytic domain in 15-LOX-2 upon lipid binding.** H/D exchange was performed for 15-LOX-2 in 4 different states: (1) 15-LOX-2 with  $\text{Ca}^{2+}$  present (blue square); (2) 15-LOX-2 with  $\text{Ca}^{2+}$  and AA present (green diamond); (3) 15-LOX-2 with  $\text{Ca}^{2+}$  and 15-HpETE present (red circle); and (4)  $\text{Ca}^{2+}$ -free 15-LOX-2 with AA present (black triangle). Peptides exhibiting changes greater than 10% at 2 minutes of exchange are shown.

When  $\text{Ca}^{2+}$ -15-LOX-2 is in the presence of AA or 15-HpETE, five peptides (45-52, 54-67, 67-87, 185-191, and 418-438) demonstrate a similar and significant decrease in deuterium incorporation when compared to  $\text{Ca}^{2+}$ -15-LOX-2 alone (Figures 22 and 23). Two of the peptides that demonstrated a reduction in deuterium incorporation were part of the 15-LOX-2 active site. The segment corresponding to  $\alpha$ -helix 2 (peptide 185-191), which forms the exterior of the active site, displayed a 21% decrease in deuterium incorporation at 120 seconds of deuterium incubation relative to substrate free  $\text{Ca}^{2+}$ -15-LOX-2 (Figure 22). Peptide 419-438 located at the active site entrance exhibited a 12% reduction in H/D exchange at 120 seconds of deuterium incubation relative to substrate free  $\text{Ca}^{2+}$ -15-LOX-2 (Figure 22). Decreases in deuterium incorporation upon AA and 15-HpETE binding in the active site are likely due to shielding of hydrogen exchange triggered by lipid binding protecting the peptide backbone from solvent exposure. This indicates that both lipid substrate and product are binding in a similar manner to 15-LOX-2. As an additional control, deuterium incorporation after 15 seconds of H/D exchange was measured at increasing concentrations of AA to test if the reduction in deuterium incorporation in the presence of AA was due to AA micelle formation. The smooth dose-dependent trend over the critical micelle concentration of AA ( $70 \mu\text{M}$ )<sup>144</sup> suggests that the deuterium incorporation profiles observed are not caused by the peptide backbone of 15-LOX-2 interacting with an AA micelle (Figure 24).

One of the more interesting H/D exchange results observed in this work is that binding of either AA or 15-HpETE to the 15-LOX-2 active site in the catalytic domain induces a decrease in deuterium incorporation in peptides that are located in the PLAT domain (peptides 45-52, 54-76, and 67-87) (Figure 23). Peptide 67-87 showed a 32% reduction in deuterium incorporation after 120 seconds of H/D exchange in  $\text{Ca}^{2+}$ -15-LOX-2 with bound AA relative to  $\text{Ca}^{2+}$ -15-LOX-2 alone (Figure 23). Peptide 45-52 experienced a 30% reduction in deuterium incorporation after 120

seconds of H/D exchange (Figure 23). This suggests that AA binding to the catalytic domain either reduces the conformational freedom of the PLAT domain or induces conformational changes that limit solvent exposure.

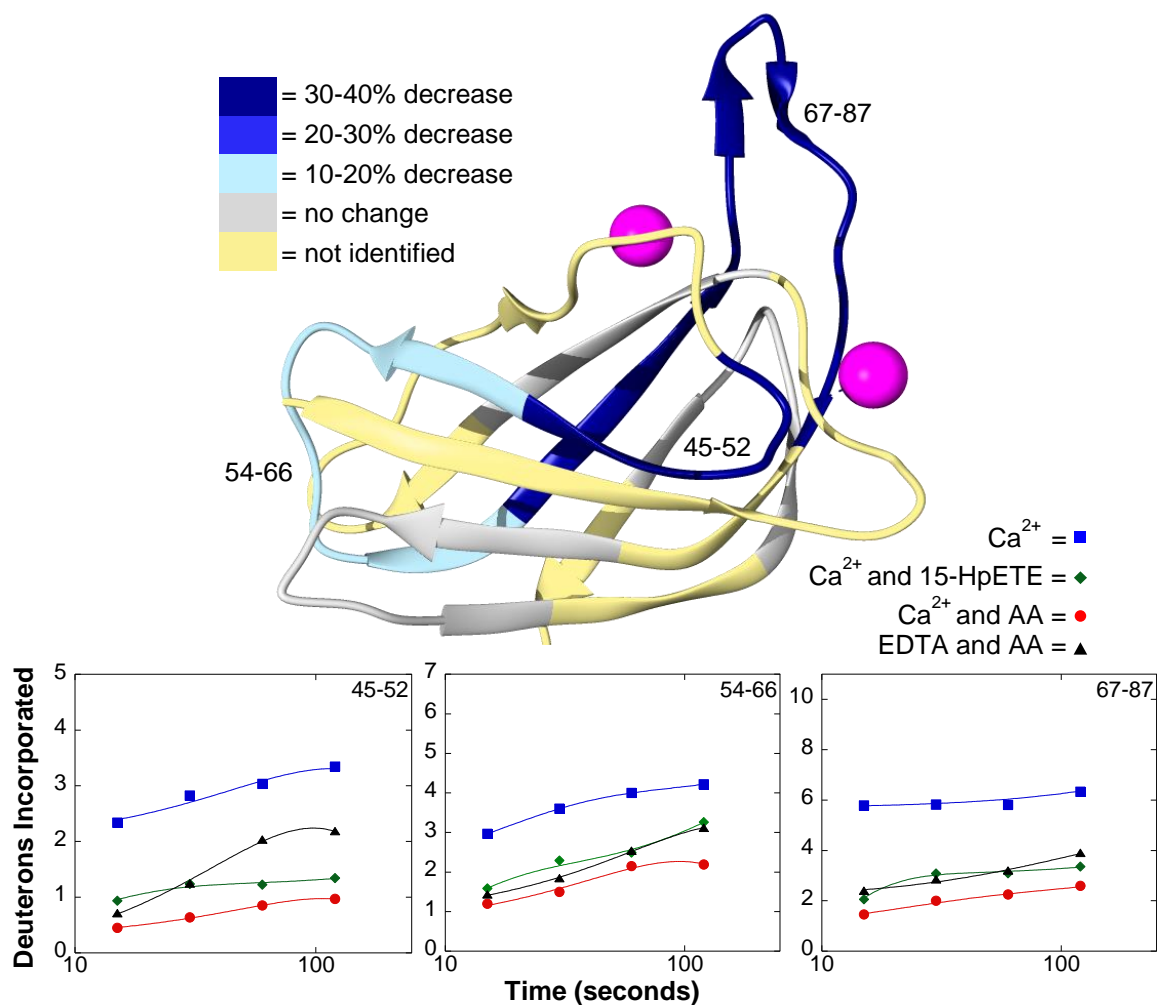


**Figure 23. Deuterium exchange in the PLAT domain in 15-LOX-2 upon lipid binding.** Addition of substrate and product to 15-LOX-2 resulted in unexpected decreases in H/D exchange in the PLAT domain. H/D exchange was performed for 15-LOX-2 in 4 different states: (1) 15-LOX-2 with  $\text{Ca}^{2+}$  present (blue square); (2) 15-LOX-2 with  $\text{Ca}^{2+}$  and AA present (green diamond); (3) 15-LOX-2 with  $\text{Ca}^{2+}$  and 15-HpETE present (red circle); and (4)  $\text{Ca}^{2+}$ -free 15-LOX-2 with AA present (black triangle). Peptides with changes greater than 10% after 2 minutes of exchange are shown.

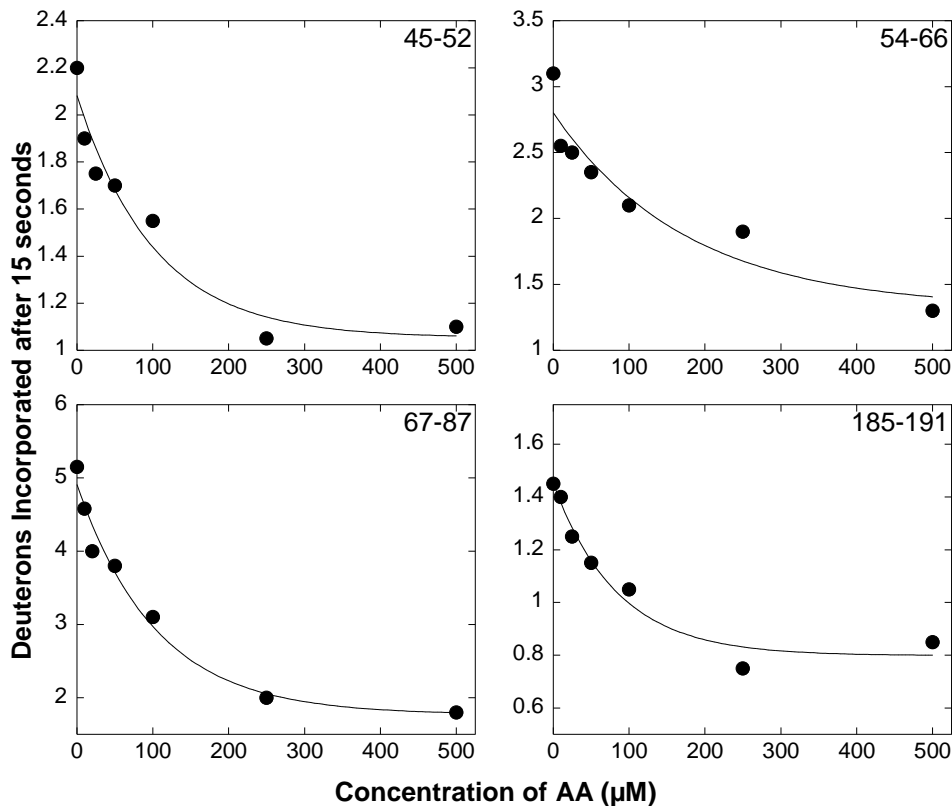


**Figure 24. AA dose dependence of deuterium incorporation.** Deuterons incorporated after 15 seconds of D<sub>2</sub>O incubation were measured and plotted vs concentration of AA. This showed a dose-dependent response with a smooth transition moving from below to above the critical micelle concentration of AA (70 μM)<sup>144</sup>. This indicates that decreases in deuterium incorporation observed at 250 mM AA are not dependent on AA micelle formation.

To test if the reductions in deuterium incorporation in peptides derived from the PLAT domain in the presence of AA are Ca<sup>2+</sup> dependent, 15-LOX-2 was chelated with EGTA before the addition of AA followed by H/D exchange experiments. Two of the three peptides in the PLAT domain (peptide 54-66, and 67-87) demonstrated no change in deuterium incorporation, indicating that neither peptide is affected by removal of Ca<sup>2+</sup>. A third peptide (peptide 45-52) demonstrated a 20% increased deuterium incorporation after 120 seconds of H/D exchange in the absence of



Ca<sup>2+</sup> (Figure 23), suggesting that this peptide is destabilized upon Ca<sup>2+</sup> removal in the presence of AA. This peptide is part of  $\beta$ -7, which is located close to the Ca<sup>2+</sup> binding site, but does not have any amino acids that directly coordinate Ca<sup>2+</sup>.

### *Structural studies of the allosteric regulation of 15-LOX-2*

Allostery is the process by which proteins transmit the effect of binding at one site to another, often distal, functional site allowing for regulation of enzymatic activity. Since allostery is a thermodynamic process, the communication across a protein can be facilitated by both static and dynamic conformational fluctuations.<sup>145</sup> 15-LOX-2 oxygenation of AA is positively allosterically regulated by the binding of 13-HODE.<sup>110</sup> To identify the 13-HODE binding site and the structural mechanism of allostery in 15-LOX-2, H/D exchange MS studies were carried out for Ca<sup>2+</sup>-15-LOX-2 in the presence of 13-HODE, and 15-HpETE.

When analyzing the H/D exchange kinetics it is important to consider that 13-HODE is the reduced product of 13-HpODE, which in turn is an enzymatic product of 15-LOX-2. Therefore, 13-HODE can potentially bind to both the active and allosteric sites. H/D exchange kinetics for Ca<sup>2+</sup>-15-LOX-2 with 13-HODE bound revealed changes in deuterium incorporation in 5 peptides (45-52, 67-87, 117-134, 185-191, and 419-438) when compared to Ca<sup>2+</sup>-15-LOX-2 (Figure 25). Peptides 45-52, 67-87, and 185-191 all experienced a decrease in deuterium incorporation upon ligand binding. These peptides also exhibited reductions in deuterium incorporation upon 15-HpETE binding, implying the ligands are binding in similar locations and inducing similar conformational changes. As 15-HpETE binds to the 15-LOX-2 active site, but does not allosterically regulate 15-LOX-2 the decrease in deuterium incorporation in these peptides are thought to be associated with binding to the active site.

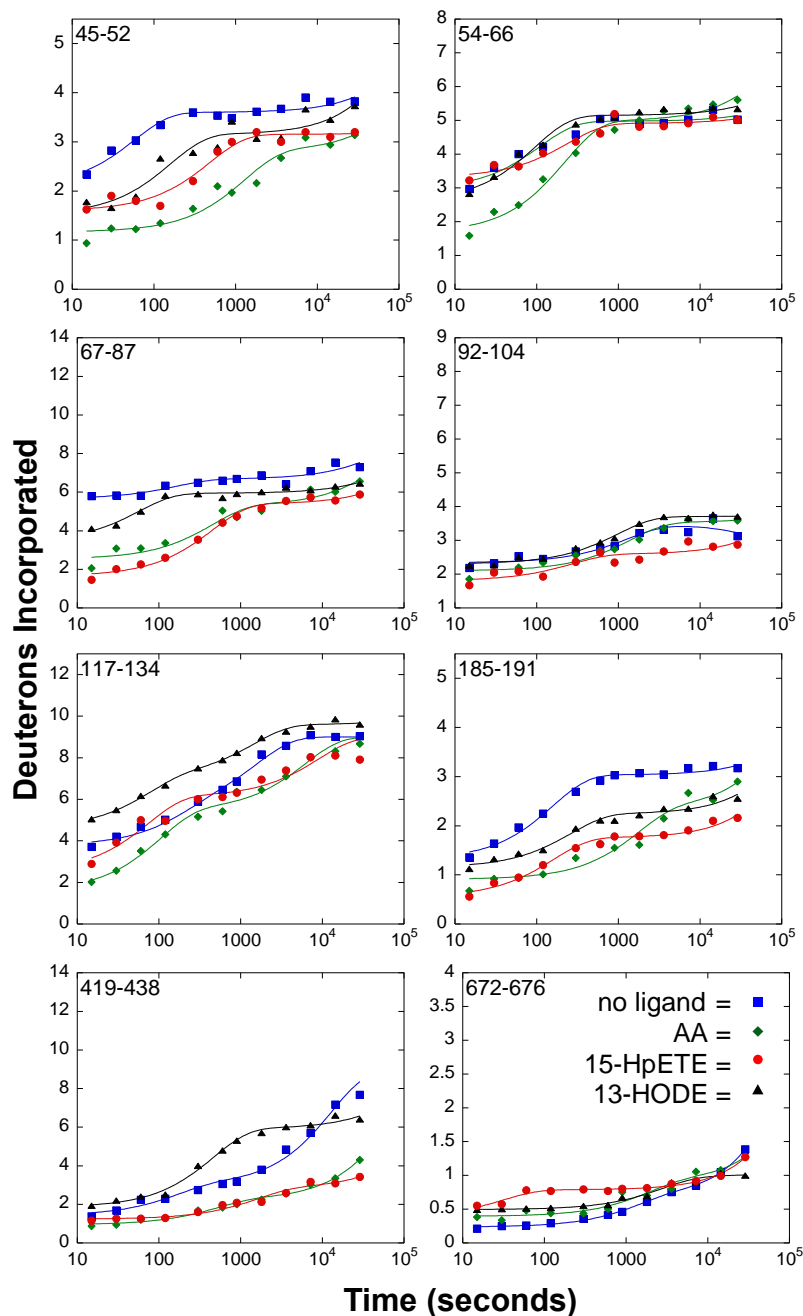


**Figure 25. Effects of ligand binding to 15-LOX-2.** The H/D exchange kinetic profiles of 15-LOX-2 are shown as a function of time. The y-axis represents the number of exchangeable sites in the peptide. Four different Ca<sup>2+</sup>-15-LOX-2 states are shown: (1) 15-LOX-2 with no ligand bound, (2) 15-LOX-2 with 250  $\mu$ M AA, (3) 15-LOX-2 with 250  $\mu$ M 15-HpETE, and (4) 15-LOX-2 with 250  $\mu$ M 13-HODE. The rate constants and amplitudes from this data are provided in Table 4.

An interesting observation from this data is that the deuterium incorporation for peptides 45-52, 67-87, and 185-191 in Ca<sup>2+</sup>-15-LOX-2 with bound 15-HpETE is less than the deuterium incorporation for Ca<sup>2+</sup>-15-LOX-2 with bound 13-HODE (Figure 25). For example, peptide 67-87 shows approximately 4 deuterons incorporated after 15 seconds of H/D exchange in the Ca<sup>2+</sup>-15-LOX-2 complex with 13-HODE compared to approximately 2 deuterons incorporated in Ca<sup>2+</sup>-15-LOX-2 complexed with 15-HpETE. Another, interesting result for the Ca<sup>2+</sup>-15-LOX-2/ 13-HODE complex is that peptides 117-134 and 419-438 exhibit increased deuterium incorporation when compared to Ca<sup>2+</sup>-15-LOX-2. This indicated the protein backbone becomes either more flexible or more solvent exposed due to conformational changes that occur upon ligand binding.

## Discussion

### *Conformational changes in the 15-LOX-2 PLAT domain upon lipid binding*

Knowledge of substrate binding in LOX has significantly improved since the first mammalian LOX, rabbit 15-LOX-1, was crystalized in 1997.<sup>106</sup> The active site in LOXs is hypothesized to be highly dynamic as binding of an inhibitor to rabbit 15-LOX-1 structure induced a 12 Å movement in  $\alpha$ -helix 2 and a substantial rearrangement of the active site shape. In addition, 15-LOX is able to oxygenate AA-containing phospholipids and cholesteryl esters, which implies the active site is able to adapt to bind ligands with bulky head groups.<sup>131</sup> As previously discussed, the H/D exchange data in our research also indicates that the exterior of the active site is highly dynamic.

In the H/D exchange experiments featured in this chapter that focus on substrate binding in Ca<sup>2+</sup>-15-LOX-2 we observe a decrease in deuterium incorporation at the exterior region of the active site (peptides 185-191 and 419-418) upon substrate binding. This implies that lipids in the

active site are coordinated by the exterior of the active site in a way that shields the peptide backbone from H/D exchange. An alternative explanation is that lipid binding reduces the flexibility of the active site exterior. Interestingly, there was no corresponding observable change in the H/D exchange in the interior of the active site. As these peptides experience low deuterium even incorporation in ligand free 15-LOX-2 it would be difficult to detect solvent shielding effects. Nevertheless, the lack of changes in H/D exchange in the active site interior in the presence of AA does, at the very least, suggest that the active site is not opened in a way that allows solvent accessibility upon substrate binding.

AA-induced changes in H/D exchange kinetic profiles were observed in both the active site in the catalytic domain and select regions of the PLAT domain. Traditionally, PLAT and C2 domains were primarily thought to function only as membrane associating domains.<sup>36</sup> However, recent work suggests a plausible communication site between the PLAT and catalytic domains in LOXs that implies the PLAT domain may play a role in regulating LOX activity.<sup>72</sup> There is a conserved  $\pi$ -cation interaction between a tryptophan in the PLAT domain and lysine or arginine in the catalytic domain observed in all mammalian LOX crystal structures. Moreover, multiple sequence alignments reveal the amino acids involved in this interaction are conserved throughout the enzyme superfamily (Figure 26). In 15-LOX-2, this interaction is between W109 on PLAT domain  $\beta$ -strand 7 and K175 on catalytic domain  $\alpha$ -helix 2. A crystal structure of a truncated version of 12S-LOX that lacks the PLAT domain revealed significant positional shifts in  $\alpha$ -helix 2 when compared to other LOX crystal structures, implying the physical restraint imposed by the PLAT domain may play a role in positioning  $\alpha$ -helix 2.<sup>83</sup> In addition, a W98A mutation in 12/15-LOX, which corresponds to W109 in 15-LOX-2 (see Figure 26), decreased the enzymatic turnover rate. This loss of activity was associated with changes in inter-domain orientations, as the 12/15-

LOX molecular diameter increased and its thermal stability decreased. These studies imply an important role for PLAT and catalytic domain communication in the LOX catalytic mechanism.<sup>84</sup>

15-LOX-2	99	GHLLFPCYQWL	170	LELNIKY
15-LOX-1	89	DEVRFPCYRWV	160	LPVDERF
5-LOX	92	DYIEFPCYRWI	163	LPRDIQF
12-LOX	88	AEVAFPCYRWV	160	LPPNMRF
12-LOX-2	94	RIYHFPAYQWM	196	LNLNLRV

**Figure 26. The conserved  $\pi$ -cation bridge that connects the PLAT and catalytic domains.** A partial sequence alignment of the PLAT domain and the loop that leads to  $\alpha$ -helix 2 is shown to demonstrate the amino acids that create the  $\pi$ -cation interaction. The amino acids that form the interaction are in blue, while other conserved amino acids are in red.

One of the more interesting results of this work was that there are changes in H/D exchange in the PLAT domain upon lipid binding to the catalytic domain, which supports the importance of the previously-hypothesized interdomain communication (Figure 27). Exactly how occupation of the active site alters the structure of the PLAT domain is not established by our data, but our results support the presence of important interdomain communications, as it appears lipid binding to the active site alters H/D exchange profiles in the PLAT domain.

An alternative explanation for substrate-induced decreases in deuterium incorporation in the PLAT domain is AA binding to a secondary allosteric site that is proposed to be located between the PLAT and catalytic domains.<sup>110</sup> LOX have been shown to be allosterically regulated by their enzymatic products.<sup>146</sup> However, the allosteric site in 15-LOX-2 is highly specific to 13-HODE, the oxygenated product of LA. This site binds 13-HODE but not 15-HpETE or 12-HpETE.<sup>110</sup> This suggests it is unlikely that the decreases in deuterium incorporation in the PLAT domain are due to direct AA binding to the secondary allosteric site. In addition H/D exchange with 13-HODE was investigated and displayed differences in some unliganded 15-LOX-2 peptide

H/D exchange profiles, when compared to conditions with bound AA. Another explanation could be a nonspecific hydrophobic interaction between an AA micelle and the PLAT domain. However, this seems unlikely as the shielding of H/D exchange that results from the presence of AA was not observed when nanodiscs or other micelles were present (Figures 17 and 20).

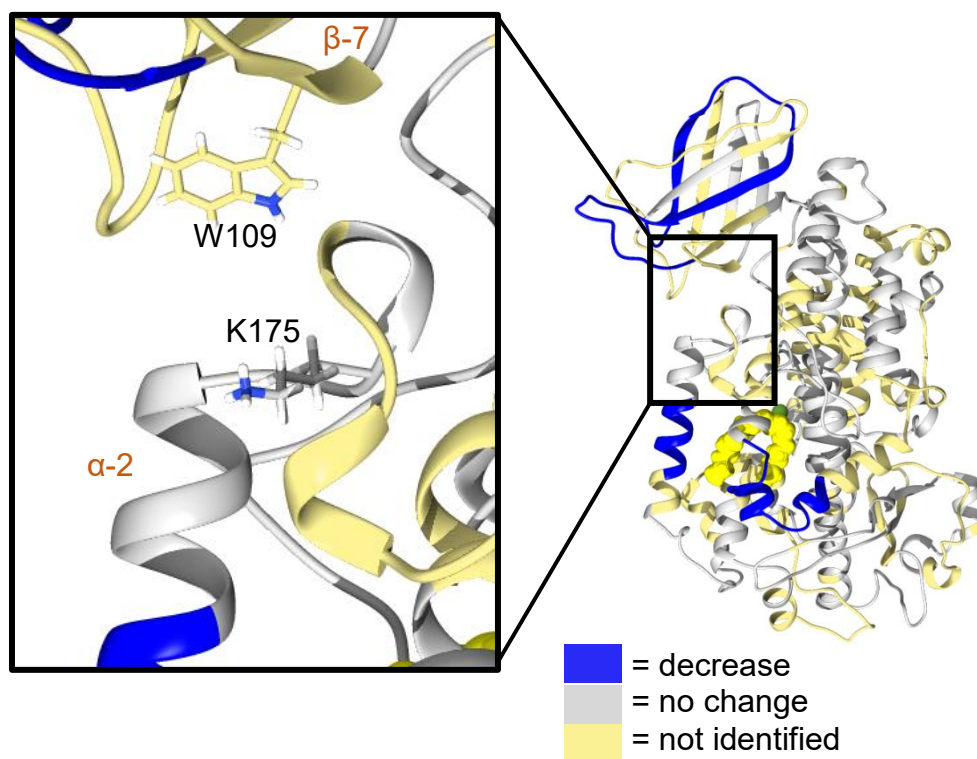


**Figure 27. The conserved  $\pi$ -cation bridge that binds the PLAT and catalytic domain. W109 and K175 are invariant amino acids in the LOX superfamily and are proposed to play a role in domain communication. Here they are highlighted as the possible lynchpin linking decreases in  $\alpha$ -helix 2 H/D exchange upon AA binding to the decreases observed in the PLAT domain.**

### *Binding of 13-HODE to 15-LOX-2 changes the active site structure*

Previous work by Dr. Theodore Holman's laboratory demonstrated the role of 13-HODE as an allosteric regulator for 15-LOX-2. These studies were unable to identify the allosteric binding site or elucidate the molecular or structural mechanism of allostery.<sup>110</sup> Binding of 13-HODE to 15-LOX-2 activates the oxygenation of AA and inhibits the oxygenation of another 15-LOX-2 substrate, GLA. This indicates the allosteric structural changes at the active site are able to discriminate between differences in the length and unsaturation of these ligands. The structural changes that result upon 13-HODE binding were investigated in this study by H/D exchange MS techniques. The differentiation between structural changes induced upon 13-HODE binding to the allosteric site and structural changes induced upon 13-HODE binding to the active site was achieved by comparing H/D exchange results to Ca<sup>2+</sup>-15-LOX-2 with bound 15-HpETE. 15-HpETE binds to the active site, but does not allosterically regulate 15-LOX-2.

Peptides 45-52, 67-87, and 185-191 from both the PLAT and catalytic domains experienced a decrease in deuterium incorporation upon 13-HODE and 15-HpETE binding indicating these effects are due to ligand binding to the active site and shielding of the peptide backbone from H/D exchange (Figure 28). In addition, comparison of deuterium incorporation in Ca<sup>2+</sup>-15-LOX-2 with bound 13-HODE and Ca<sup>2+</sup>-15-LOX-2 with bound 15-HpETE revealed less deuterium incorporation upon 15-HpETE binding in select peptides (Figure 25) implying 15-HpETE has a greater shielding effect on the active site. This data corresponds with enzyme kinetic studies that show AA (converted to 15-HpETE) has a greater K<sub>m</sub> than LA (converted to 13-HpODE). Therefore, these studies indicate that the active site favors the longer carbon chains with higher degrees of unsaturation.<sup>146</sup>

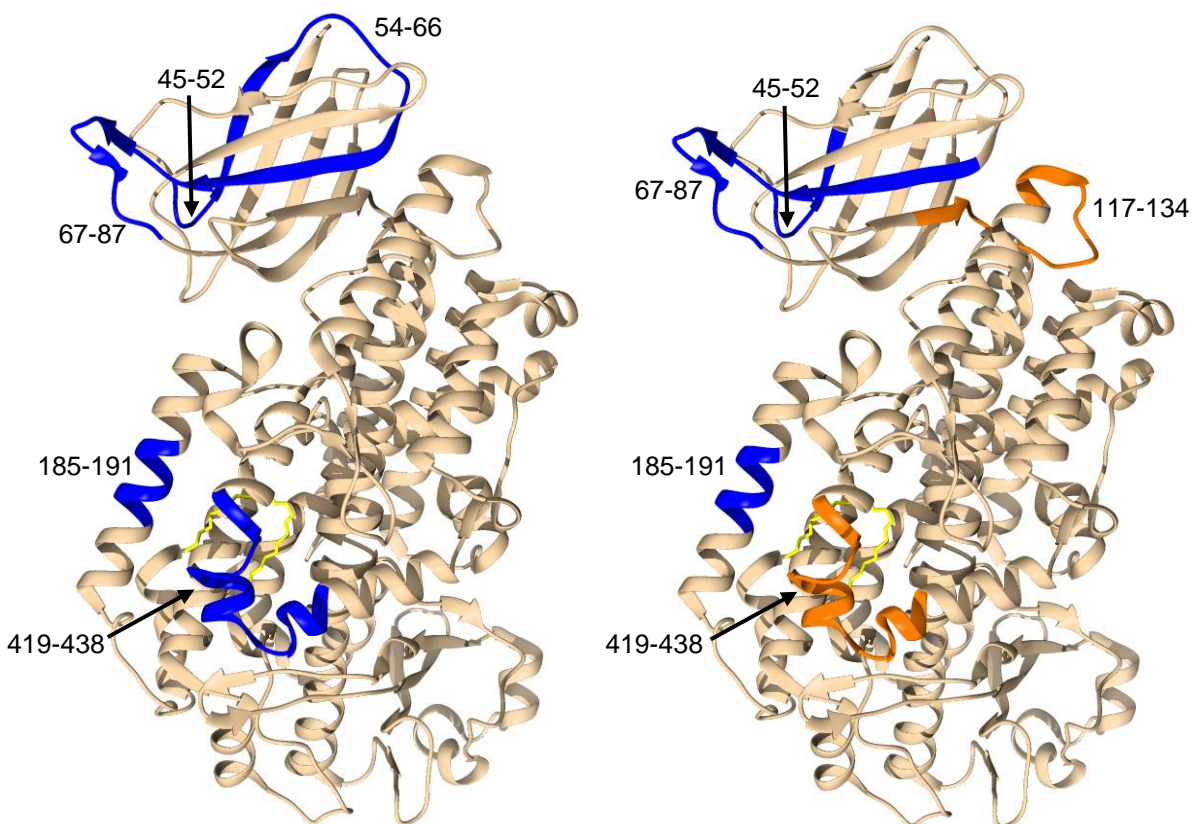


**Figure 28. Comparison of H/D exchange kinetics upon 15-HpETE and 13-HODE binding to 15-LOX-2.** (A) The impact of ligand binding on the H/D exchange behavior of 15-LOX-2. The effects of 15-HpETE are shown in A, and the effects of 13-HODE are in B. Peptides exhibiting enhanced exchange are shown in orange while regions with decreased exchange are in blue. 15-LOX-2 active site is emphasized by showing the binding of C8E4 to 15-LOX-2 active site.

Protection from H/D exchange due to 13-HODE interacting with the peptide backbone of 15-LOX-2 in the allosteric binding site was not observed. This could be due to the site being located in an area of 15-LOX-2 that does not have analyzable peptides or that 13-HODE is bound in a way that does not shield the peptide backbone from H/D exchange. Peptides 117-134 and 419-438 undergo an increase in deuterium incorporation upon 13-HODE binding to  $\text{Ca}^{2+}$ -15-LOX-2, indicating the peptide backbone is becoming more solvent exposed through increases in backbone flexibility or structural changes. The explanation for peptide 117-134 H/D exchange kinetics upon



13-HODE binding is not obvious as this peptide forms the unstructured linker between the PLAT and catalytic domain, and no previous work has implicated this part of the structure in regulation of enzymatic activity. The allosteric site is predicted to lie in the cleft located between the PLAT and catalytic domains. Therefore, it is possible that binding of 13-HODE forces the domains of 15-LOX-2 into an arrangement that changes the orientation of the linker. Peptide 419-438 forms the exterior of the active site entrance. Increased deuterium incorporation implies the active site entrance is more solvent exposed or more dynamic. A common paradigm in positive allosteric interactions is modification of an active site that facilitates substrate binding.<sup>147</sup> An opening of the active site in 15-LOX-2 would allow for an increase in substrate binding, however it does not explain how binding 13-HODE changes substrate specificity.

Synthetic allosteric regulators present an opportunity to specifically regulate LOXs enzymatic activity. Changing the proportions of LOX products, as opposed to inhibiting the enzymatic activity could allow beneficial LOX activity to continue while still down-regulating the biosynthesis of inflammatory mediators. Further studies on 13-HODE allosteric regulation of 15-LOX-2 are needed to fully interpret the H/D exchange data obtained in this study.

### *Conclusions*

Backbone amide H/D exchange analysis is an excellent tool to map the structural dynamics of purified protein targets upon ligand binding. Differentiation between direct effects of ligand binding and the impact of binding on global conformational dynamics is difficult and requires previous structural and molecular studies for interpretation. One of the more intriguing results from this study is that despite the lack of strong conformational coupling between the PLAT and catalytic domains, the data presented in this study nevertheless suggest that binding of AA to the

active site plays a role in regulating the structural dynamics of the PLAT domain. In addition, our H/D exchange studies with allosteric regulator, 13-HODE, suggest a structural mechanism for allostery, in which binding of 13-HODE results in the increased flexibility of the active site entrance. The H/D exchange kinetics reported here presents the first physical evidence for the role of structural dynamics in the enzymatic and allosteric mechanisms of 15-LOX-2.

## CHAPTER V

### EFFORTS TOWARDS DETERMINING 5-LIPOXYGENASE AND 5-LIPOXYGENASE ACTIVATING PROTEIN COMPLEX INTERACTIONS

5-LOX is the only identified LOX that requires complex formation with a membrane scaffolding protein (FLAP) for optimal activity in intact cells. FLAP is an integral membrane protein that is hypothesized to facilitate the transfer of AA from the nuclear membrane to 5-LOX for conversion to 5-HpETE and initiation of the LT biosynthesis pathway. However, this putative role of FLAP requires additional information for verification. The AA binding site in FLAP and the protein-protein interaction sites in the 5-LOX-FLAP complex have not been identified. This work sought to use H/D exchange to elucidate the protein and ligand interactions in this important protein complex.

#### Results

##### *Expression and Purification of FLAP*

Expression and purification protocols for recombinant 5-LOX and FLAP have been published;<sup>116,88</sup> however, these protocols are hindered by low yields for FLAP and loss of enzymatic activity for 5-LOX. Therefore, the initial step of this investigation was to optimize protein expression and purification. Increased FLAP expression was achieved by expression trials utilizing differing expression vectors, competent cells, growth media, and induction points. Expression trials with different vectors revealed that vectors with low copy numbers (pET-28b and pET-21b) increased FLAP expression when compared to a vector with a high copy number (pUC57). Competent cells that are selected for increased membrane protein expression, such as

C41(DE3) and C43(DE3), increased FLAP expression when compared to the standard BL21 cells used in the previously published protocol.<sup>116</sup> Expression tests with different types of growth media showed minimal media supplemented with glucose as a carbon source, and casamino acids, increased FLAP expression compared to the nutrient rich Terrific Broth and Luria Broth. Combining the data from the expression trials led to a protocol for optimal FLAP expression. A gene encoding full-length FLAP with a C-terminal His-tag and optimized codons was cloned into the pET-21b vector for *E. coli* expression. This vector was transformed into C43(DE3) competent cells and cells were grown at 37 °C in minimal media. Recombinant protein expression was induced with 1 mM IPTG when OD<sub>600</sub> reached approximately 0.4. The optimized protocol described here produced between 2 and 5 mg of FLAP in 9 L of cell culture (Figure 29).

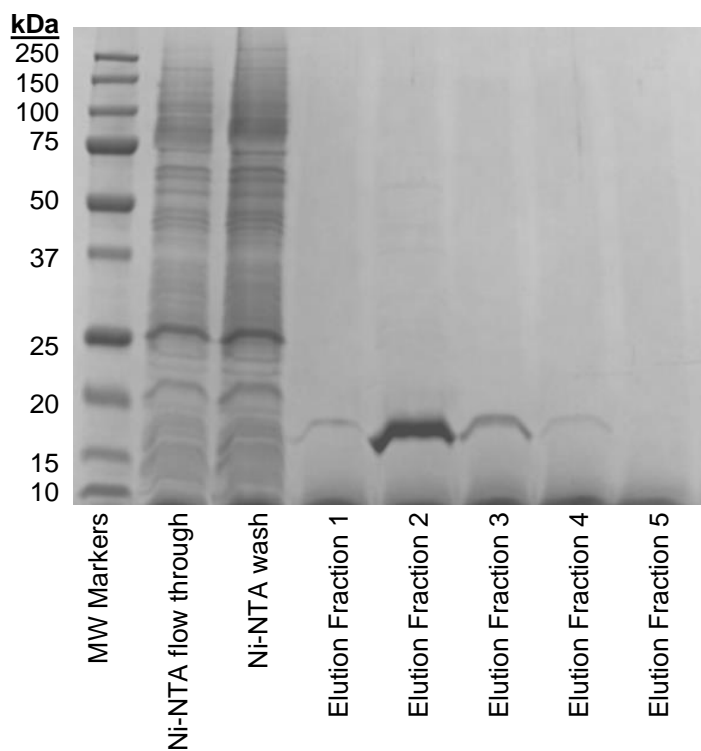


**Figure 29. SDS-page gel of purified FLAP.** FLAP was eluted from a gravity flow Ni-NTA column with an elution buffer containing 200 mM imidazole. 5 mL fractions were collected and run on an SDS-PAGE gel. All fractions were concentrated and used for FLAP experiments.

Purification of FLAP was accomplished by ultracentrifugation of the cell lysate to isolate the membrane fraction and subsequent solubilization of the membrane fraction in detergent micelles. To prevent protein aggregation, detergent screening was completed with different nonionic or zwitterionic detergents. The structural integrity and oligomeric state of FLAP were investigated by size exclusion chromatography (Figure 30). Elution from a High-Prep 16/60 Sephacryl-200 HR column was monitored by absorbance at 280 nm. A monodisperse signal peak was observed at 45 mL, which corresponds to an approximate Stokes radius of 5 nm. This radius reflects the homotrimer formation of FLAP. Fractions were collected between 40 to 50 mL for further studies (Figure 30).

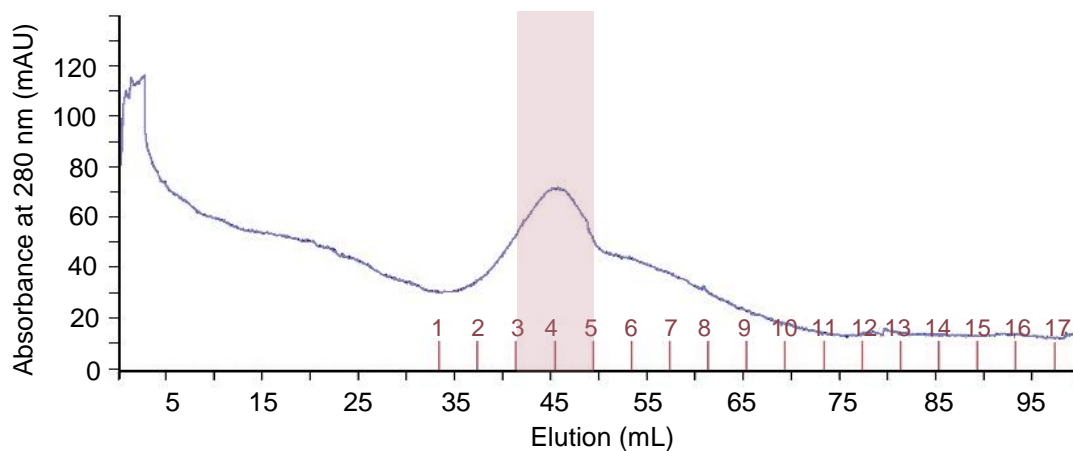


**Figure 30. Size exclusion chromatography of FLAP.** FLAP was purified on a High-Prep 16/60 Sephacryl-200 HR column to analyze FLAP size homogeneity. FLAP eluted with a Stokes radius of 5 nm corresponding to a FLAP homotrimer.

#### *Activity of 5-Lipoxygenase*

The published protocol for expressing and isolating 5-LOX produces sufficient yields for H/D exchange studies, and the slight changes in the expression and purification protocols

completed in this work did not affect the protein yield. However, 5-LOX has been observed to lose activity after purification.<sup>86</sup> Therefore, 5-LOX was mutated in previous work to increase the enzymatic half-life. The mutated version of 5-LOX, Stable 5-LOX, was used in these studies, but there was an inconsistency in activity between various protein purification batches. The highest specific activity measured was  $35 \frac{\text{nmol}}{\text{min}\cdot\text{mg}}$  which is significantly less than the previously published kinetic data.<sup>87</sup> To observe the time dependence of the enzymatic activity, 5-LOX activity was monitored 1, 8, and 20 hours after purification and stored at 4 °C in between time points. The specific activity was reduced by half after 8 hours and decreased to less than  $1 \frac{\text{nmol}}{\text{min}\cdot\text{mg}}$  after 20 hours. Addition of oxygenated product has been shown to increase LOX activity by activating the catalytic iron.<sup>86</sup> However, in this study addition of 13-HODE and 15-HpETE to 5-LOX activity assays did not increase the specific activity of 5-LOX.

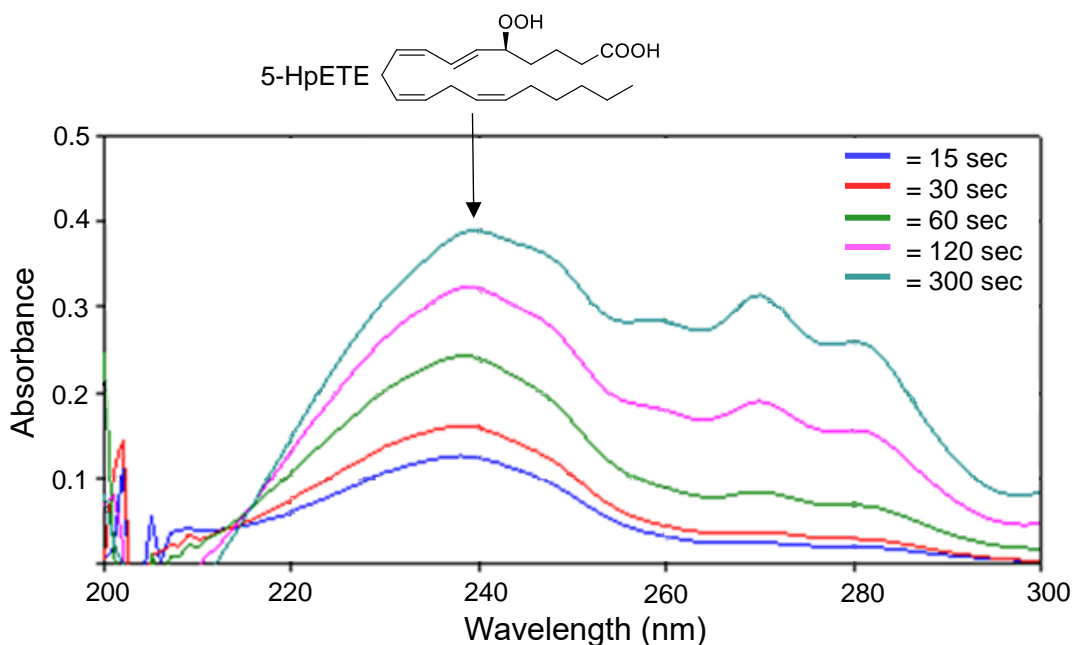


**Figure 31. 5-LOX dual activity.** The UV-Vis spectrum of 5-LOX used for activity assays shows several peaks, with the first peak at 238 nm corresponding to the HpETE product and the second peak at 270 nm corresponding to hydrolysis products of LTA<sub>4</sub>.

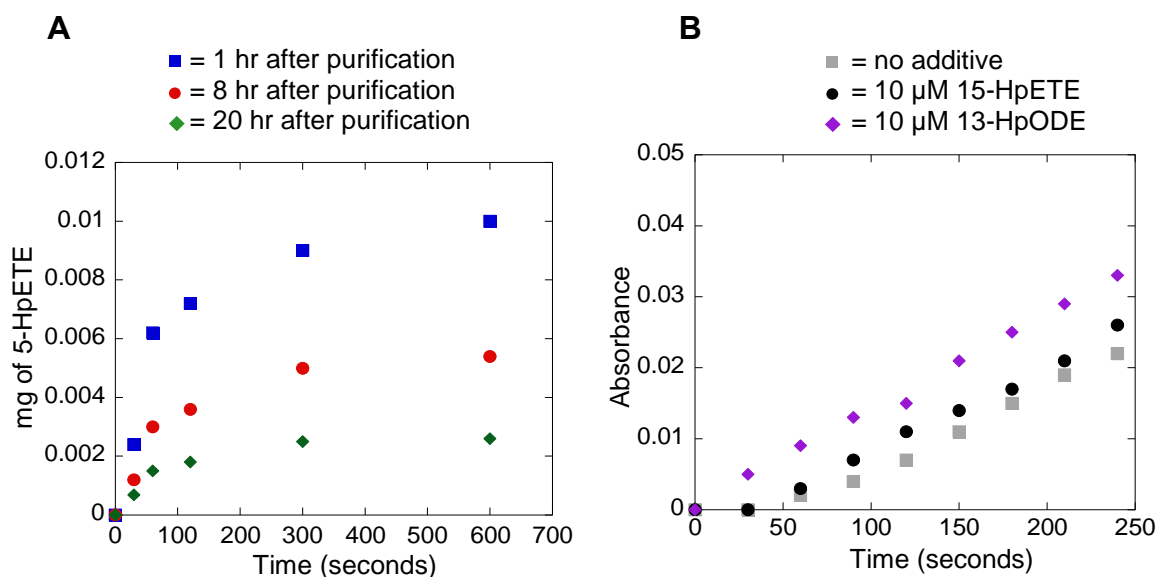


**Figure 32. 5-LOX loss of activity.** (A) Formation of the HpETE product plotted vs time to determine 5-LOX activity. Protein stored at 4 °C was tested at different time points after the final purification step to observe loss of 5-LOX activity over time. (B) Testing the effect of adding oxidized lipids to reactive the catalytic iron on 5-LOX activity assay. No significant increase in 5-LOX activity was observed.

#### *Peptide Mapping of 5-LOX and FLAP*

Prior to collecting H/D exchange-MS data, peptide maps of FLAP and 5-LOX were determined. Optimization of peptide mapping was completed by varying sample conditions, MS parameters, and HPLC gradients. For 5-LOX, three different proteases (pepsin, protease XIII, and protease XVIII) were tested at various molar ratios with 5-LOX. A 1:3 5-LOX: pepsin molar ratio provided higher coverage when compared to the other acidic proteases. In addition, digestion times from 4 to 11 minutes were tested, with 9 minutes providing optimal peptide generation. A peptide map with 88% sequence coverage and 115 peptides (ranging from 4 to 24 residues) was created by using these digestion conditions for sample preparation (Figure 33). This high sequence coverage allowed us to continue with H/D exchange experiments.

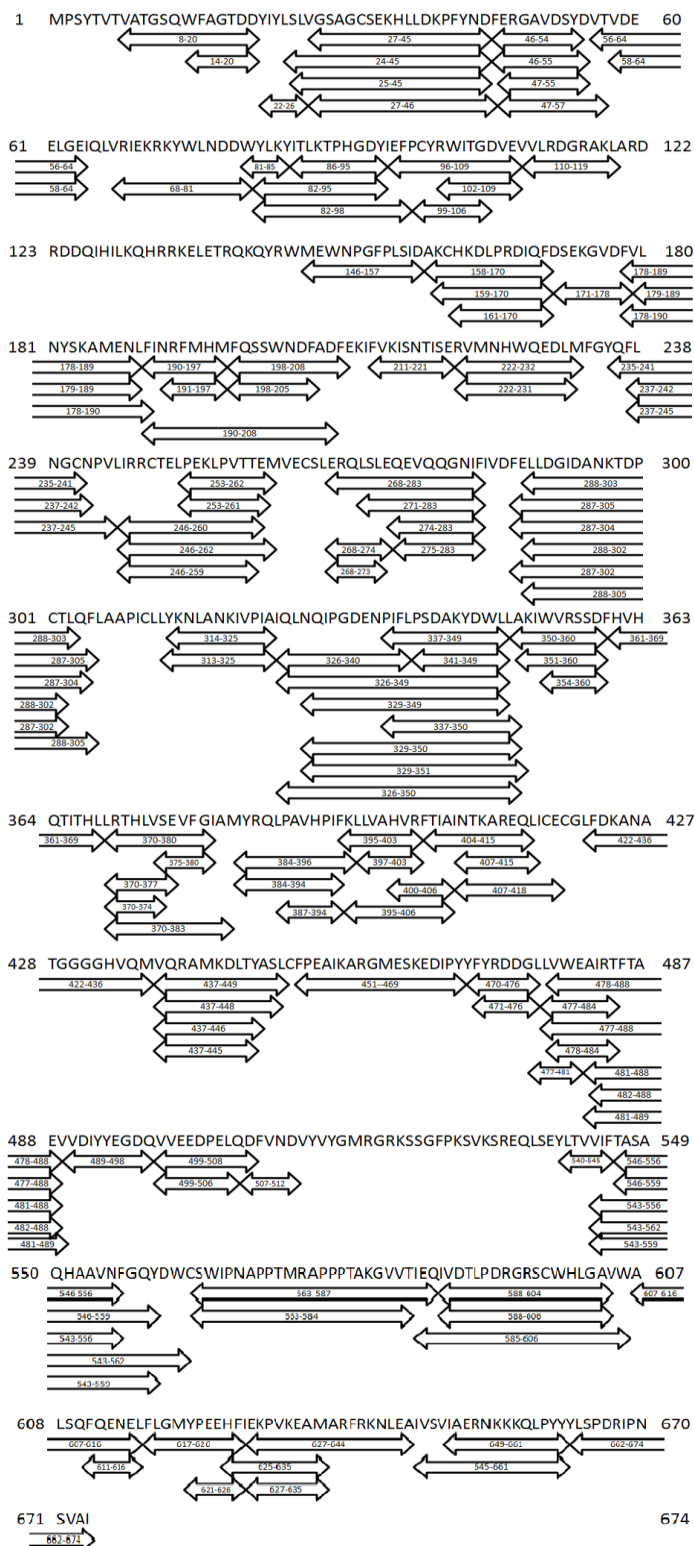


**Figure 33. Preliminary Peptide Map of 5-LOX.** Peptide map created by pepsin digest of 5-LOX. Peptides were separated, ionized, and fragmented using HPLC coupled to MS/MS. Peptides were identified using the computational program PEAKS.



Peptide mapping of FLAP was completed in a manner similar to that of 5-LOX, but was complicated by the presence of detergent. Detergents suppress the ionization of sample through charge competition in ESI. Therefore, initial detergent trials with various concentrations of DDM and CHAPS were completed to find the minimal concentration of each detergent required to avoid protein aggregation. FLAP was stable at 4 °C for several days in 0.05% DDM and 0.7% CHAPS. FLAP in DDM micelles provided greater peptide coverage compared to FLAP in CHAPS micelles and was used in peptide mapping optimization trials. However, FLAP still experienced consistently low sequence coverage. Adding denaturing agents such as urea and guanidine hydrochloride increased the peptide coverage from approximately 30% to 50%. The highest sequence coverage was obtained with FLAP stored in 20 mM Tris, 300 mM KCl, 2.5% glycerol, 1 mM DTT, 0.05% DDM, pH=7.5. A 1:1.5 FLAP: pepsin molar ratio and a 7 minute digestion time provided 54% sequence coverage. Due to low ion envelope resolution, only select peptides could be analyzed in subsequent H/D exchange experiments; therefore the coverage dropped to 35.4%.

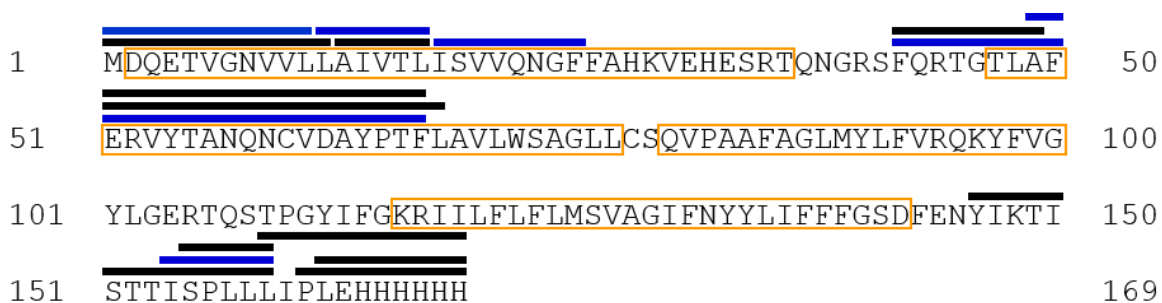


**Figure 34. Peptide Map of FLAP.** Peptide map created by pepsin digestion of FLAP. Peptides that were identified and had measurable ion envelope resolutions are labeled in blue and were used in subsequent H/D exchange studies. Peptides in black were identified by fragmentation but could not be analyzed due to low  $m/z$  signal.

### *H/D exchange of native and ligand bound FLAP*

H/D exchange experiments with FLAP were completed with the limited peptide map to determine structural dynamics in regions of the FLAP trimer. The levels of deuteration for six peptides were analyzed for FLAP without ligand bound. Several of the peptides (12-18, 18-25, and 150-159) demonstrated less than 20% deuteration after 2 hours of H/D exchange (Figure 35). This indicates the peptides are protected from solvent exposure by interactions due to stable secondary structure or burial in detergent micelles. Peptide 42-50 is 75% deuterated during this time period, indicating it is highly flexible and partially solvent exposed (Figure 35). Peptide 49-67 experienced a significant increase in deuterium incorporation between 15 and 60 seconds, indicating local fluctuations in folding that allow solvent to access a protected region of the protein. (Figure 36)

When FLAP was in the presence of AA (250  $\mu$ M), only one of the six peptides showed a difference in deuterium incorporation over 2 hours of H/D exchange. Peptide 49-67 showed a significant decrease in the rate of deuterium incorporation at the 15 and 60 second time points, indicating this area of the protein either undergoes conformational changes that leads to solvent protection or is involved with ligand binding (Figure 36). Data collection with FLAP in the presence of inhibitor MK-886 (100  $\mu$ M) was complicated by low signal. When FLAP was in the presence of MK-886, only peptides 12-18, 18-25, 42-50, and 150-159 could be measured for deuterium incorporation (Figure 36). All of these peptides showed similar deuterium incorporation for native and MK-886 bound FLAP, indicating inhibitor binding does not change the structural dynamics for the segments from which these peptides were derived.

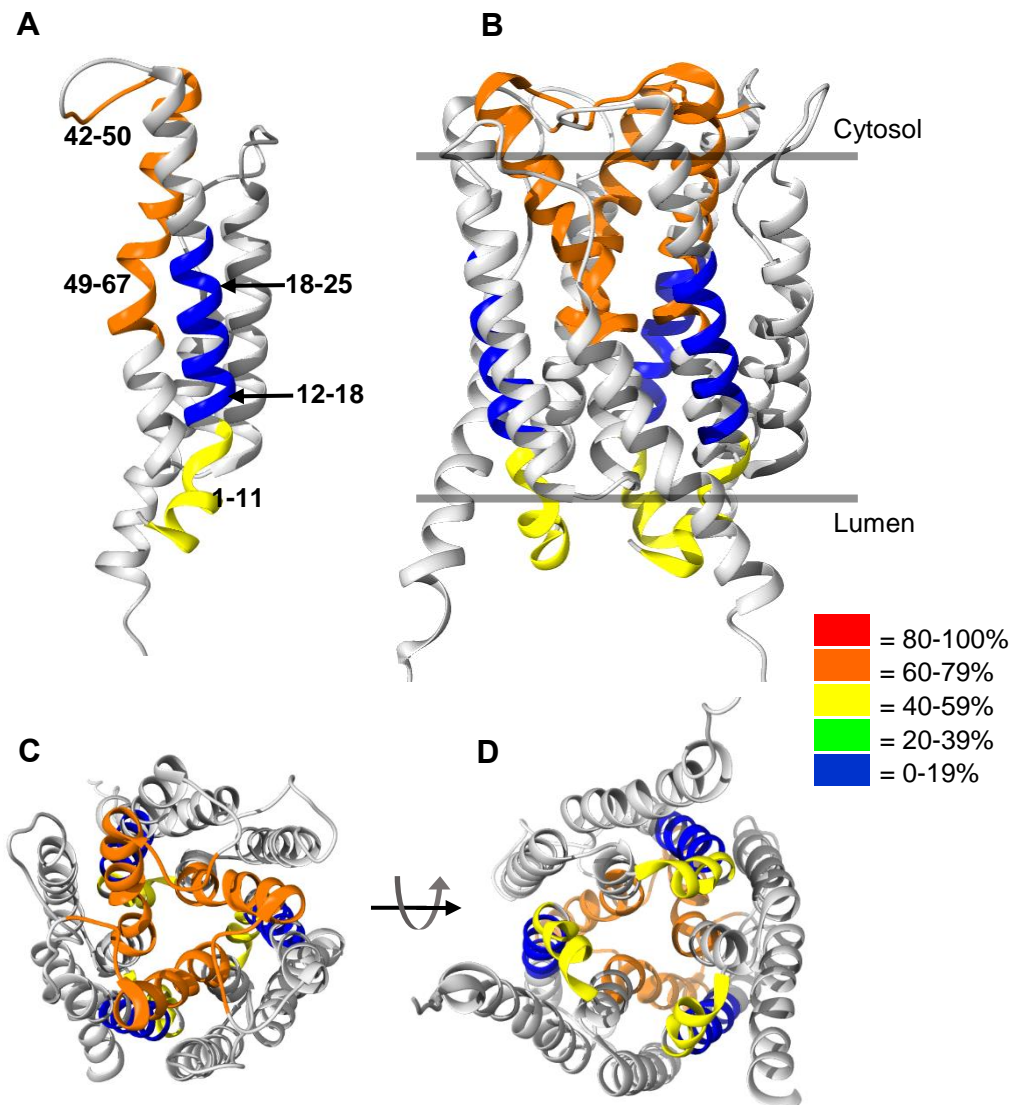


**Figure 35. Structural dynamics of apo-FLAP.** Deuteration levels following 2 hour of incubation in  $D_2O$  in apo-FLAP are mapped onto the crystal structure (PDB entry 2Q7R, with LT biosynthesis inhibitor MK-591 bound) to provide information on general flexibility and solvent exposure. Gray indicates that peptides were not identified in that area. (A) FLAP monomer with peptides referred to in this work designated by their sequence range. (B) FLAP trimer. (C) View from cytosol of FLAP. (D) View from lumen of FLAP.

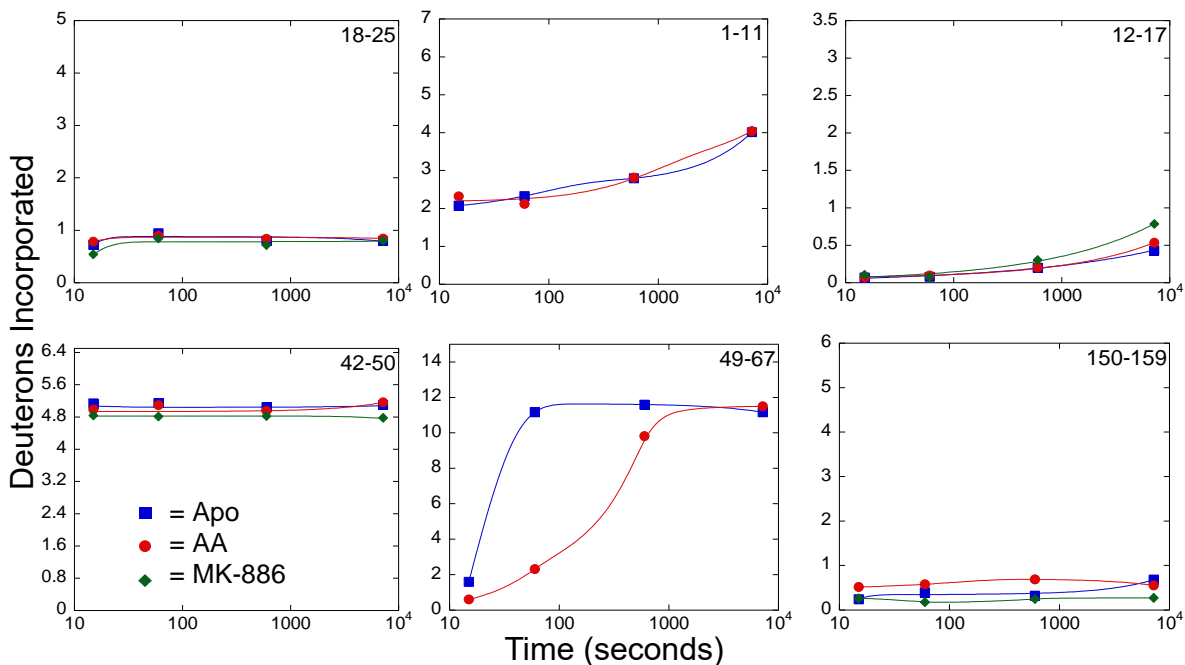


**Figure 36. H/D exchange profiles for FLAP peptides.** Deuterium incorporation at 15, 60, 600, and 7,200 seconds was measured and plotted for each peptide. Three different states of FLAP were tested; (1) apo-FLAP, (2) FLAP with AA bound, and (3) FLAP with MK-886 bound.

## Discussion

### *FLAP protein expression is limited due to cell toxicity*

The initial step in this project was to increase the expression of FLAP. Membrane protein expression can be complicated by the tendency for membrane proteins to form inclusion bodies and the potential toxicity associated with their heterologous overexpression in *E. coli* cells, frequently resulting in cell death. Toxicity can be caused by overexpression of membrane proteins leading to membrane destabilization and leakage or pore formation.<sup>148</sup> The published protocol for expression of FLAP utilized BL21 cells and the pET28 vector.<sup>116</sup> When that protocol was used for these studies, only micrograms of FLAP could be purified from 9 L cell cultures. Here, an optimized protocol utilizing C43 competent cells and pET 21b was derived from systematic

expression tests. These tests indicated that use of competent cells optimized for membrane protein expression dramatically increased FLAP expression. C43 competent cells overexpress AtpF, the *E. coli*  $\beta$ -subunit of the  $H^+$ -ATP synthase. This results in a large network of internal membranes providing a suitable environment for membrane protein folding. We found that plasmids with high copy numbers were unfavorable for expression, most likely due to rapid protein production and the subsequent cell death associated with toxicity. The protocol established in this work produced approximately 2 to 5 mg of FLAP from 9 L cell cultures. Proper folding and trimer formation for FLAP was indicated by size exclusion chromatography.

#### *Recombinant 5-LOX activity significantly decreases after protein purification*

The specific activity observed for 5-LOX in these studies was inconsistent and significantly less than previously reported.<sup>88</sup> One possible explanation for low 5-LOX activity may be the method of measuring product formation in this work. The UV-Vis spectrometer assay monitors the absorbance of the conjugated double bonds formed in the HpETE product at 238 nm. 5-LOX is a dual function enzyme that transforms 5-HpETE to LTA<sub>4</sub>, the hydrolysis products of which have a max absorbance at 270 nm (Figure 31). Low and inconsistent activity observed in 5-LOX may be due to structural damage leading to loss of the catalytic iron coordination.

An alternative explanation for 5-LOX loss of activity is an inactive oxidation state of the catalytic iron upon 5-LOX purification. LOX kinetics have demonstrated a relatively long lag phase preceding steady-state kinetics due to the oxidation state of the catalytic iron. When 5-LOX is in an inactive state, the catalytic iron is in the ferrous state and it does not oxidize to a ferric state in the presence of molecular oxygen. *In vivo*, it is hypothesized that autoxidation of substrates leads to a small amount of non-enzymatically produced LOOH. These LOOH are able to oxidize

the catalytic iron to the active Fe<sup>3+</sup> oxidation state.<sup>130</sup> In these studies, addition of 13-HpODE and 15-HpETE to activity assays did not significantly increase 5-LOX enzymatic activity, indicating the loss of activity observed for 5-LOX is most likely due to structural integrity as opposed to the catalytic iron (Figure 32).

*AA binding results in shielding of the FLAP hydrophobic cavity from H/D exchange*

Due to low peptide coverage in FLAP, minimal H/D exchange data could be analyzed (Figure 34). The detergents used to solubilize membrane proteins contribute to suppression of ion generation in ESI. Ion suppression results from the presence of less volatile compounds changing the efficiency of droplet formation or droplet evaporation in ESI, decreasing the amount of charged ions in the gas phase that reaches the detector, thereby lowering sample signal.<sup>149</sup> Multiple attempts at decreasing detergent concentration in FLAP H/D exchange samples and adjusting MS parameters did not increase peptide identification or improve the ion envelope signal in H/D exchange.

Little insight has been obtained regarding how AA binds to FLAP. The H/D exchange studies in this work provided some evidence. We observed a decrease in deuterium incorporation in peptide 49-67 upon addition of AA to FLAP (Figure 36). The remaining peptides analyzed do not experience any changes in H/D exchange profiles. Mapping the H/D exchange data onto the crystal structure of FLAP (that has inhibitor MK-591 bound) indicated that the central cavity of FLAP experienced protection from H/D exchange upon AA binding (Figure 37). Due to the inherent complications in interpreting H/D exchange data, the decrease could be due to ligand binding to this peptide or conformational changes upon AA binding, resulting in less solvent exposure. Previously published radioligand binding assays indicated the AA binding site overlaps

with the binding site for MK-591, which is between helix 1 on one monomer and helix 4 on the adjacent monomer in the FLAP homotrimer.<sup>150</sup>

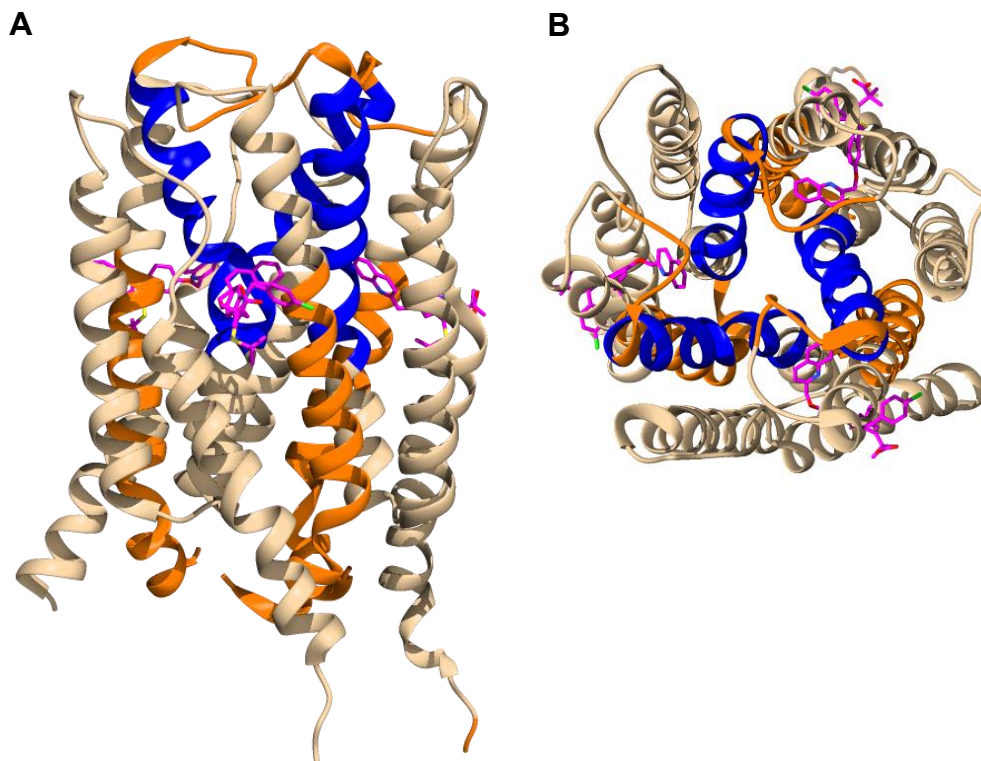


**Figure 37. AA binding induces changes in H/D exchange in FLAP.** Effects of AA binding to FLAP are mapped onto the FLAP crystal structure (with MK-591 bound, PDB entry 3O8Y). Peptides that experienced decreases in deuterium incorporation are in blue. Peptides that did not experience changes in deuterium incorporation are in orange, and peptides that are not identified are in gray.

This limited information on the AA binding site supports both proposed explanations of the H/D exchange data. The indole moiety of MK-591, which binds in a similar position as MK-886, is directed towards helix-2 (which contains peptide 49-67 and its part of the hydrophobic cavity); therefore AA could be directly interacting with this helix upon binding (Figure 37).<sup>116</sup> Alternatively, FLIM studies completed with an acceptor fluorophore on the C-terminus of FLAP and a donor fluorophore on the N-terminus indicated substrate induced changes in the orientation of the termini, supporting the hypothesis that the orientations of the TM helices shift upon AA

binding. It is plausible that changes in helical orientations lead to different conformations of FLAP that decrease solvent accessibility to the hydrophobic cavity.<sup>34</sup> A more complete peptide map of FLAP would provide essential information for a specific explanation of the H/D exchange data collected.

### *Conclusions*

This work has established an optimized expression protocol and a purification method that maintains proper membrane protein folding for FLAP. H/D exchange studies with 5-LOX were prevented due to structural degradation of 5-LOX leading to decreased activity over the time periods required for H/D exchange. Additional experiments are needed to establish a more stable form of 5-LOX that maintains its enzymatic activity and structural components. Deuteration levels of peptides after 2 hours of D<sub>2</sub>O incubation in FLAP indicate that local structural fluctuations allow solvent to access the hydrophobic cavity formed by the FLAP trimer. The hydrophobic cavity experiences significant decreases in deuteration upon AA binding, indicating that AA binds to the cavity, resulting in protection of the protein backbone from H/D exchange. An alternative explanation is that AA binding induces conformational changes that prevents solvent accessibility to the hydrophobic cavity. Additional experimental methods such as utilizing a peptide trap to remove detergent from FLAP H/D exchange samples before MS injection could be used to increase sequence coverage in the FLAP peptide map and improve ion envelope signal to complete the partial data collected in this study.



## CHAPTER VI

### CONCLUSIONS

Inflammation is part of the protective immune response that is important in the healing process. However, when not properly regulated, inflammation can trigger or contribute to a variety of diseases. Therefore, a large focus in pharmaceutical development is on therapeutics that regulate inflammation. This includes targeting the actions of proteins involved with the synthesis of eicosanoids. Eicosanoids are potent lipid mediators of inflammation. Two protein superfamilies involved in the biosynthesis of eicosanoids are the LOX and MAPEG superfamilies. This work focused on analyzing the structure and function of three proteins in these superfamilies, 15-LOX-2, 5-LOX, and FLAP. There is a large amount of information available on the structure and biological activity of these proteins, but information on the protein structural dynamics that play a role in ligand binding and LOX membrane association has been limited. Therefore, this work utilized H/D exchange MS to analyze 15-LOX-2 structural dynamics upon ligand binding, and membrane association. Moreover, the preliminary studies completed in this work with 5-LOX/FLAP protein and ligand interactions provide directions for future work.

#### *15-LOX-2*

We initiated these studies using H/D exchange MS to determine secondary structure flexibility and solvent exposure in native 15-LOX-2. Mapping the deuterium incorporation levels of excised 15-LOX-2 peptides onto the crystal structure of 15-LOX-2 led to several interesting observations for the possible roles of structural dynamics in 15-LOX-2 function.<sup>107</sup> The PLAT

domain is highly flexible, whereas the catalytic domain is much more ordered. In addition, H/D exchange profiles revealed the importance of structural dynamics in the exterior of the active site for the observed substrate promiscuity in 15-LOX-2. Moreover, the deuterium incorporation in the linker between the domains and in the domain interface suggests the likelihood of a high-degree of inter-domain flexibility. Protein dynamics upon  $\text{Ca}^{2+}$  binding were also investigated. However, no significant differences in H/D exchange were observed, indicating that 15-LOX-2 does not undergo structural changes upon binding  $\text{Ca}^{2+}$ .

We completed further analysis by comparing the H/D exchange kinetics of  $\text{Ca}^{2+}$ -15-LOX-2, both in solution and when the complex was associated with membrane-mimetic, nanodiscs. The H/D exchange profiles of peptides derived from nanodisc-associated  $\text{Ca}^{2+}$ -15-LOX-2 did not significantly differ from soluble  $\text{Ca}^{2+}$ -15-LOX-2, indicating that significant structural changes are not required for membrane association. The hydrophobic loop that protrudes from the PLAT domain (Figure 17), observed in the crystal structure, is not deeply buried in the membrane. Overall, our results challenge the previous hypothesis that  $\text{Ca}^{2+}$  binding induced-structural changes of the PLAT domain in 15-LOX-2 promote membrane association. An alternative method of membrane association is suggested in this work, in which the binding of  $\text{Ca}^{2+}$  changes the electrostatic potential of the PLAT domain to positive without changing the structural dynamics of 15-LOX-2. This allows the PLAT domain to interact with the negatively charged head group of PS. Further experiments on 15-LOX-2 membrane association are needed to assess this suggested model of membrane association.

In addition to investigating structural changes upon membrane association, we used H/D exchange MS to test the impact of substrate and allosteric ligands on 15-LOX-2. Addition of AA, and 15-HpETE resulted in shielding from H/D exchange in select peptides derived from the 15-

LOX-2 active site and PLAT domain when compared to ligand free  $\text{Ca}^{2+}$ -15-LOX-2. The changes in H/D exchange between the states were not  $\text{Ca}^{2+}$  dependent. There is no previous structural evidence for AA or its oxygenated products directly interacting with the PLAT domain, which led me to conduct several additional control experiments. The deuterium incorporation was observed to be dose dependent with a smooth decrease in deuterium incorporation associated with increased AA concentrations, indicating the changes in H/D exchange are not due to interaction with an AA micelle. Moreover, involvement of an unidentified allosteric binding site for AA seems unlikely as 15-HpETE binding also induces changes in H/D exchange. Previous studies found that 15-HpETE does not allosterically regulate 15-LOX-2 activity, and the allosteric site is highly specific for 13-HODE.<sup>110,151</sup> An alternative explanation is that binding of AA to the active site could regulate the structural dynamics of the PLAT domain. This data is most intriguing, particularly in light of the lack of strong structural coupling between the PLAT and catalytic domains.

The structural dynamics involved with the allosteric regulation of 15-LOX-2 oxygenation of AA was also investigated by H/D exchange MS. In these studies  $\text{Ca}^{2+}$ -15-LOX-2 and  $\text{Ca}^{2+}$ -15-LOX-2 with 13-HODE bound were compared. The data did not indicate the location of the 13-HODE allosteric binding site but did suggest a possible structural mechanism of allostery. The entrance of the active site appears to become more dynamic upon the binding of 13-HODE, suggesting that the active site is opened to increase substrate binding and promote 15-LOX-2 activity. The H/D exchange kinetics also implied that the linker between the PLAT and catalytic domain is affected by 13-HODE binding, suggesting that the interdomain conformations are changed during allosteric regulation. This work suggests that the structural dynamics of 15-LOX-2 play an important role in its enzymatic activity and allosteric regulation. Pharmaceuticals that alter the structural dynamics of 15-LOX-2, as opposed to a substrate antagonist that block substrate

binding, could lead to highly specific regulation of 15-LOX-2 activity. Our data suggest that it is plausible a drug that shifts the inter-domain conformation or decreases the flexibility of the active site could be a promising treatment for diseases that are associated with 15-LOX-2.

### *FLAP and 5-LOX*

Previous studies have shown a direct binding interaction between 5-LOX, and FLAP.<sup>115</sup> In addition, a direct interaction between AA and FLAP has been observed.<sup>34</sup> Combining this knowledge with the results of other studies can create a working model of how the 5-LOX-FLAP complex functions: Substrate AA that is trapped in the membrane binds to FLAP, which is an integral membrane protein. FLAP then facilitates AA transfer from the membrane to the active site of 5-LOX located above the membrane surface. Here we sought to use H/D exchange MS to analyze 5-LOX and FLAP protein-protein and protein-ligand interactions. We initiated this project by completing expression trials that lead to an optimization of FLAP expression in *E. coli*. Competent cells specialized for expressing toxic proteins, such as membrane proteins, were used. We also systematically tested expression conditions. These efforts led to greatly increased FLAP expression that facilitated H/D exchange experiments. However, this project was greatly hindered by loss of 5-LOX enzymatic activity upon protein purification. Another complication was the suppression of ion generation in ESI during peptide mapping for FLAP from the detergents used to solubilize FLAP. Nevertheless, a partial peptide map of FLAP provided limited H/D exchange data that allowed the identification of a putative AA binding location in the hydrophobic cavity formed by the FLAP homotrimer. The data also suggests that AA enters the cavity through the small opening between the TM helices. This is interesting because the passage of AA through this cavity in route to the 5-LOX active site is a key component of our working model for the

mechanism of FLAP/5-LOX action. This work is the first to identify regions of FLAP that interact with AA, which is a crucial step in structure-based drug development. While these results are limited, they do pave the way for possible future studies.

### Future Studies

In this work we found that changes in structural dynamics are not needed for 15-LOX-2 membrane association. We also completed experiments with PIP and SpingoStrips to reveal that 15-LOX-2 preferentially associated to PS. However, binding of 15-LOX-2 to PS in actual membranes or model membranes such as nanodiscs has not yet been verified and additional experiments are needed. For example, we could repeat our SEC experiment that verified binding of 15-LOX-2 to PS-containing nanodiscs (Figure 19), using nanodiscs that do not contain PS. Isothermal titration calorimetry can be used to measure the dissociation constant ( $K_D$ ) for 15-LOX-2 with unilamellar vesicles with PS and anionic phospholipids at varying molar ratios to confirm 15-LOX-2 phospholipid preference. Surface plasmon resonance is an alternative technique that could be used to determine the  $K_D$  for 15-LOX-2 with vesicles. This technique has the advantage of “real time” kinetics, however, it requires a Biacore instrument and biosensor chips with the immobilized lipid vesicles.<sup>152</sup> In addition, a comparison of 15-LOX-2 structural dynamics upon membrane association with other human LOXs such as human 5-LOX, 12-LOX, and 12/15-LOX, would be interesting. Alignment of the primary sequence in the PLAT domains in these proteins suggest different mechanism for membrane association from LOX to LOX (Figure 10). Performing H/D exchange MS on these various LOXs in soluble  $Ca^{2+}$  free, soluble  $Ca^{2+}$  bound, and  $Ca^{2+}$  nanodisc-associated states would provide evidence needed to determine the degree to which LOX superfamily members differ in terms of membrane association mechanism.

Much of the data presented in this study could be further illuminated if additional crystal structures of 15-LOX-2 were determined under conditions that are similar to those used in some of our H/D exchange experiments. For example, this work suggest that 13-HODE may positively allosterically regulate 15-LOX-2 activity by increasing the fluctuations of the active site entrance, allowing for facile substrate binding. However, a direct binding site for 13-HODE was not identified. A crystal structure of 15-LOX-2 with 13-HODE bound to the allosteric site would provide information on the molecular mechanism of allostery and could assist with the interpretation of the H/D exchange MS results in this work.

Our work supports the notion that there is communication between the PLAT and catalytic domain. The role interdomain allostery plays in 15-LOX-2 biological function can be further investigated by completing site mutagenesis of K175 or W109 to disrupt the  $\pi$ -cation interaction. Analysis of the mutated 15-LOX-2 catalytic properties, in addition to analysis of its structure and structural dynamics, will provide essential information on the role of the PLAT domain in 15-LOX-2 activity.

Studies are needed to further investigate the 5-LOX and FLAP protein complex and complex-ligand interactions. Alternative expression systems for 5-LOX may assist in protein folding and allow post-translational modifications that improve 5-LOX structural stability. H/D exchange studies with FLAP could be improved by ultra performance liquid chromatography (UPLC). UPLC employs smaller particle sizes in ESI to produce superior resolution, speed, and sensitivity and recent work demonstrates its compatibly with H/D exchange MS methods.<sup>153</sup> In addition, methods that remove of non-ionic detergents prior to sample injection are being optimized.<sup>154</sup> Both of these methods could improve the resolution of the peptide ion envelope and

improve the fragmentation data that leads to improved sequence coverage. These methods can be supplemented with other structural dynamics-dependent labeling techniques coupled with MS.

### *Concluding Remarks*

The study of inflammation has progressed from treating inflammatory symptoms with natural products to developing a molecular understanding of the cellular pathways involved in inflammation. Although the body of knowledge related to inflammation is already vast each new study on key mediators brings the scientific community a step closer to being able to properly regulate the cellular pathways that lead to harmful inflammatory symptoms. This work focused on the structural dynamics of three proteins involved in the biosynthesis of a few subclasses of eicosanoids, which is an essential part of these cellular pathways. These studies are representative of the fact that we are now in the stage of not only observing the biological functions of proteins involved in inflammation, but also being able to utilize their structure and structural dynamics as the basis for designing molecules to target them for therapeutic purposes. It is my hope that the work of this dissertation will contribute to this important field of research.

APPENDIX A

AMPLITUDES AND RATE CONSTANTS FOR AMIDE H/D EXCHANGE PROFILES

**Table 2. Amplitudes and rate constants for amide H/D exchange profiles in Figure 17.** H/D exchange profiles for select peptides in 15-LOX-2 are shown in Figure 17 in the following states; (1) Ca<sup>2+</sup> free 15-LOX-2 (blue),(2) Ca<sup>2+</sup>-15-LOX-2 (red), and (3) nanodisc-associated Ca<sup>2+</sup>-15-LOX-2 (green). The data was fit to a sum of first-order rate terms, and the following values were calculated.

Peptide/ State	A <sub>fast</sub> (D)	A <sub>1</sub> (D)	k <sub>1</sub> (min <sup>-1</sup> )
<b>A 45-52</b>			
EGTA	2.2	1.41 ± 0.24	0.015 ± 0.005
Ca <sup>2+</sup>	2.3	1.52 ± 0.20	0.017 ± 0.004
Ca <sup>2+</sup> and ND	2.8	1.0 ± 0.4	≤ 1 x 10 <sup>-4</sup>
<b>B 54-66</b>			
EGTA	3.1	2.01 ± 0.19	0.01 ± 0.002
Ca <sup>2+</sup>	3	2.02 ± 0.23	0.009 ± 0.002
Ca <sup>2+</sup> and ND	3.1	1.79 ± 0.30	0.001 ± 0.001
<b>C 67-87</b>			
EGTA	6	1.01 ± 0.24	≤ 1 x 10 <sup>-4</sup>
Ca <sup>2+</sup>	5.8	2	0.006 ± 0.004
Ca <sup>2+</sup> and ND	4.7	2.33 ± 0.2	0.003 ± 0.001
<b>D 92-104</b>			
EGTA	2.7	0.48 ± 0.09	0.0005 ± 0.0002
Ca <sup>2+</sup>	2.2	1.13 ± 0.17	0.0007 ± 0.0002
Ca <sup>2+</sup> and ND	2.1	1.35 ± 0.16	0.0006 ± 0.0002



**Table 3. Amplitudes and rate constants for amide H/D exchange profiles in Figure 22.** H/D exchange profiles for select peptides in 15-LOX-2 are shown in Figure 22 in the following states; (1) Ca<sup>2+</sup>-15-LOX-2 (blue); (2) Ca<sup>2+</sup>-15-LOX-2 with AA present (green); (3) Ca<sup>2+</sup>-15-LOX-2 with 15-HpETE present (red); and (4) Ca<sup>2+</sup>-free 15-LOX-2 with AA present (black). The data was fit to a sum of first- or second-order rate terms, and the following values were calculated.

Peptide/ State	A <sub>fast</sub> (D)	A <sub>1</sub> (D)	k <sub>1</sub> (min <sup>-1</sup> )	A <sub>2</sub> (D)	k <sub>2</sub> (min <sup>-1</sup> )
<b>A 185-191</b>					
Ca <sup>2+</sup>	1.4	1.72 ± 0.08	0.006 ± 0.0009		
Ca <sup>2+</sup> and AA	0.7	0.60 ± 0.24	0.007 ± 0.001	1.26 ± 0.38	≤ 1 x 10 <sup>-4</sup>
Ca <sup>2+</sup> and 15-HpETE	0.5	1.16 ± 0.07	0.007 ± 0.001	1.45 ± 0.3	≤ 1 x 10 <sup>-4</sup>
EGTA and AA	0.6	1.41 ± 0.11	0.007 ± 0.002	1.76 ± 0.002	≤ 1 x 10 <sup>-5</sup>
<b>B 419-438</b>					
Ca <sup>2+</sup>	1.4	1.56 ± 0.35	0.006 ± 0.004	6.01 ± 0.24	≤ 1 x 10 <sup>-5</sup>
Ca <sup>2+</sup> and AA	1.0	0.96 ± 0.14	0.005 ± 0.002	1.92 ± 0.35	≤ 2 x 10 <sup>-4</sup>
Ca <sup>2+</sup> and 15-HpETE	0.9	0.58 ± 0.29	0.004 ± 0.004	1.37 ± 0.32	≤ 2 x 10 <sup>-4</sup>
EGTA and AA	1.2	0.82 ± 0.30	0.017 ± 0.014	1.60 ± 0.47	≤ 2 x 10 <sup>-4</sup>

**Table 4. Amplitudes and rate constants for amide H/D exchange profiles in Figure 23.** H/D exchange profiles for select peptides in 15-LOX-2 are shown in Figure 23 in the following states; (1) Ca<sup>2+</sup>-15-LOX-2 (blue); (2) Ca<sup>2+</sup>-15-LOX-2 with AA present (green); (3) Ca<sup>2+</sup>-15-LOX-2 with 15-HpETE present (red); and (4) Ca<sup>2+</sup>-free 15-LOX-2 with AA present (black). The data was fit to a sum of first- or second-order rate terms, and the following values were calculated.

Peptide/ State	A <sub>fast</sub> (D)	A <sub>1</sub> (D)	k <sub>1</sub> (min <sup>-1</sup> )	A <sub>2</sub> (D)	k <sub>2</sub> (min <sup>-1</sup> )
<b>A 45-52</b>					
Ca <sup>2+</sup>	1.21	1.51 ± 0.2	0.017 ± 0.004		
Ca <sup>2+</sup> and AA	0.82	0.68 ± 0.25	0.006 ± 0.005	1.38 ± 0.30	≤ 3 x 10 <sup>-4</sup>
Ca <sup>2+</sup> and 15-HpETE	0.43	0.76 ± 0.11	0.021 ± 0.006	1.32 ± 0.010	≤ 1 x 10 <sup>-4</sup>
EGTA and AA	0.75	2.55 ± 0.63	0.023 ± 0.009	1.6 ± 0.015	≤ 1 x 10 <sup>-5</sup>
<b>B 54-66</b>					
Ca <sup>2+</sup>	3.1	2.02 ± 0.23	0.009 ± 0.002	4.02 ± 0.09	≤ 1 x 10 <sup>-6</sup>
Ca <sup>2+</sup> and AA	1.4	3.3 ± 0.19	0.004 ± 0.0008	4.02 ± 0.12	≤ 1 x 10 <sup>-6</sup>
Ca <sup>2+</sup> and 15-HpETE	1.2	3.8 ± 0.25	0.003 ± 0.0006	3.99 ± 0.18	≤ 1 x 10 <sup>-6</sup>
EGTA and AA	1.6	3.04 ± 0.25	0.003 ± 0.001	4.3 ± 0.17	≤ 1 x 10 <sup>-6</sup>
<b>C 67-87</b>					
Ca <sup>2+</sup>	5.8	1.01 ± 0.24	0.0061 ± 0.004	2.33 ± 0.13	≤ 1 x 10 <sup>-5</sup>
Ca <sup>2+</sup> and AA	2.0	2.76 ± 0.36	0.002 ± 0.0008	3.69 ± 0.30	≤ 1 x 10 <sup>-5</sup>
Ca <sup>2+</sup> and 15-HpETE	1.6	3.73 ± 0.15	0.0022 ± 0.0002	3.62 ± 0.3	≤ 1 x 10 <sup>-6</sup>
EGTA and AA	2.2	3.10 ± 0.25	0.0045 ± 0.0010	3.49 ± 0.15	≤ 1 x 10 <sup>-6</sup>

**Table 5. Amplitudes and rate constants for amide H/D exchange profiles in Figure 23.** H/D exchange profiles for select peptides in 15-LOX-2 are shown in Figure 23 in the following states; (1) Ca<sup>2+</sup>-15-LOX-2 (blue); (2) Ca<sup>2+</sup>-15-LOX-2 and AA present (green); (3) Ca<sup>2+</sup>-15-LOX-2 and 15-HpETE present (red); and (4) Ca<sup>2+</sup>-15-LOX-2 and 13-HODE present (black). The data was fit to a sum of first- or second-rate terms, and the following values were calculated.

Peptide/ State	A <sub>fast</sub> (D)	A <sub>1</sub> (D)	k <sub>1</sub> (min <sup>-1</sup> )	A <sub>2</sub> (D)	k <sub>2</sub> (min <sup>-1</sup> )
<b>A 45-52</b>					
Ca <sup>2+</sup>	1.21	1.51 ± 0.2	0.017 ± 0.004		
Ca <sup>2+</sup> and AA	0.82	0.68 ± 0.25	0.006 ± 0.005	1.38 ± 0.30	≤ 4 x 10 <sup>-4</sup>
Ca <sup>2+</sup> and 15-HpETE	0.43	0.76 ± 0.11	0.021 ± 0.006	1.32 ± 0.010	≤ 1 x 10 <sup>-4</sup>
Ca <sup>2+</sup> and 13-HODE	1.8	1.62 ± 0.23	0.006 ± 0.002	0.81 ± 0.12	≤ 1 x 10 <sup>-6</sup>
<b>B 54-66</b>					
Ca <sup>2+</sup>	3.1	2.02 ± 0.23	0.009 ± 0.002	4.02 ± 0.09	≤ 1 x 10 <sup>-6</sup>
Ca <sup>2+</sup> and AA	1.4	3.3 ± 0.19	0.004 ± 0.0008	4.02 ± 0.12	≤ 1 x 10 <sup>-6</sup>
Ca <sup>2+</sup> and 15-HpETE	1.2	3.8 ± 0.25	0.003 ± 0.0006	3.99 ± 0.18	≤ 1 x 10 <sup>-6</sup>
Ca <sup>2+</sup> and 13-HODE	1.2	2.55 ± 0.19	0.01 ± 0.001	3.85 ± 0.07	≤ 1 x 10 <sup>-6</sup>
<b>C 67-87</b>					
Ca <sup>2+</sup>	5.8	1.01 ± 0.24	0.0061 ± 0.004	2.33 ± 0.13	≤ 1 x 10 <sup>-5</sup>
Ca <sup>2+</sup> and AA	2.0	2.76 ± 0.36	0.002 ± 0.0008	3.69 ± 0.30	≤ 1 x 10 <sup>-5</sup>
Ca <sup>2+</sup> and 15-HpETE	1.6	3.73 ± 0.15	0.0022 ± 0.0002	3.62 ± 0.30	≤ 1 x 10 <sup>-6</sup>
Ca <sup>2+</sup> and 13-HODE	4	2.55 ± 0.26	0.017 ± 0.003	3.06 ± 0.07	≤ 1 x 10 <sup>-5</sup>
<b>D 92-104</b>					
Ca <sup>2+</sup>	2.1	1.13 ± 0.17	0.0008 ± 0.0002		
Ca <sup>2+</sup> and AA	1.9	1.42 ± 0.15	0.0007 ± 0.0001		
Ca <sup>2+</sup> and 15-HpETE	1.7	0.78 ± 0.16	0.0036 ± 0.002		
Ca <sup>2+</sup> and 13-HODE	2.2	1.40 ± 0.075	0.0010 ± 0.001		
<b>E 117-134</b>					
Ca <sup>2+</sup>	3.7	1.76 ± 0.50	0.005 ± 0.003	3.46 ± 0.58	≤ 7 x 10 <sup>-4</sup>
Ca <sup>2+</sup> and AA	2	3.87 ± 0.36	0.010 ± 0.002	3.55 ± 0.23	≤ 2 x 10 <sup>-4</sup>
Ca <sup>2+</sup> and 15-HpETE	2.9	3.62 ± 0.61	0.013 ± 0.02	2.88 ± 0.32	≤ 1 x 10 <sup>-4</sup>
Ca <sup>2+</sup> and 13-HODE	5.1	2.42 ± 0.25	0.013 ± 0.003	2.56 ± 0.22	≤ 8 x 10 <sup>-4</sup>
<b>F 185-191</b>					
Ca <sup>2+</sup>	1.4	1.72 ± 0.08	0.006 ± 0.0009		
Ca <sup>2+</sup> and AA	0.7	0.60 ± 0.24	0.007 ± 0.001	1.26 ± 0.38	≤ 1 x 10 <sup>-4</sup>
Ca <sup>2+</sup> and 15-HpETE	0.5	1.16 ± 0.07	0.007 ± 0.001	1.45 ± 0.3	≤ 1 x 10 <sup>-4</sup>
Ca <sup>2+</sup> and 13-HODE	1.2	1.09 ± 0.08	0.003 ± 0.0009		
<b>G 419-438</b>					
Ca <sup>2+</sup>	5.8	1.01 ± 0.24	0.0061 ± 0.004	2.33 ± 0.13	≤ 1 x 10 <sup>-5</sup>
Ca <sup>2+</sup> and AA	2.0	2.76 ± 0.36	0.002 ± 0.0008	3.69 ± 0.30	≤ 1 x 10 <sup>-5</sup>
Ca <sup>2+</sup> and 15-HpETE	1.6	3.73 ± 0.15	0.0022 ± 0.0002	3.62 ± 0.30	≤ 1 x 10 <sup>-6</sup>
Ca <sup>2+</sup> and 13-HODE	2.0	4.06 ± 0.17	0.002 ± 0.0002		
<b>H 672-676</b>					
Ca <sup>2+</sup>	0.25	0.44 ± 0.019	≤ 8 x 10 <sup>-4</sup>		
Ca <sup>2+</sup> and AA	0.4	0.50 ± 0.10	≤ 6 x 10 <sup>-4</sup>		
Ca <sup>2+</sup> and 15-HpETE	0.6	0.49 ± 0.06	≤ 3 x 10 <sup>-4</sup>		
Ca <sup>2+</sup> and 13-HODE	0.5	0.42 ± 0.10	≤ 2 x 10 <sup>-4</sup>		

APPENDIX B

ADDITIONAL H/D EXCHANGE PROFILES FOR 15-LOX-2

**Figure 38. H/D exchange kinetic profiles for 15-LOX-2 as a function of  $\text{Ca}^{2+}$  binding and nanodisc-association, Resides 1-364.** The number of deuterons incorporated is plotted vs time for 15-LOX-2 peptides analyzed but not directly discussed throughout this work. The following 15-LOX-2 states are shown; (1)  $\text{Ca}^{2+}$  free 15-LOX-2 (blue squares), (2)  $\text{Ca}^{2+}$ -15-LOX-2 (red circle), and (3) nanodisc-associated  $\text{Ca}^{2+}$ -15-LOX-2 (green triangle).

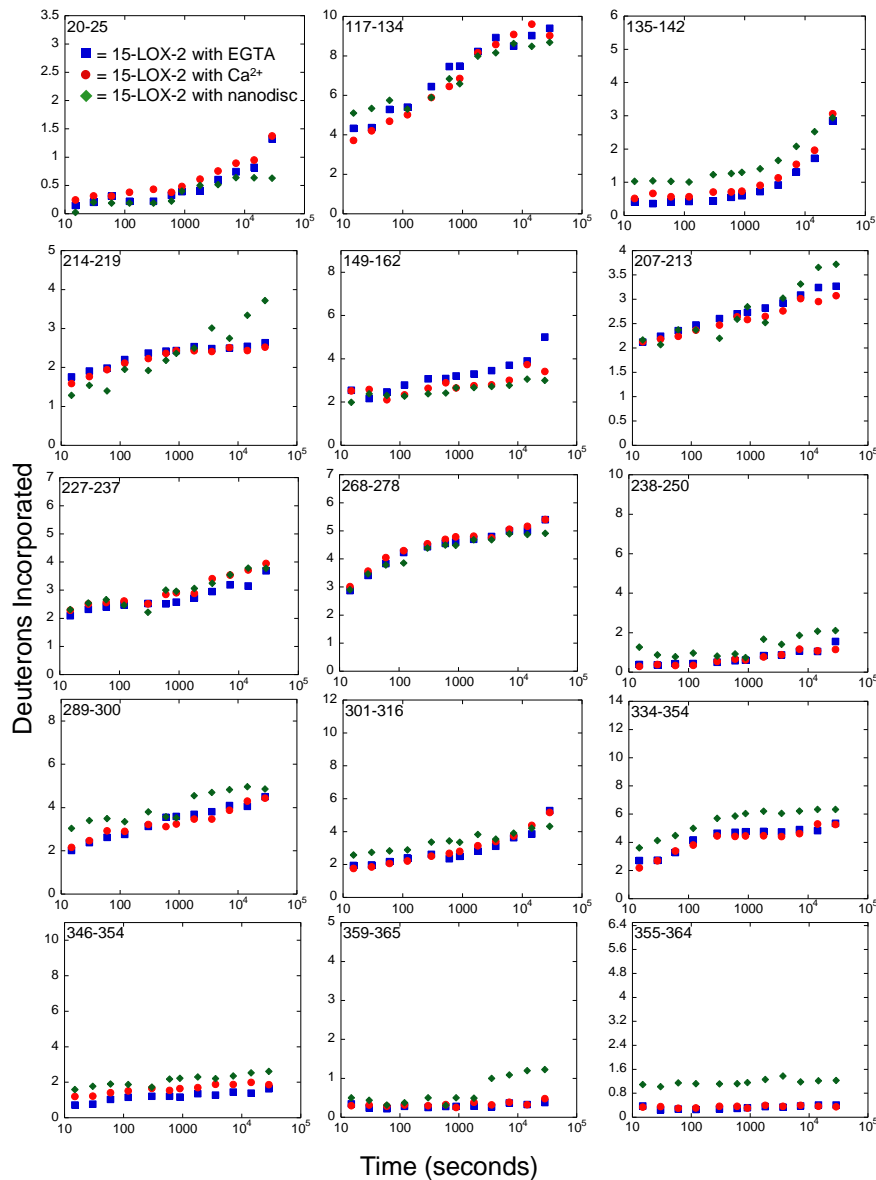


**Figure 39. H/D exchange kinetic profiles for 15-LOX-2 as a function of  $\text{Ca}^{2+}$  binding and nanodisc-association, Residues 345-676.** The number of deuterons incorporated is plotted vs time for 15-LOX-2 peptides analyzed but not directly discussed throughout this work. The following 15-LOX-2 states are shown; (1)  $\text{Ca}^{2+}$  free 15-LOX-2 (blue squares), (2)  $\text{Ca}^{2+}$ -15-LOX-2 (red circle), and (3) nanodisc-associated  $\text{Ca}^{2+}$ -15-LOX-2 (green triangle).

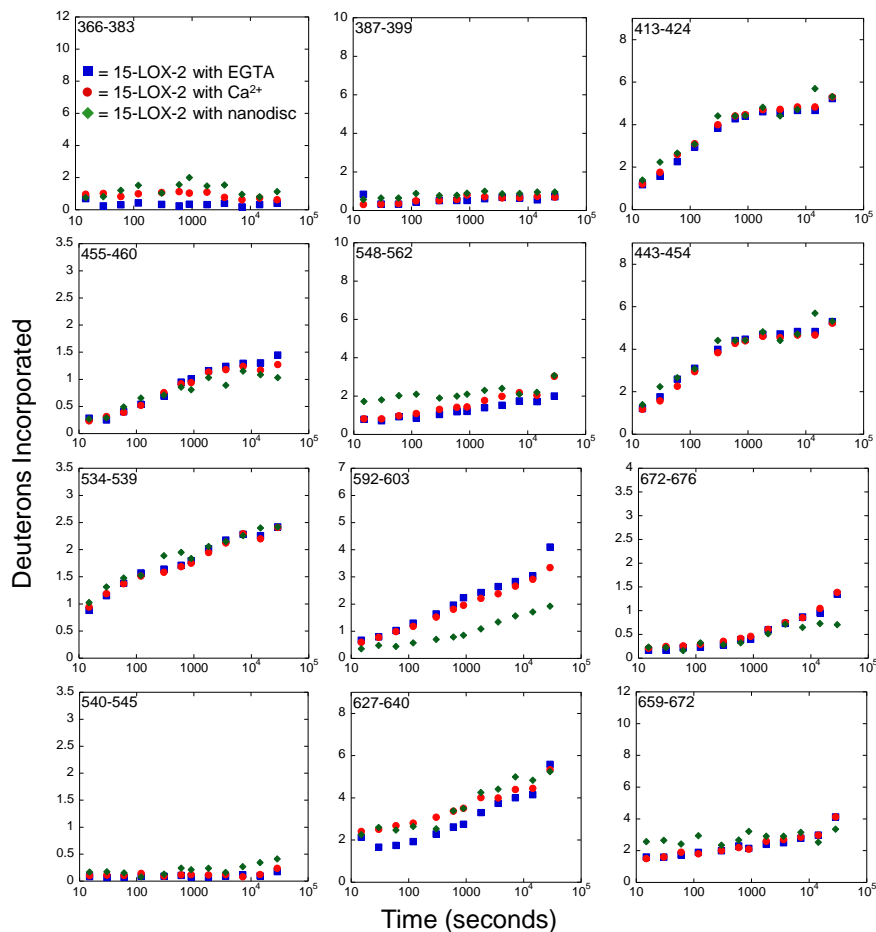


**Figure 40. H/D exchange kinetic profiles for 15-LOX-2 as a function of AA and 15-HpETE binding, Residues 1-354.** The number of deuterons incorporated is plotted vs time for 15-LOX-2 peptides analyzed but not directly discussed throughout this work. The following 15-LOX-2 states are shown; (1)  $\text{Ca}^{2+}$ -15-LOX-2 (blue squares), (2)  $\text{Ca}^{2+}$ -15-LOX-2 with AA present (green triangle), and (3)  $\text{Ca}^{2+}$ -15-LOX-2 with 15-HpETE present (red circle).

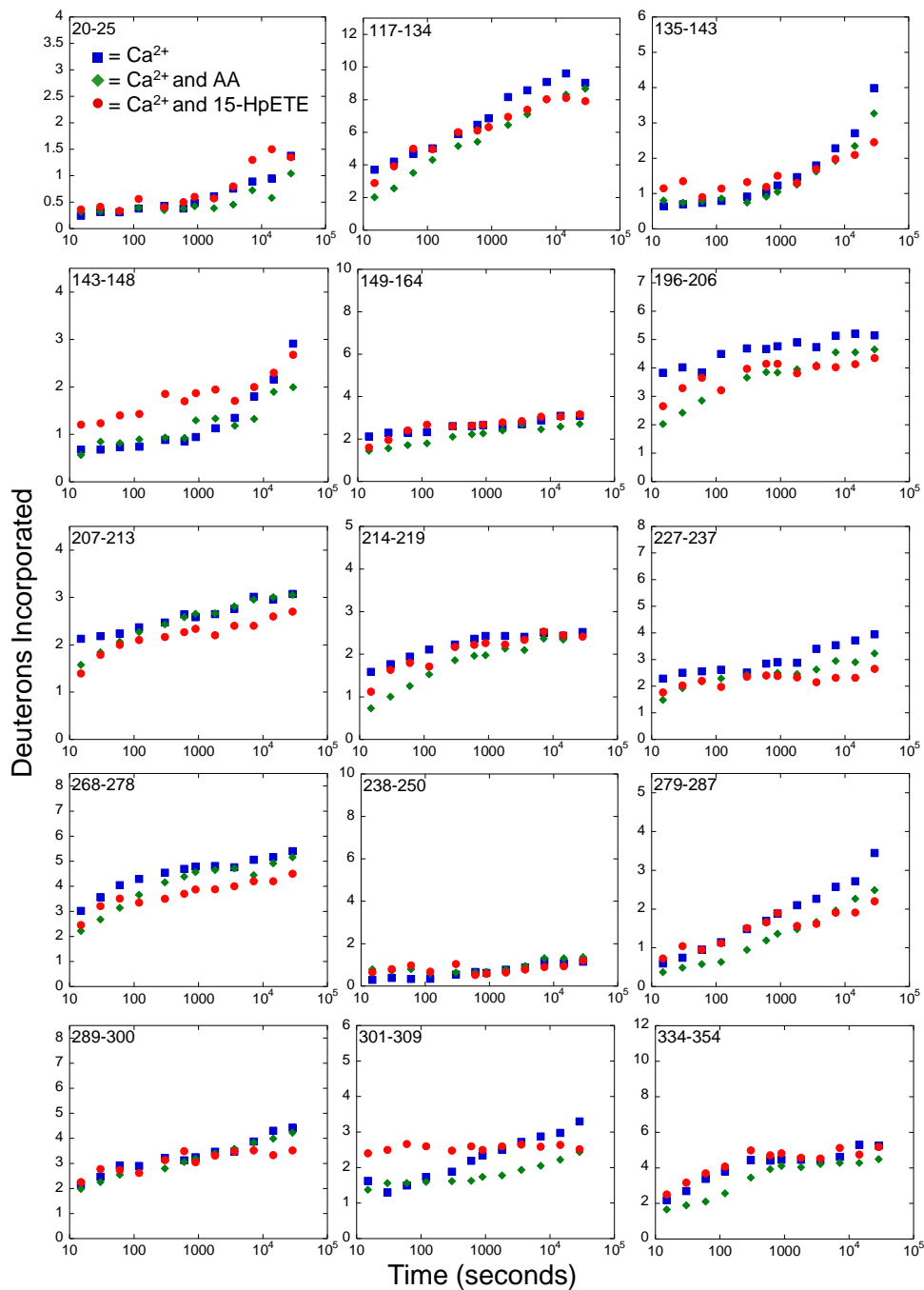
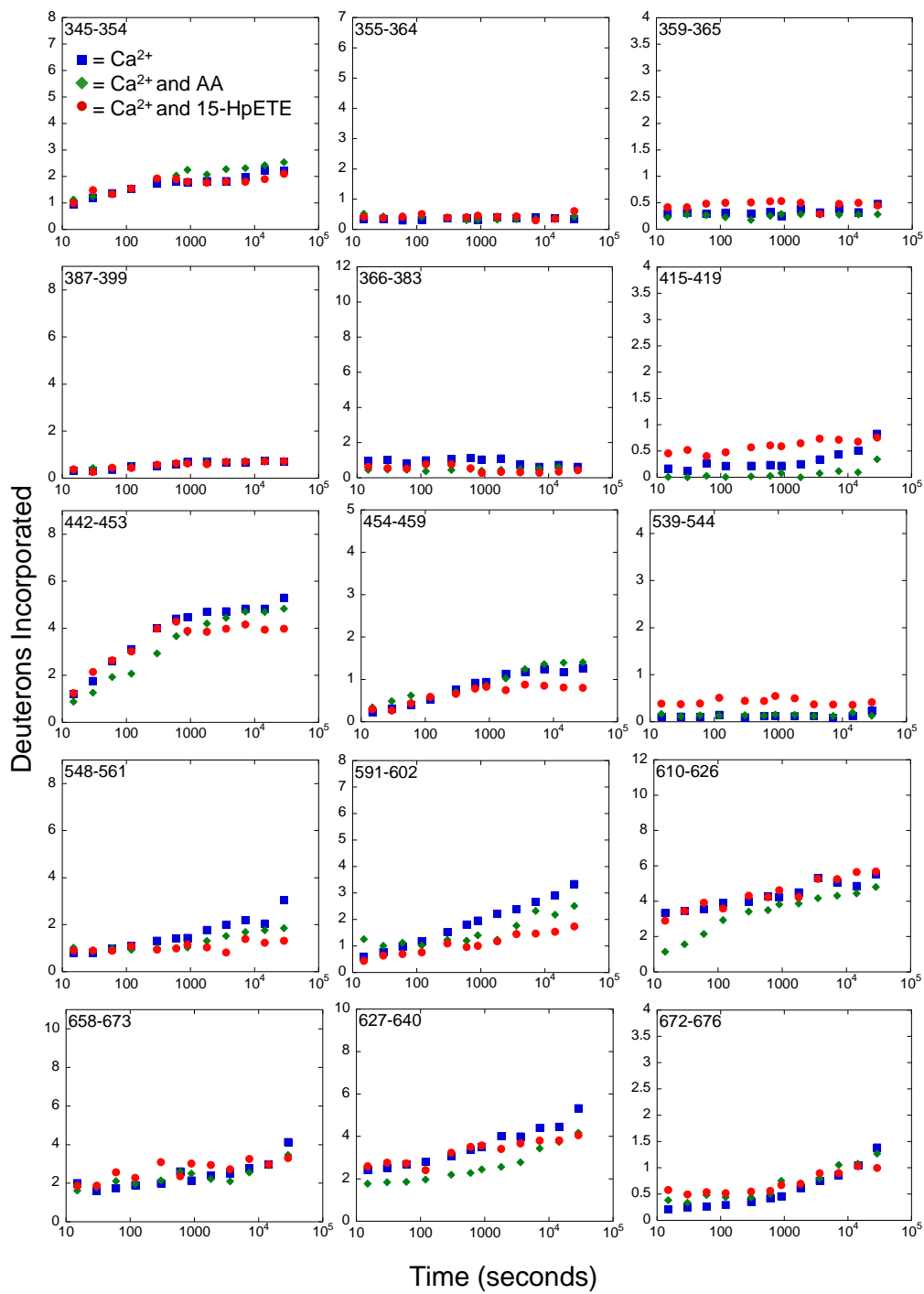


**Figure 41. H/D exchange kinetic profiles for 15-LOX-2 as a function of AA and 15-HpETE binding, Residues 345-676.** The number of deuterons incorporated is plotted vs time for 15-LOX-2 peptides analyzed but not directly discussed throughout this work. The following 15-LOX-2 states are shown; (1)  $\text{Ca}^{2+}$ -15-LOX-2 (blue squares), (2)  $\text{Ca}^{2+}$ -15-LOX-2 with AA present (green triangle), and (3)  $\text{Ca}^{2+}$ -15-LOX-2 with 15-HpETE present (red circle).



## APPENDIX C

### SUPPLEMENTAL INFORMATION FOR CHAPTER III

**Figure 42. SDS-PAGE gel of 15-LOX-2 associated with nanodiscs.** The fractions collected from the elution of nanodisc associated 15-LOX-2 from a HiLoad 16/60 Superdex 200 pg column (Figure 29) were analyzed by a SDS-PAGE gel. 1 mL fractions from the peak at 8.5 mL were used to determine the protein content. A band indicative of 15-LOX-2 (76 kDa) and a band indicative of the nanodisc scaffold protein (MSP1e3d1, 37 kDa) was observed, indicating that 15-LOX-2 is associated to nanodiscs.

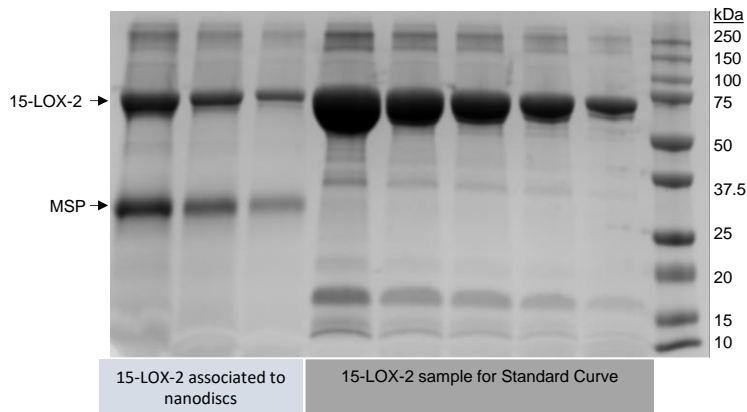
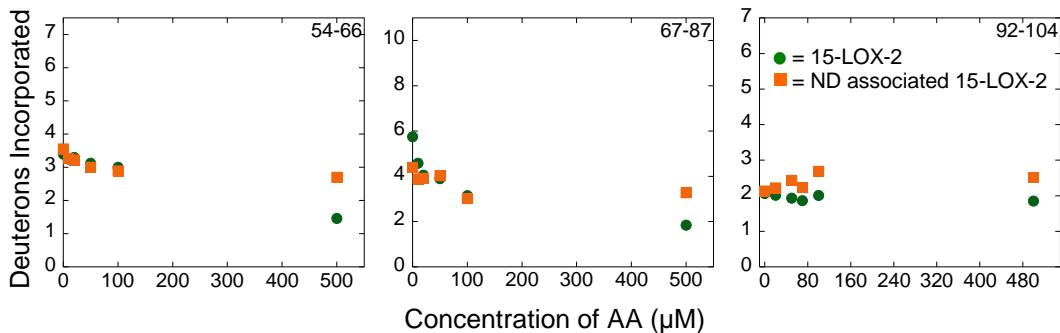


**Figure 43. H/D exchange of 15-LOX-2 associated with nanodiscs containing AA.** To determine if presence of substrate increases the “tightness” of membrane association nanodiscs composed of phospholipids and increasing concentration of AA were created and had 15-LOX-2 associated with them. H/D exchange was measured at 15 seconds. The similarities in deuterium incorporation between nanodisc associated soluble  $\text{Ca}^{2+}$ -15-LOX-2 (green) and nanodisc associated  $\text{Ca}^{2+}$ -15-LOX-2 suggest AA presence does not affect 15-LOX-2 association.

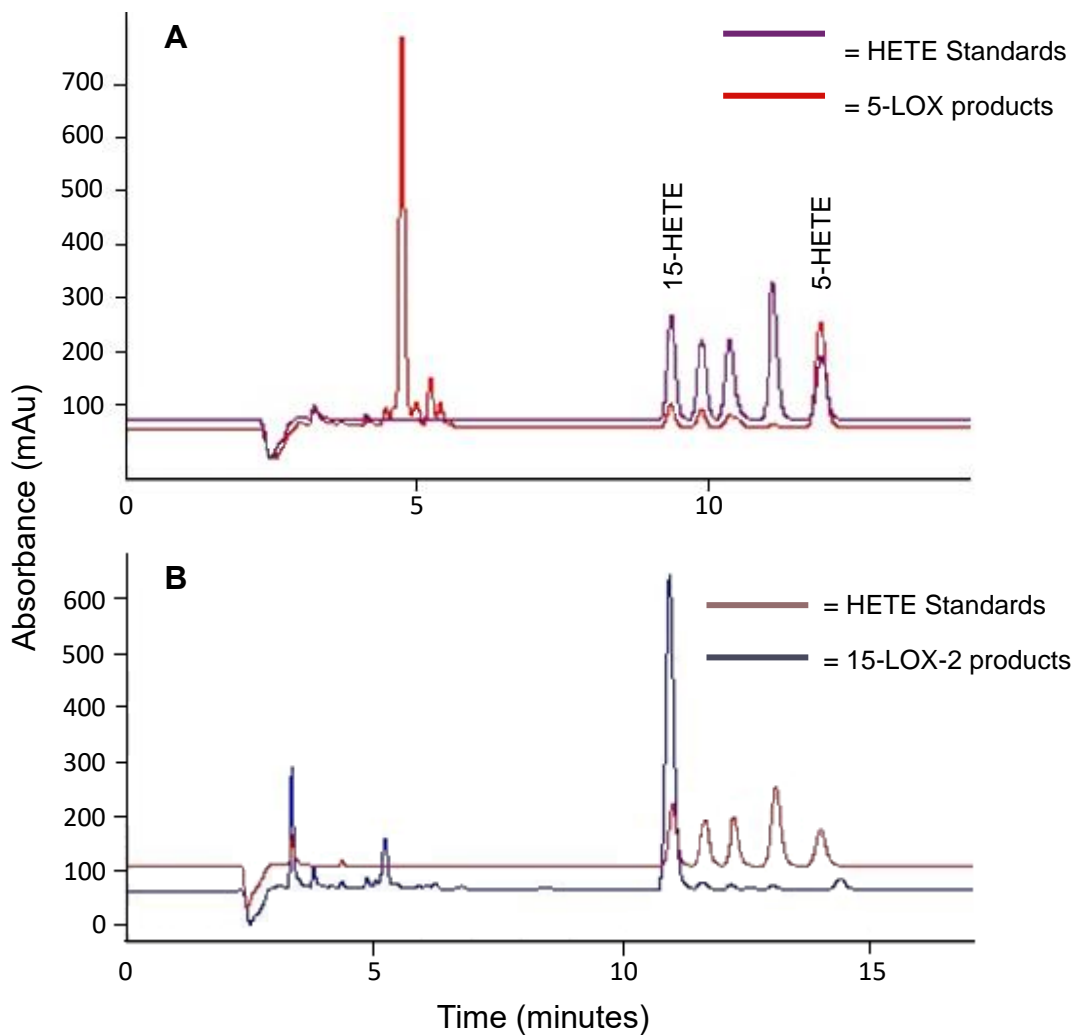




APPENDIX D

SUPPLEMENTAL INFORMATION FOR CHAPTER V

**Figure 44. HPLC chromatogram of LOX products.** Product analysis of (A) Stable 5-LOX reveals that 5-HpETE is the major product of 5-LOX enzymatic oxygenation of AA. (B) Similar methods reveal that 15-LOX-2 primarily produces 15-HpETE upon AA oxygenation.



## APPENDIX E

### CURRICULUM VITAE

---

**Kristin D. Droege**

2300 Sharondale Dr.  
Nashville, TN 372015

Phone Number: (618) 946-2471  
Email: kristin.d.droege@vanderbilt.edu

---

#### Education

- **Ph.D.**      **Vanderbilt University**, Nashville, TN      Expected: June 2017  
Department of Chemistry  
*Advisor:* Richard N. Armstrong, Ph.D. (Deceased June 2015)  
Charles R. Sanders, Ph.D.  
*Thesis:* Elucidation of lipoxygenase structural dynamics upon regulatory  
and enzymatic mechanisms. (in progress)
- **B.S.**      **Illinois State University**, Normal, IL      May 2011  
Major in Chemistry- Chemistry Education sector (*cum laude*)

#### Endorsements

- Illinois State Board of Education: Endorsed in Initial Secondary Teaching Grade 6 to 12  
(Science- Chemistry)

#### Teaching Experience

**Vanderbilt University**      Center for Teaching      Jan 2016-Present  
**BOLD Fellow**, *Teaching as Research Project*

- Designed and implemented science education research project (Project Title: *Does online homework format effect students learning and self-assessment?*)
- Created online homework for introductory biochemistry undergraduate course at Vanderbilt University for 5 coordinating professors.
- Developed and administered 2 different homework formats (tradition multiple choice, and case-study multiple choice), online homework site, and post-homework survey.
- Obtained Vanderbilt Institutional Review Board approval for research project
- A description of the project can be found at  
<https://www.vanderbilt.edu/bold/docs/biochemistry-bsci2520/>

**Vanderbilt University** Department of Biological Sciences Nov 2016  
**Guest Lecturer, Biochemistry 2520**

- Taught 1 lecture on amino acid catabolism.
- Developed a lesson plan with PowerPoint that integrated class discussion and group problem solving.

**Vanderbilt University** Programs for Talented Youth July 2015-Present  
**Summer Academy for Vanderbilt Youth (SAVY) Instructor, It's Elemental and Culinary Chemistry**

- Attended two orientations involving focused on research and teaching methods for gifted students and emergency first aid.
- Organized week long lesson plan that utilized a combination of lecture, discussion, guided experiments, and group activities for gifted students.
- Created and instructed course (Culinary Chemistry) with focuses on chemical composition of food, and chemical techniques involved in food processing (ex. fermentation, blanching, canning, and calorie determination) to fourth and fifth grade students.
- Created and instructed course (It's Elemental) that focused on the uses, and information provided by the periodic table such as observing patterns, molecular numbers, ionic formation, and chemical reaction predictions.

**Vanderbilt University** Department of Chemistry Aug 2013-2015  
**Graduate Teaching Assistant, Organic Chemistry I and II Laboratory**

- Prepared laboratory apparatuses and benches for 12-18 students.
- Created and implemented pre-lab lectures for chemistry undergraduate students with variety of backgrounds and abilities.
- Created and graded quizzes to assess students' preparedness and prior knowledge.
- Planned and applied rubrics for grading weekly laboratory reports.

**Vanderbilt University** Center for Teaching Aug 2014-2015  
**Graduate Teaching Affiliate**

- Attended a two week orientation covering how students learn, leading discussions, effective lecturing, and information for new teaching assistants (TA's).
- Led a full day Teaching Assistant Orientation for incoming chemistry TA's, which included approximately 20 graduate students.
- Created an educational video on faculty expectations for incoming TA's in the Departments of Chemistry and Biological Science.

**Bloomington High School** Jan 2011- May 2011  
**Student Teacher, Chemistry and Advanced Chemistry**

- Collaborated with teaching mentor to create and implement lesson plans that meet Illinois State Board of Education standards for students ranging from 10<sup>th</sup> to 12<sup>th</sup> grade.

- Created projects and experiments that focused on promoted science literacy, problem solving skills, and critical thinking.
- Implemented alternative testing methods, and assignments with multiple opinions to promote learning for differentiate learners with autism, dyslexia, and ADHD.
- Attended monthly meetings with additional student teachers to assess novel teaching methods, and learn new classroom technology available.
- Provided a weekly journal on classroom techniques and experiences to professor of student teachers for review and assessment.
- Conducted communication with students' parents via parent-teacher conferences, monthly newsletters, phone calls, and good-news post cards.

**Illinois State University** Department of Chemistry Aug 2010-Dec 2010  
**Undergraduate Teaching Assistant, *Organic Chemistry***

- Assisted instructor in preparing laboratory equipment and solutions.
- Graded student assignments and assessed student's pre and post-laboratory notebooks.

### Research Experience

**Vanderbilt University** Department of Chemistry Aug 2011-Present  
**Graduate Research Fellow**

*Advisor:* Richard N. Armstrong, Ph.D. (Decreased June 2015)  
 Charles R. Sanders, Ph.D.

*Topic:* Utilization of hydrogen-deuterium exchange mass spectrometry to elucidate lipoxygenase structural dynamics upon regulatory and enzymatic mechanisms.

**Illinois State University** Department of Chemistry Aug 2009-Aug 2011  
**Undergraduate Researcher**

*Advisor:* Marjorie Jones, Ph.D.

*Topic:* Investigation of the inhibitory effect of protophyrin derivatives and super oxide production on *Leishmania tarentola* proliferation.

### Additional Experiences

**Vanderbilt Children's Hospital** Eskind Diabetes Clinic March 2017-Present  
**Volunteer**

- Volunteered two hours a week as waiting room/lifestyle room attendant.
- Interacted with children through play and activities while they were waiting throughout appointments in order to create a calming and beneficial experience.

**Vanderbilt University** May 2013  
**Conference Session Chair, *Biomolecular Structure, Dynamic, Function: Membrane Protein***

- Served as a session chair during keynote speaker session.
- Introduced speaker, assisted in time management, and organized questions for speakers.

### Publications

- Dungeng Peng, Ji-Hun Kim, Brett M. Kroncke, Cheryl L. Law, Yan Xia, **Kristin D. Droege**, Wade D. Van Horn, Carlos G. Vanoye, and Charles R. Sanders (2014) Purification and structural study of the voltage-sensor domain of the human KCNQ1 potassium ion channel. *Biochemistry* 53, 2032-2042.
- Victoria H. Nguyen, **Kristin D. Droege**, Matthew L. Beio, Ancuta Carcu, Jaqueline D. Hooker, Conor McMahon, David L. Cedeno, Viviana Taylor, Sara Robiedo, Ivan D. Velez, and Marjorie A. Jones (2012) The photodynamic effects of protoporphyrin IX, protoporphyrin IX dimethyl ester or metallated protoporphyrin IX on *Leishmania tarentolae* in culture. *Trends in Photochemistry and Photobiology* 14, 39-46.

### Peer Reviewed Presentations

<b>Poster presenter</b>	251 <sup>st</sup> ACS National Meeting and Exposition San Diego Convention Center, San Diego, CA <i>Title: Elucidation of lipoxygenase membrane association via hydrogen deuterium exchange</i>	Mar 2016
<b>Poster presenter</b>	36 <sup>th</sup> Annual Steenbock Symposium University of Wisconsin, Madison, WI <i>Title: The Elucidation of Lipoxygenase Mechanism and Regulation via Hydrogen-Deuterium Exchange Mass Spectrometry</i>	May 2014
<b>Poster presenter</b>	Biomolecular Structure, Dynamic, Function: Membrane Protein Vanderbilt University, Nashville, TN <i>Title: The elucidation of lipoxygenase mechanism and regulation via hydrogen-deuterium exchange mass spectrometry</i>	May 2014
<b>Poster presenter</b>	Vanderbilt Institute of Chemical Biology Student Symposium Vanderbilt University, Nashville, TN <i>Title: Characterization of interactions in 5-lipoxygenase and 5-lipoxygenase activating protein complexes in leukotriene biosynthesis</i>	Sept 2013
<b>Poster presenter</b>	240 <sup>th</sup> ACS National Meeting and Exposition Boston Convention and Exhibition Center, Boston, MA <i>Title: Protoporphyrin IX and metallated protoporphyrin IX dose dependent effects on Leishmania</i>	Aug 2010

### Additional Presentations

- Poster presenter** Teaching Tools and Approaches in the Classroom May 2016  
Central Library, Vanderbilt University, Nashville, TN  
*Title: Does online homework format impact student learning and self-assessment in biochemistry?*
- Oral presenter** Department of Chemistry Forum Oct 2015  
Vanderbilt University, Nashville, TN  
*Title: 15-lipoxygenase-2 structural dynamics upon ligand binding and membrane association via hydrogen-deuterium exchange*
- Oral presenter** Chemical Biology Association of Students Dec 2014  
Vanderbilt University, Nashville, TN  
*Title: Elucidation of lipoxygenase regulatory and enzymatic mechanism*

### Research Skills

- Standard molecular biological techniques such as cloning, gel electrophoresis, western blotting and site-directed mutagenesis
- Monitoring cell viability via MTT assay
- Recombinant protein expression in *Escherichia coli*
- Expression and purification of difficultly expressed membrane proteins
- Protein purification via affinity tags
- Enzymatic synthesis and purification of enzyme substrates
- UV and HPLC-based enzyme assays
- Mass spectrometry protein sequencing
- Hydrogen-deuterium exchange mass spectrometry (HDX-MS)
- Formation and purification of nanodiscs and alternative membrane substitutions
- Molecular graphics including Pymol and Chimera
- Computer Software: HDExaminer, Prism, QualBrowser, PEAKS, MagTran, MassXpert, Kaleidagraph, Microsoft Office Suite

### References

Charles R. Sanders, Ph.D.  
Provisional Advisor (in lieu of Richard N. Armstrong, Ph.D.)  
Professor of Biochemistry  
Associate Editor of Biochemistry  
Aileen M Lange and Annie Mary Lyle Chair of Cardiovascular Research  
Vanderbilt University  
5110C MRBIII  
465 21<sup>st</sup> Ave S.  
Nashville, TN 37232-8725

Phone: (615) 936-3756  
Email: chuck.sanders@vanderbilt.edu

Matthew K. Thompson, Ph.D.  
Postdoctoral Fellow  
Department of Biochemistry  
Vanderbilt University  
5144E MRBIII  
465 21<sup>st</sup> Ave S.  
Nashville, TN 37232-8725  
Phone: (919) 455-1775  
Email: matthew.k.thompson@vanderbilt.edu

Cynthia J. Brame, Ph.D.  
Assistant Director, Center for Teaching  
Director, BOLD Fellows program  
Senior Lecturer, Biological Sciences  
PMB 183  
230 Appleton Place  
Nashville, TN 37203-5721  
Phone: (615) 322-7290  
Email: Cynthia.brame@vanderbilt.edu

---

## REFERENCES

1. Helming, L. Inflammation: Cell Recruitment versus Local Proliferation. *Curr. Biol.* **21**, R548–R550 (2011).
2. Dennis, E. A. & Norris, P. C. Eicosanoid Storm in Infection and Inflammation. *Nat. Rev. Immunol.* **15**, 511–523 (2015).
3. Harizi, H., Corcuff, J.-B. & Gualde, N. Arachidonic-acid-derived eicosanoids: roles in biology and immunopathology. *Trends Mol. Med.* **14**, 461–468 (2008).
4. Pesic, M. & Greten, F. R. Inflammation and cancer: tissue regeneration gone awry. *Curr. Opin. Cell Biol.* **43**, 55–61 (2016).
5. Turner, H. & Kinet, J.-P. Signalling through the high-affinity IgE receptor FcεRI. *Nature* **402**, 24–30 (1999).
6. Ravetch, J. V. & Bolland, S. IgG Fc Receptors. *Annu. Rev. Immunol.* **19**, 275–290 (2001).
7. Markiewski, M. M. & Lambris, J. D. The Role of Complement in Inflammatory Diseases From Behind the Scenes into the Spotlight. *Am. J. Pathol.* **171**, 715–727 (2007).
8. Boe, A., Baiocchi, M., Carbonatto, M., Papoian, R. & Serlupi-Crescenzi, O. Interleukin 6 knock-out mice are resistant to antigen-induced experimental arthritis. *Cytokine* **11**, 1057–1064 (1999).
9. Neumann, E., Lefèvre, S., Zimmermann, B., Gay, S. & Müller-Ladner, U. Rheumatoid arthritis progression mediated by activated synovial fibroblasts. *Trends Mol. Med.* **16**, 458–468 (2010).
10. Köhl, J. in *Current Topics in Complement*. 71–94 (Springer US, 2006). doi:10.1007/0-387-34134-X\_6
11. Bäck, M. *et al.* Update on leukotriene, lipoxin and oxoeicosanoid receptors: IUPHAR Review 7. *Br. J. Pharmacol.* **171**, 3551–74 (2014).
12. George, B. & Burr, M. M. A new deficiency disease produced by the rigid exclusion of fat from the diet. *J. Biol. Chem.* **82**, 346–367 (1929).
13. George, B. & Burr, M. M. On the nature and role of the fatty acids essential in nutrition. *J. Biol. Chem.* **86**, 578–621 (1930).
14. Goldblatt, M. W. Properties of human seminal plasma. *J. Physiol.* **84**, 208–218 (1935).
15. von Euler, U. S. On the specific vaso-dilating and plain muscle stimulating substances from accessory genital glands in man and certain animals (prostaglandin and vesiglandin). *J. Physiol.* **88**, 213–34 (1936).
16. Bergstrom, S., Ryhage, R., Samuelsson, B. & Sjovall, J. Prostaglandins and related factors: The structure of postaglandin E1, F1alpha and F1beta. *J. Biol. Chem.* **238**, 3555–3561 (1963).



17. Buczynski, M. W., Dumlao, D. S. & Dennis, E. A. Thematic Review Series: Proteomics. An integrated omics analysis of eicosanoid biology. *J. Lipid Res.* **50**, 1015–38 (2009).
18. Serhan, C. N. *et al.* Novel functional sets of lipid-derived mediators with antiinflammatory actions generated from omega-3 fatty acids via cyclooxygenase 2-Nonsteroidal Antiinflammatory drugs and transcellular processing. *J. Exp. Med.* **192**, 1197–1204 (2000).
19. Serhan, C. N. *et al.* Resolvins: A Family of Bioactive Products of Omega-3 Fatty Acid Transformation Circuits Initiated by Aspirin Treatment that Counter Proinflammation Signals. *J. Exp. Med.* **101300**, 1025–1037 (2002).
20. Funk, C. D. Prostaglandins and Leukotrienes: Advances in Eicosanoid Biology. *Science* (80-. ). **294**, 1871–1875 (2001).
21. Norris, P. C., Reichart, D., Dumlao, D. S., Glass, C. K. & Dennis, E. A. Specificity of eicosanoid production depends on the TLR-4-stimulated macrophage phenotype. *J. Leukoc. Biol.* **90**, 563–74 (2011).
22. Tilley, S. L., Coffman, T. M. & Koller, B. H. Mixed messages: modulation of inflammation and immune responses by prostaglandins and thromboxanes. *J. Clin. Invest.* **108**, 15–23 (2001).
23. Hartung, H. P., Hadding, U., Bitter-Suermann, D. & Gemsa, D. Stimulation of prostaglandin E and thromboxane synthesis in macrophages by purified C3b. *J. Immunol.* **130**, 2861–2865 (1983).
24. Wallace, J. L., McKnight, W., Reuter, B. K. & Vergnolle, N. NSAID-induced gastric damage in rats: Requirement for inhibition of both cyclooxygenase 1 and 2. *Gastroenterology* **119**, 706–714 (2000).
25. Huber, M., Beutler, B. & Keppler, D. Tumor necrosis factor  $\alpha$  stimulates leukotriene production in vivo. *Eur. J. Immunol.* **18**, 2085–2088 (1988).
26. Borgeat, P., Hamberg, M. & Samuelsson, B. Transformation of arachidonic acid and homo-gamma-linolenic acid by rabbit polymorphonuclear leukocytes. Monohydroxy acids from novel lipoxygenases. *J. Biol. Chem.* **251**, 7816–20 (1976).
27. Borgeat, P. & Samuelsson, B. Transformation of arachidonic acid by rabbit polymorphonuclear leukocytes. Formation of a novel dihydroxyeicosatetraenoic acid. *J. Biol. Chem.* 2643–2646 (1979).
28. Murphy, R. C., Hammarström, S. & Samuelsson, B. Leukotriene C: a slow-reacting substance from murine mastocytoma cells. *Proc. Natl. Acad. Sci. U. S. A.* **76**, 4275–9 (1979).
29. Wong, A. *et al.* Stimulation of leukotriene production and membrane translocation of 5-lipoxygenase by cross-linking of the IgE receptors in RBL-2H3 cells. *Biochemistry* **31**, 4046–53 (1992).
30. Glover, S. *et al.* Translocation of the 85-kDa phospholipase A2 from cytosol to the

- nuclear envelope in rat basophilic leukemia cells stimulated with calcium ionophore or IgE/antigen. *J. Biol. Chem.* **270**, 15359–67 (1995).
31. Petersgolden, M. & Mcnish, R. W. Redistribution of 5-Lipoxygenase and Cytosolic Phospholipase A2 to the Nuclear Fraction upon Macrophage Activation. *Biochem. Biophys. Res. Commun.* **196**, 147–153 (1993).
  32. Hammarberg, T., Provost, P., Persson, B. & Rådmark, O. The N-terminal domain of 5-lipoxygenase binds calcium and mediates calcium stimulation of enzyme activity. *J. Biol. Chem.* **275**, 38787–93 (2000).
  33. Lichtenbergova, L., Yoon, E. T. & Cho, W. Membrane Penetration of Cytosolic Phospholipase A 2 Is Necessary for Its Interfacial Catalysis and Arachidonate Specificity. *Biochemistry* **37**, 14128–14136 (1998).
  34. Bair, A. M., Turman, M. V, Vaine, C. A., Panettieri, R. A. & Soberman, R. J. The nuclear membrane leukotriene synthetic complex is a signal integrator and transducer. *Mol Biol Cell* **23**, 4456–4464 (2012).
  35. Rouzer, C., Matsumoto, T. & Samuelsson, B. Single protein from human leukocytes possesses 5-lipoxygenase and leukotriene A4 synthase activities. *Proc. Natl. Acad. Sci. USA* **83**, 857–861 (1986).
  36. Newcomer, M. & Gilbert, N. Location, Location, Location: Compartmentalization of Early Events in Leukotriene Biosynthesis. *J. Biol. Chem.* **285**, 25109–25114 (2010).
  37. Raulf, M., Stuning, M. & Konig, W. Metabolism of leukotrienes by L-gamma-glutamyl-transpeptidase and dipeptidase from human polymorphonuclear granulocytes. *Immunology* **55**, 135–147 (1985).
  38. Yokomizo, T., Izumi, T., Chang, K., Takuwa, Y. & Shimizu, T. A G-protein-coupled receptor for leukotriene B4 that mediates chemotaxis. *Nature* **387**, 620–624 (1997).
  39. Maekawa, A., Kanaoka, Y., Xing, W. & Austen, K. F. Functional recognition of a distinct receptor preferential for leukotriene E4 in mice lacking the cysteinyl leukotriene 1 and 2 receptors. *Proc. Natl. Acad. Sci. U. S. A.* **105**, 16695–700 (2008).
  40. Bankova, L. G. *et al.* Leukotriene E4 elicits respiratory epithelial cell mucin release through the G-protein-coupled receptor, GPR99. *Proc. Natl. Acad. Sci. U. S. A.* **113**, 6242–7 (2016).
  41. Dannull, J. *et al.* Leukotriene C4 induces migration of human monocyte-derived dendritic cells without loss of immunostimulatory function. *Blood* **119**, 3113–3122 (2012).
  42. Costa, M. F. de S. *et al.* Leukotriene B4 mediates gammadelta T lymphocyte migration in response to diverse stimuli. *J. Leukoc. Biol.* **87**, 323–32 (2010).
  43. Griffiths, R. J. *et al.* Leukotriene B4 plays a critical role in the progression of collagen-induced arthritis. *Proc. Natl. Acad. Sci. USA* **92**, 517–521 (1995).
  44. Serhan, C. N., Chiang, N. & Dyke, T. E. Van. Resolving inflammation: dual anti-

- inflammatory and pro- resolution lipid mediators. *Nat. Rev. Immunol.* **8**, 349–361 (2008).
45. Ueda, N. *et al.* Lipoxin synthesis by arachidonate 12-lipoxygenase purified from porcine leukocytes. *Biochem. Biophys. Res. Commun.* **149**, 1063–1069 (1987).
  46. Ueda, N., Yamamoto, S., Fitzsimmons, B. J. & Rokach, J. Lipoxin synthesis by arachidonate 5-lipoxygenase purified from porcine leukocytes. *Biochem. Biophys. Res. Commun.* **144**, 996–1002 (1987).
  47. Claria, J. & Serhan, C. N. Aspirin triggers previously undescribed bioactive eicosanoids by human endothelial cell-leukocyte interactions. *Proc. Natl. Acad. Sci. U S A* **92**, 9475–9479 (1995).
  48. Hanson, J., Ferreirós, N., Pirotte, B., Geisslinger, G. & Offermanns, S. Heterologously expressed formyl peptide receptor 2 (FPR2/ALX) does not respond to lipoxin A4. *Biochem. Pharmacol.* **85**, 1795–1802 (2013).
  49. Brink, C. *et al.* International Union of Pharmacology XXXVII. Nomenclature for Leukotriene and Lipoxin Receptors. *Pharmacol. Rev.* **55**, 195–227 (2003).
  50. Aliberti, J., Hieny, S., Reis e Sousa, C., Serhan, C. N. & Sher, A. Lipoxin-mediated inhibition of IL-12 production by DCs: a mechanism for regulation of microbial immunity. *Nat. Immunol.* **3**, 76–82 (2002).
  51. Levy, B. D. *et al.* Multi-pronged inhibition of airway hyper-responsiveness and inflammation by lipoxin A4. *Nat. Med.* **8**, 1018–1023 (2002).
  52. Barnig, C. *et al.* Lipoxin A4 Regulates Natural Killer Cell and Type 2 Innate Lymphoid Cell Activation in Asthma. *Sci. Transl. Med.* **5**, 174ra26-174ra26 (2013).
  53. Oh, S. F., Pillai, P. S., Recchiuti, A., Yang, R. & Serhan, C. Pro-resolving actions and stereoselective biosynthesis of 18S E-series resolvins in human leukocytes and murine inflammation. *J. Clin. Investig.* **21**, 569–581 (2011).
  54. Serhan, C. N. & Petasis, N. A. Resolvins and protectins in inflammation resolution. *Chem. Rev.* **111**, 5922–43 (2011).
  55. Arita, M. *et al.* Stereochemical assignment, antiinflammatory properties, and receptor for the omega-3 lipid mediator resolvin E1. *J. Exp. Med.* **201**, 713–722 (2005).
  56. Arita, M. *et al.* Resolvin E1 selectively interacts with leukotriene B4 receptor BLT1 and ChemR23 to regulate inflammation. *J. Immunol.* **178**, 3912–3917 (2007).
  57. Krishnamoorthy, S. *et al.* Resolvin D1 binds human phagocytes with evidence for proresolving receptors. *Proc. Natl. Acad. Sci. U S A* **107**, 1660–1665 (2010).
  58. Oh, S. F. *et al.* Resolvin E2 formation and impact in inflammation resolution. *J. Immunol.* **188**, 4527–34 (2012).
  59. Sun, Y.-P. *et al.* Resolvin D1 and its aspirin-triggered 17R epimer. Stereochemical assignments, anti-inflammatory properties, and enzymatic inactivation. *J. Biol. Chem.* **282**, 9323–34 (2007).

60. Steinhilber, D. & Hofmann, B. Recent Advances in the Search for Novel 5-Lipoxygenase Inhibitors. *Basic Clin. Pharmacol. Toxicol.* **114**, 70–77 (2014).
61. Tardif, J. C. *et al.* Treatment With 5-Lipoxygenase Inhibitor VIA-2291 (Atreleuton) in Patients With Recent Acute Coronary Syndrome. *Circ. Cardiovasc. Imaging* **3**, 298–307 (2010).
62. Kuhn, H., Banthiya, S. & van Leyen, K. Mammalian lipoxygenases and their biological relevance. *Biochim. Biophys. Acta - Mol. Cell Biol. Lipids* **1851**, 308–330 (2015).
63. Brash, A. R. Lipoxygenases: occurrence, functions, catalysis, and acquisition of substrate. *J. Biol. Chem.* **274**, 23679–82 (1999).
64. Hansen, J. *et al.* Bacterial lipoxygenases, a new subfamily of enzymes? A phylogenetic approach. *Appl. Microbiol. Biotechnol.* **97**, 4737–4747 (2013).
65. Boeglin, W. E., Kim, R. B. & Brash, A. R. A 12R-lipoxygenase in human skin: Mechanistic evidence, molecular cloning, and expression. *Biochemistry* **95**, 6744–6749 (1998).
66. Rapoport, S. M. *et al.* The Lipoxygenase of Reticulocytes. Purification, Characterization and Biological Dynamics of the Lipoxygenase; Its Identity with the Respiratory Inhibitors of the Reticulocyte. *Eur. J. Biochem.* **96**, 545–561 (1979).
67. Maskrey, B. H. *et al.* Activated platelets and monocytes generate four hydroxyphosphatidylethanolamines via lipoxygenase. *J. Biol. Chem.* **282**, 20151–63 (2007).
68. Schilstra, M. J., Veldink, G. A., Verhagen, J. & Vliegthart, J. F. Effect of lipid hydroperoxide on lipoxygenase kinetics. *Biochemistry* **31**, 7692–9 (1992).
69. Schneider, C., Pratt, D. A., Porter, N. A. & Brash, A. R. Control of oxygenation in lipoxygenase and cyclooxygenase catalysis. *Chem. Biol.* **14**, 473–88 (2007).
70. Ivanov, I. *et al.* Molecular enzymology of lipoxygenases. *Arch. Biochem. Biophys.* **503**, 161–174 (2010).
71. Sloane, D. L., Leung, R., Craik, C. S. & Sigal, E. A primary determinant for lipoxygenase positional specificity. *Nature* **354**, 149–152 (1991).
72. Eek, P. *et al.* Structure of a Calcium-dependent 11R-Lipoxygenase Suggests a Mechanism for Ca<sup>2+</sup> Regulation. *J. Biol. Chem.* **287**, 22377–22386 (2012).
73. Egmond, M. R., Vliegthart, J. F. G. & Boldingh, J. Stereospecificity of the hydrogen abstraction at carbon atom n-8 in the oxygenation of linoleic acid by lipoxygenases from corn germs and soya beans. *Biochem. Biophys. Res. Commun.* **48**, 1055–1060 (1972).
74. Coffa, G. & Brash, A. R. A single active site residue directs oxygenation stereospecificity in lipoxygenases: stereocontrol is linked to the position of oxygenation. *Proc. Natl. Acad. Sci. U. S. A.* **101**, 15579–84 (2004).
75. Boyington, J. C., Gaffney, B. J. & Amzel, L. M. The three-dimensional structure of an

- arachidonic acid 15-lipoxygenase. *Science* (80-. ). **260**, 1482–1486 (1993).
76. Garreta, A. *et al.* Structure and interaction with phospholipids of a prokaryotic lipoxygenase from *Pseudomonas aeruginosa*. *FASEB J.* **27**, 4811–4821 (2013).
  77. Newcomer, M. E. & Brash, A. R. The structural basis for specificity in lipoxygenase catalysis. *Protein Sci.* **24**, 298–309 (2015).
  78. Neau, D. B. *et al.* Crystal structure of a lipoxygenase in complex with substrate: the arachidonic acid-binding site of 8R-lipoxygenase. *J. Biol. Chem.* **289**, 31905–13 (2014).
  79. Hammel, M., Walther, M., Prassl, R. & Kuhn, H. Structural Flexibility of the N-terminal b-Barrel Domain of 15-Lipoxygenase-1 Probed by Small Angle X-ray Scattering. Functional Consequences for Activity Regulation and Membrane Binding. *J. Mol. Biol.* **343**, 917–929 (2004).
  80. Hammarberg, T., Provost, P., Persson, B. & Rådmark, O. The N-terminal domain of 5-lipoxygenase binds calcium and mediates calcium stimulation of enzyme activity. *J. Biol. Chem.* **275**, 38787–93 (2000).
  81. Kulkarni, S., Das, S., Funk, C. D., Murray, D. & Cho, W. Molecular Basis of the Specific Subcellular Localization of the C2-like Domain of 5-Lipoxygenase. *J. Biol. Chem.* **277**, 13167–13174 (2002).
  82. Jarving, R. *et al.* Activation of 11R-lipoxygenase is fully Ca<sup>2+</sup>-dependent and controlled by the phospholipid composition of the target membrane. *Biochemistry* **51**, 3310–3320 (2012).
  83. Xu, S., Mueser, T. C., Marnett, L. J. & Funk, M. O. Crystal Structure of 12-Lipoxygenase Catalytic Domain-Inhibitor Complex Identifies a Substrate Binding Channel for Catalysis. *Structure* **20**, 1490–1497 (2012).
  84. Ivanov, I. *et al.* Tight association of N-terminal and catalytic subunits of rabbit 12/15-lipoxygenase is important for protein stability and catalytic activity. *Biochim. Biophys. Acta - Mol. Cell Biol. Lipids* **1811**, 1001–1010 (2011).
  85. Murphy, R. C. & Gijón, M. A. Biosynthesis and metabolism of leukotrienes. *Biochem. J.* **405**, 379–395 (2007).
  86. Zhang, Y.-Y., Hamberg, M., Radmark, O. & Samuelsson Bengt. Stabilization of Purified Human 5-Lipoxygenase with Glutathione Peroxidase and Superoxide Dismutase. *Anal. Biochem.* **220**, 28–35 (1994).
  87. Gilbert, N. C. *et al.* The structure of human 5-lipoxygenase. *Science* (80-. ). **331**, 217–219 (2011).
  88. Gilbert, N. C. *et al.* The structure of human 5-lipoxygenase. *Science* (80-. ). **331**, 217–219 (2011).
  89. Pande, A. H. *et al.* Modulation of Human 5-Lipoxygenase Activity by Membrane Lipids. *Biochemistry* **43**, 14653–14666 (2004).

90. Pande, A. H., Qin, S. & Tatulian, S. A. Membrane fluidity is a key modulator of membrane binding, insertion, and activity of 5-lipoxygenase. *Biophys. J.* **88**, 4084–94 (2005).
91. Ochi, K., Yoshimoto, T., Yamamoto, S., Taniguchi, K. & Miyamoto, T. Arachidonate 5-lipoxygenase of guinea pig peritoneal polymorphonuclear leukocytes. Activation by adenosine 5'-triphosphate. *J. Biol. Chem.* **258**, 5754–8 (1983).
92. Lepley, R. A., Muskardin, D. T. & Fitzpatrick, F. A. Tyrosine kinase activity modulates catalysis and translocation of cellular 5-lipoxygenase. *J. Biol. Chem.* **271**, 6179–84 (1996).
93. Werz, O., Klemm, J., Samuelsson, B. & Rådmark, O. 5-lipoxygenase is phosphorylated by p38 kinase-dependent MAPKAP kinases. *Proc. Natl. Acad. Sci. U. S. A.* **97**, 5261–6 (2000).
94. Werz, O., Burkert, E., Samuelsson, B., Radmark, O. & Steinhilber Dieter. Activation of 5-lipoxygenase by cell stress is calcium independent in human polymorphonuclear leukocytes. *Blood* **99**, 1044–1052 (2002).
95. Werz, O. *et al.* Extracellular signal-regulated kinases phosphorylate 5-lipoxygenase and stimulate 5-lipoxygenase product formation in leukocytes. *FASEB J.* **16**, 1441–3 (2002).
96. Luo, M. *et al.* Phosphorylation by protein kinase a inhibits nuclear import of 5-lipoxygenase. *J. Biol. Chem.* **280**, 40609–16 (2005).
97. Gilbert, N. C. *et al.* Conversion of human 5-lipoxygenase to a 15-lipoxygenase by a point mutation to mimic phosphorylation at Serine-663. *FASEB J.* **26**, 3222–9 (2012).
98. Takano, T., Clish, C. B., Gronert, K., Petasis, N. & Serhan, C. N. Lipoxin Analogues Inhibit Neutrophil-mediated Leakage Permeability Neutrophil-mediated Changes in Vascular Permeability Are Inhibited by Topical Application of Aspirin-triggered 15-epi-lipoxin A 4 and Novel Lipoxin B 4 Stable Analogues. *J. Clin. Invest* **101**, 819–826 (1998).
99. Sendobry, S. M. *et al.* Attenuation of diet-induced atherosclerosis in rabbits with a highly selective 15-lipoxygenase inhibitor lacking significant antioxidant properties. *Br. J. Pharmacol.* **120**, 1199–1206 (1997).
100. Harats, D. *et al.* Overexpression of 15-Lipoxygenase in Vascular Endothelium Accelerates Early Atherosclerosis in LDL Receptor-Deficient Mice. *Arterioscler. Thromb. Vasc. Biol.* **20**, (2000).
101. Harats, D. *et al.* Overexpression of 15-Lipoxygenase in Vascular Endothelium Accelerates Early Atherosclerosis in LDL Receptor-Deficient Mice. *Arterioscler. Thromb. Vasc. Biol.* **20**, 2100–2105 (2000).
102. Funk, C. D., Chen, X.-S., Johnson, E. N. & Zhao, L. Lipoxigenase genes and their targeted disruption. *Prostaglandins Other Lipid Mediat.* **68–69**, 303–312 (2002).
103. Gulliksson, M. *et al.* Expression of 15-lipoxygenase type-1 in human mast cells. *Biochim. Biophys. Acta - Mol. Cell Biol. Lipids* **1771**, 1156–1165 (2007).

104. Kü Hn, H. & O 'donnell, V. B. Inflammation and immune regulation by 12/15-lipoxygenases. *Prog. Lipid Res.* **45**, 334–356 (2006).
105. Brash, A. R., Boeglin, W. E. & Chang, M. S. Discovery of a second 15S-lipoxygenase in humans. *Proc. Natl. Acad. Sci. U. S. A.* **94**, 6148–6152 (1997).
106. Gillmor, S. A., Villaseñor, A., Fletterick, R., Sigal, E. & Browner, M. F. The structure of mammalian 15-lipoxygenase reveals similarity to the lipases and the determinants of substrate specificity. *Nat. Struct. Biol.* **4**, 1003–9 (1997).
107. Kobe, M. J., Neau, D. B., Mitchell, C. E., Bartlett, S. G. & Newcomer, M. E. The structure of human 15-lipoxygenase-2 with a substrate mimic. *J. Biol. Chem.* **289**, 8562–9 (2014).
108. Andersson, E., Schain, F., Svedling, M., Claesson, H.-E. & Forsell, P. K. A. Interaction of human 15-lipoxygenase-1 with phosphatidylinositol bisphosphates results in increased enzyme activity. *Biochim. Biophys. Acta - Mol. Cell Biol. Lipids* **1761**, 1498–1505 (2006).
109. Ruddat, V. C., Whitman, S., Holman, T. R. & Bernasconi, C. F. Stopped-flow kinetic investigations of the activation of soybean lipoxygenase-1 and the influence of inhibitors on the allosteric site. *Biochemistry* **42**, 4172–8 (2003).
110. Joshi, N. *et al.* Kinetic and structural investigations into the allosteric and pH effect on the substrate specificity of human epithelial 15-lipoxygenase-2. *Biochemistry* **52**, 8026–35 (2013).
111. Miller, D. K. *et al.* Identification and isolation of a membrane protein necessary for leukotriene production. *Nature* **343**, 278–281 (1990).
112. Young, R. N. Development of novel leukotriene--based anti-asthma drugs: MK-886 and MK-571. *Agents Actions. Suppl.* **34**, 179–87 (1991).
113. Müller-Peddinghaus, R. *et al.* BAY X1005, a new selective inhibitor of leukotriene synthesis: pharmacology and pharmacokinetics. *J. Lipid Mediat.* **6**, 245–8 (1993).
114. Mancini, J. A. *et al.* 5-lipoxygenase-activating protein is an arachidonate binding protein. *FEBS Lett.* **318**, 277–281 (1993).
115. Mandal, A. K. *et al.* The nuclear membrane organization of leukotriene synthesis. *Proc. Natl. Acad. Sci. U. S. A.* **105**, 20434–9 (2008).
116. Ferguson, A. D. *et al.* Crystal Structure of Inhibitor-Bound Human 5-Lipoxygenase-Activating Protein. *Science (80-. ).* **317**, (2007).
117. Niegowski, D. *et al.* Crystal Structures of Leukotriene C 4 Synthase in Complex with Product Analogs. *J. Biol. Chem.* **289**, 5199–5207 (2014).
118. Sjögren, T. *et al.* Crystal structure of microsomal prostaglandin E 2 synthase provides insight into diversity in the MAPEG superfamily. *Proc. Natl. Acad. Sci.* **110**, 3806–3811 (2013).
119. S.P. Sansom, M. & Weinstein, H. Hinges, swivels and switches: the role of prolines in

- signalling via transmembrane  $\alpha$ -helices. *Trends Pharmacol. Sci.* **21**, 445–451 (2000).
120. Pettersen, D., Davidsson, O. & Whatling, C. Recent advances for FLAP inhibitors. *Bioorg. Med. Chem. Lett.* **25**, 2607–2612 (2015).
  121. Hutchinson, J. H. *et al.* 5-lipoxygenase-activating protein inhibitors: Development of 3-[3-tert-butylsulfanyl-1-[4-(6-methoxy-pyridin-3-yl)-benzyl]-5-(pyridin-2-ylmethoxy)-1H-indol-2-yl]-2,2-dimethyl-propionic acid (AM103). *J. Med. Chem* **52**, 5803–5815 (2009).
  122. Carpenter, E. P., Beis, K., Cameron, A. D. & Iwata, S. Overcoming the challenges of membrane protein crystallography. *Curr. Opin. Struct. Biol.* **18**, 581–6 (2008).
  123. Pirrone, G. F., Iacob, R. E. & Engen, J. R. Applications of Hydrogen/Deuterium Exchange MS from 2012 to 2014. *Anal. Chem.* **87**, 99–118 (2014).
  124. Hvidt, A. & Linderstrom-Lang, K. Exchange of hydrogen atoms in insulin with deuterium atoms in aqueous solutions. *Biochim. Biophys. Acta* **14**, 574–5 (1954).
  125. Zhang, Z. & Smith, D. L. Determination of amide hydrogen exchange by mass spectrometry: a new tool for protein structure elucidation. *Protein Sci.* **2**, 522–31 (1993).
  126. Johnson, R. S. & Walsh, K. A. Mass spectrometric measurement of protein amide hydrogen exchange rates of apo- and holo-myoglobin. *Protein Sci.* **3**, 2411–2418 (1994).
  127. Busenlehner, L. S. & Armstrong, R. N. Insights into enzyme structure and dynamics elucidated by amide H/D exchange mass spectrometry. *Arch. Biochem. Biophys.* **433**, 34–46 (2005).
  128. Feng, Y., Wang, B., Chu, X., Wang, Y. & Zhu, L. The Development of Protein Chips for High Throughput Screening (HTS) of Chemically Labeling Small Molecular Drugs. *Mini Rev. Med. Chem.* **16**, 846–50 (2016).
  129. Bender, A. *et al.* Which aspects of HTS are empirically correlated with downstream success? *Curr. Opin. Drug Discov. Devel.* **11**, 327–37 (2008).
  130. Schilstra, M. J., Veldink, G. A. & Vliegthart, J. F. The dioxygenation rate in lipoxygenase catalysis is determined by the amount of iron (III) lipoxygenase in solution. *Biochemistry* **33**, 3974–9 (1994).
  131. Hutchins, P. M. & Murphy, R. C. Cholesteryl ester acyl oxidation and remodeling in murine macrophages: formation of oxidized phosphatidylcholine. *J. Lipid Res.* **53**, 1588–97 (2012).
  132. Bender, G., Schexnaydre, E. E., Murphy, R. C., Uhlson, C. & Newcomer, M. E. Membrane-dependent Activities of Human 15-LOX-2 and Its Murine Counterpart. *J. Biol. Chem.* **291**, 19413–19424 (2016).
  133. Newcomer, M. E. & Brash, A. R. The structural basis for specificity in lipoxygenase catalysis. *Protein Sci.* **24**, 298–309 (2014).
  134. Gilbert, N. C. *et al.* Conversion of human 5-lipoxygenase to a 15-lipoxygenase by a point mutation to mimic phosphorylation at Serine-663. *FASEB J* **26**, 3222–3229 (2012).



135. Walther, M., Wiesner, R. & Kuhn, H. Investigations into Calcium-dependent Membrane Association of 15-Lipoxygenase-1. *J. Biol. Chem.* **279**, 3717–3725 (2004).
136. Hsu, Y.-H. *et al.* Calcium Binding Rigidifies the C2 Domain and the Intradomain Interaction of GIVA Phospholipase A 2 as Revealed by Hydrogen/Deuterium Exchange Mass Spectrometry. *J. Biochem.* **283**, 9820–9827 (2008).
137. Cao, J., Burke, J. E. & Dennis, E. A. Using hydrogen/deuterium exchange mass spectrometry to define the specific interactions of the phospholipase A2 superfamily with lipid substrates, inhibitors, and membranes. *J. Biol. Chem.* **288**, 1806–13 (2013).
138. Verdaguer, N., Corbalan-Garcia, S., Ochoa, W. F., Fita, I. & Gó Mez-Ferná Ndez, J. C. Ca<sup>2+</sup> bridges the C2 membrane-binding domain of protein kinase C $\alpha$  directly to phosphatidylserine. *EMBO J.* **18**, 6329–6338 (1999).
139. Kulkarni, S., Das, S., Funk, C. D., Murray, D. & Cho, W. Molecular Basis of the Specific Subcellular Localization of the C2-like Domain of 5-Lipoxygenase. *J. Biol. Chem.* **277**, 13167–13174 (2002).
140. Kay, J. G. & Grinstein, S. in *Advances in experimental medicine and biology* **991**, 177–193 (2013).
141. Manna, D. *et al.* Differential Roles of Phosphatidylserine, PtdIns(4,5)P<sub>2</sub>, and PtdIns(3,4,5)P<sub>3</sub> in Plasma Membrane Targeting of C2 Domains. *J. Biol. Chem.* **38**, 26047–26058 (2008).
142. Yeom, M. *et al.* Phosphatidylserine inhibits inflammatory responses in interleukin-1 $\beta$ -stimulated fibroblast-like synoviocytes and alleviates carrageenan-induced arthritis in rat. *Nutr. Res.* **33**, 242–50 (2013).
143. Ramos, G. C. *et al.* Apoptotic mimicry: phosphatidylserine liposomes reduce inflammation through activation of peroxisome proliferator-activated receptors (PPARs) in vivo. *Br. J. Pharmacol.* **151**, 844–50 (2007).
144. Glick, J., Santoyo, G. & Casey, P. J. Arachidonate and related unsaturated fatty acids selectively inactivate the guanine nucleotide-binding regulatory protein, Gz. *J. Biol. Chem.* **271**, 2949–54 (1996).
145. Motlagh, H. N., Wrabl, J. O., Li, J. & Hilser, V. J. The ensemble nature of allstery. *Nature* **508**, 331–339 (2014).
146. Wecksler, A. T., Kenyon, V., Deschamps, J. D. & Holman, T. R. Substrate Specificity Changes for Human Reticulocyte and Epithelial 15-Lipoxygenases Reveal Allosteric Product Regulation. *Biochemistry* **46**, 7364–7375 (2008).
147. Laskowski, R. A., Gerick, F. & Thornton, J. M. The structural basis of allosteric regulation in proteins. *FEBS Lett.* **583**, 1692–1698 (2009).
148. Miroux, B. & Walker, J. E. Over-production of Proteins in Escherichia coli: Mutant Hosts that Allow Synthesis of some Membrane Proteins and Globular Proteins at High Levels. *J. Mol. Biol.* **260**, 289–298 (1996).

149. Annesley, T. M. Ion suppression in mass spectrometry. *Clin. Chem.* **49**, 1041–4 (2003).
150. Evans, J. F., Ferguson, A. D., Mosley, R. T. & Hutchinson, J. H. What's all the FLAP about?: 5-lipoxygenase-activating protein inhibitors for inflammatory diseases. *Trends Pharmacol. Sci.* **29**, 72–78 (2008).
151. Joshi, N. *et al.* Kinetic and Structural Investigations into the ALlosteric and pH Effect on the Substrate Specificity of Human Epithelial 15-Lipoxygenase-2. *Biochemistry* **52**, (2013).
152. Narayan, K. & Lemmon, M. A. Determining selectivity of phosphoinositide-binding domains. *Methods* **39**, 122–33 (2006).
153. Wu, Y., Engen, J. R. & Hobbins, W. B. Ultra Performance Liquid Chromatography (UPLC) Further Improves Hydrogen/Deuterium Exchange Mass Spectrometry. *J. Am. Soc. Mass Spectrom.* **17**, 163–167 (2006).
154. Rey, M. *et al.* Effective Removal of Nonionic Detergents in Protein Mass Spectrometry, Hydrogen/Deuterium Exchange, and Proteomics. *Anal. Chem.* **82**, 5107–5116 (2010).